UNIVERSITY OF OKLAHOMA

GRADUATE COLLEGE

EFFECTS OF FIBERS AND PIPE ROTATION ON HORIZONTAL WELL CLEANOUT WITH POLYMERIC FLUIDS

A THESIS

SUBMITTED TO THE GRADUATE FACULTY

in partial fulfillment of the requirements for the

Degree of

MASTER OF SCIENCE

By

SERGIO ARMANDO GARCIA PRADA

Norman, Oklahoma

2022

EFFECTS OF FIBERS AND PIPE ROTATION ON HORIZONTAL WELL CLEANOUT WITH POLYMERIC FLUIDS

A THESIS APPROVED FOR THE

MEWBOURNE SCHOOL OF PETROLEUM AND GEOLOGICAL ENGINEERING

BY THE COMMITTEE CONSISTING OF

Dr. Hamidreza Karami, Chair

Dr. Ramadan Ahmed, Co-chair

Dr. Catalin Teodoriu

Acknowledgments

I would like to express my deepest gratitude to Dr. Hamidreza Karami, who guided me during the course of my studies at the University of Oklahoma. Studying a master's degree in Petroleum Engineering at OU was a dream come true and he was the one who gave me the opportunity to demonstrate my capabilities.

My appreciation and thanks to Dr. Ramadan Ahmed for giving me the chance of working in such an interesting research project. His knowledge and support has no limits.

I would like to thank Dr. Catalin Teodoriu, his way of teaching is something I have never seen before, and I really enjoyed it. Special thanks to Mr. Jeff McCaskill for all his amazing help during my experiments.

My life at Norman would not have been the same without my girlfriend, Lisseth. Thank you so much for all your support, and for always encouraging me to do the things I like.

I would like to thank my family for supporting me in the distance, I am the person I am today because of them. I am grateful for having my little dog, Brownie, her company kept me sane while I was writing this book.

Finally, I wish to show my appreciation to the University of Oklahoma, the Mewbourne School of Geological and Petroleum Engineering, and the Well Construction Technology Center for providing everything I needed to obtain my master's degree title.

Table of Contents

List of Tables

List of Figures

Abstract

Rock cuttings deposition is a problem commonly faced during drilling, completion, and intervention activities. Using polymer-based fluids is the to-go technique to improve horizontal hole cleaning. However, the rheological properties of such fluids are sometimes not enough to guarantee an efficient cleanout. One of the ways to improve cleanout efficiency is by rotating the pipe inside the annulus to mitigate the settling of solids. Another approach is by adding fibers to the cleaning fluid, improving its lifting capacity and moving the settled solids. This study is aimed at evaluating the cleanout performance of polymer-based and fibrous fluids in horizontal wells without and with pipe rotation using a large-scale flow loop.

The flow loop consists of a 48-ft long annular test section with a 5-in. ID wellbore and an inner 2.375-in. OD drill pipe. In each experiment, a solids bed of natural proppant is placed in the annulus. Low-viscosity polymeric suspensions are used as the drilling fluid with and without fiber. Flow rate and pipe rotation are varied while measuring the equilibrium bed height. The initial bed height is placed at a flowrate of 35 GPM without pipe rotation. Then, the flow rate is increased step by step until the bed is completely cleaned. The measured test parameters include the bed height along the horizontal annulus, flow rate, pipe rotation speed, and pressure loss, monitored and recorded using a data acquisition system. A rotational viscometer is used to monitor the rheology of the fluids.

The results show that fiber improves the effectiveness of hole cleanout in horizontal wellbores. When a small amount of fiber (0.04% wt.) is added to the base fluid, the cleanout performance improves significantly. Despite negligible impact on the rheological characteristics of the fluid, the fiber improves the solid lifting capacity to induce motion in the settled bed particles in horizontal well configurations. The addition of fiber causes a lack of homogeneity in the bed

profile, an effect known as duning. The presence of pipe rotation also shows excellent cleanout efficiencies. In some cases, even the slightest rotation speed is enough to obtain almost complete cleanout at significantly lower flowrates.

The experimental results were compared to mechanistic models predicting the pressure drop and the bed height, and showed an acceptable agreement. The presence of dunes increases the error in the pressure drop prediction because the model assumes a uniform bed height. A correction factor is developed to mitigate the duning effect, giving new pressure drop predictions within an acceptable error range. The results of the bed height prediction are excellent for the base fluid and inferior for the fibrous fluid. A sensitivity analysis is done for the mechanistic model, identifying the most important predictor parameters.

Chapter 1: Introduction

This chapter covers the main concepts targeted in this study. First, an overview of the problem in hand is detailed and described. Then, the main objectives set to address with regards to this problem are presented. Finally, the scope of the work required to reach the objectives is explained.

1.1 Problem Statement

Drilling a well is the process required to connect to the reservoir and produce hydrocarbons from the sub-surface. Rock cuttings are generated when drilling, normally settling at the bottom of the annulus. If a well is vertical, the cuttings are fully suspended and transported to the surface by maintaining appropriate annular fluid velocity and viscosity. In horizontal configurations, however, the cuttings often accumulate throughout the horizontal section on the low side of the annulus. The accumulation of cuttings (poor hole cleaning) can cause several problems, such as stuck pipe, formation damage, high drag and torque, fluid loss, and so on.

The drilling fluid circulating through the drill-pipes and annulus is supposed to clean the well from the cuttings. In vertical wells, the upward drag of the fluid directly opposes the gravity and helps clean the cuttings falling in the opposite direction. In horizontal wells, however, the cuttings commonly fall after traveling short distances by the horizontal drag of the liquid and settle in a deposit bed. Once they settle, the cuttings have little chance of being picked up and transported because of the low local fluid velocities near the bed (Sifferman and Becker, 1990). Increasing the flowrate could improve the cleaning efficiency in horizontal configurations and resolve this issue.

However, excessive annular velocity may lead to borehole erosion and high pressure drop (Ahmed et al, 2002) that could cause of formation damage, lost circulation and formation fracturing.

The horizontal drag force generated by the fluid velocity doesn't help with the un-settling of cuttings in horizontal wells. Nevertheless, depending on the fluid's rheological properties, some fluids have good solids carrying capacity (higher vertical drag force opposing the motion of settling particles) to limit the deposition of solids. Rotating the drill pipe is another way to prevent settling of cuttings in horizontal configurations resulting in an increased hole cleaning efficiency. Regardless of the technique, hole cleaning in horizontal wells is the most challenging task for field engineers.

Wellbore cleanout issues have been widely studied in the last few decades. Several experimental studies (Sanchez et al. 1999; Masuda et al. 2000; Power et al. 2000; Walker and Li 2000; Duan et al. 2008; Valluri et al. 2008; Rodriguez Corredor et al. 2014; Naik 2015; Allahvirdizadeh et al. 2016; Bizhani et al. 2016; Egbue 2017; Song et al. 2017; Ozbayoglu et al. 2007; Pandya et al. 2019, 2020) investigated the influence of operational parameters. There is a consensus that fluid rheology and drill-string rotation are the most important factors that influence solids transport in deviated wells (Elgaddafi et al, 2021).

Using fibers with polymer-based fluids is an option to increase cleaning efficiency by improving the drag force acting on the deposited particles. Limited studies (Ahmed et al. 2009; Ahmed and Takach 2009; Cheung et al. 2012; George et al. 2014; Elgaddafi and Ahmed 2020) have been conducted to investigate the effect of fibers on cleanout efficiency in deviated and horizontal wells. This study aims to evaluate the effects of fiber and pipe rotation on downhole cleaning in horizontal wells using a large-scale flow loop.

1.2 Objectives

The principal objective of this investigation is to examine the effect of fiber on cleaning and hydraulic performances of polymeric fluids in horizontal configuration. The specific objectives of this study includes:

- Evaluating the cleaning efficiency of a low viscosity polymeric fluid at different flowrates with and without adding fiber at different concentrations.
- Investigating the effects of pipe rotation on the cleaning efficiency of a low viscosity polymeric fluid at different flowrates with and without adding fiber.
- Evaluating the accuracy of existing hydraulic and hole cleaning models by comparing predictions with measurements.
- Developing techniques to minimize discrepancies between model predictions and experimental data.

1.3 Scope of Work

The scope of this work includes experimental investigation and modeling of wellbore hydraulics and hole cleaning in horizontal wells. The experimental investigation was conducted in a large-scale flow loop with an eccentric annular test section. Low-viscosity polymeric suspensions were used with and without fiber. The effects of mudflow rate, pipe rotation speed, and fluid rheology on the hole cleaning performance were investigated by measuring the equilibrium bed height after the erosion of stationary solids bed at a constant flow rate. In addition, a pipe section viscometer was installed in parallel with the annular test section to study the effect of fiber on the hydraulics of the fluid flow. Also, a standard Model 35 rotational viscometer was used to monitor the rheology of the fluids before each test.

After obtaining the experimental investigation results, two different models are going to be evaluated to predict the differential pressure drop of each experiment. Furthermore, a bed height prediction model is going to be tested for the obtained experimental data. All the mentioned models are presented in Elgadaffi et al (2021).

Chapter 2: Literature Review

This chapter consist of a review of different studies conducted over time that are related to this work. The focus will be on the effect of fluid properties and wellbore geometry. Overall, there are two major approaches when studying solid transportation: mechanistic modeling and experimental approaches. These two approaches will be summarized and reviewed in the following sections.

2.1 Experimental Approaches

The experimental approaches to study solid transportation can be classified as steady solid transport and stationary bed erosion (Li and Luft 2014). The stationary bed erosion approach is focused on investigating the equilibrium concentration of solids (bed height) under several operating conditions or studying the erosion rate as a function of bed height for various operating conditions.

2.1.1 Bed Erosion

Normally, for stationary bed erosion, the solid concentration is reported as a solid bed height, cross-sectional area of wellbore covered by solids or volumetric fraction in the annulus.

2.1.1.1 Cleaning without Pipe Rotating

Cleaning horizontal wellbore without pipe rotation is challenging due to the lack of a lifting mechanism that re-suspends the deposited particles. Walker and Li (2000) analyzed the effects of particle size, fluid rheology, and pipe eccentricity on cuttings transport. They considered both cases of the circulation of the cuttings until the bed is formed (deposition phase) and the hole

cleaning once the bed is formed (erosion phase). The experiments were carried out using a 6.09-m long flow loop with 0.127-m transparent acrylic pipe to simulate the wellbore and 0.0603-m pipe to simulate the coiled tubing. The authors determined that the best way to pick up deposited solids is with a low viscosity fluid in a turbulent flow regime. However, a gel or a multiphase fluid should be used to maximize the carrying capacity. The effect of the particle size is more important at higher inclination angles for particles less than 7 mm. With regards to the position of the drill pipe, the more eccentric it becomes, the more difficult it gets to clean the particles. This is due to the lower local velocities in the narrow gaps close to the inner pipe, causing a rapid deposition of solids. The effect of eccentricity increases with the inclination of the wellbore.

A more recent study (Pandya et al. 2019) performed solids bed erosion experiments on a flow loop with a 10.36-m long horizontal test section and eccentric annular geometry, in which the ID of the outer pipe was 0.127 m and the OD of the inner pipe was 0.060 m. Water and two polymer-based (guar gel) fluids at concentrations of 1.2 and 2.4 g/L were used to analyze the cleaning efficiency of the fluids at different flow rates. Results showed superior cleanout efficiency of low viscosity fluids, due to higher local fluid velocity aiding the lifting of deposited solid particles. Water showed the highest overall cleaning efficiency because of a thinner hydrodynamic boundary than the polymer-based fluids.

Often polymers used in drilling fluids application exhibits drag reducing behavior under turbulent flow conditions which may affect their hole cleaning performance. Rodriguez Corredor et al. (2014) carried out an experimental study of hole cleaning performance, comparing water and drag reducing fluids. The experiments were conducted using a 9-m long horizontal flow loop with concentric annular geometry (95 mm outer pipe ID, and 38 mm inner pipe OD). Besides water, two drag reducing fluids with 0.07% V/V and 0.1% V/V concentrations of partially hydrolyzed

polyacrylamide (PHPA) were used. Their results showed that the solid removal efficiency of the drag reducing fluid is higher with coarse particles than finer particles. When using drag reducing fluids, lower pressure losses are obtained and the carrying capacity is increased. Higher critical velocities are required when transporting solids with drag reducing fluids in comparison to water. However, lower critical velocities are needed to initiate the movement of settled coarse cuttings, meaning that the diameter of the particles is a very important parameter related to hole cleaning.

Drilling sweep is a fluid which is different from the mud used for drilling the well. It is often circulated to clean the wellbore before making trips. The property difference between sweep fluid and drilling mud can be viscosity or density. Field study on hole cleaning (Power et al. 2000) suggested various operating parameters to optimize drilling sweeps. The study used data from two geological sidetracks drilled from the same vertical wellbore and demonstrated that using weighted sweeps is more efficient than high viscosity sweeps to clean the cuttings. The recommendations also included periodical application of drill pipe rotation with circulation to mitigate the formation of a stationary bed. The importance of this study is mainly related to its real-life field situation, rather than a lab scale, giving it an aggregated value. Another drilling sweep study (Valluri et al. 2006) focused on fluid rheology and its effect on sweep performance. The results demonstrated that regardless of the test conditions, high viscosity fluids without inner pipe rotation are ineffective in cuttings removal. This is in agreement with what has been discussed so far about thicker fluids being effective to carry solid particles in vertical wells but not as effective when a settled bed is formed.

2.1.1.2 Cleaning with Pipe Rotation

Drill pipe rotation is a parameter of interest with regards to hole cleaning. Sanchez et al. (1999) investigated the effect of drill pipe rotation during directional drilling, using a 30.48-m long

and 0.2032-m diameter wellbore simulator with a 0.1143-m drill pipe. The considered experimental variables were rotary speed, hole inclination, mud rheology, cuttings size, and mud flow rate. They conducted over 600 experiments. The results showed a significant effect of pipe rotation on hole cleaning, in which the level of enhancement was a function of the mud rheology, cuttings size, and mud flow rate. The dynamic behavior of the drill pipe (steady state vibration, unsteady state vibration, whirling rotation, true axial rotation in parallel with the wellbore axis) plays a major role in the cleaning efficiency. Typically, smaller cuttings are more difficult to transport. But at higher rotary speeds with high viscosity muds, that problem is mitigated. In highly inclined wells, low viscosity muds clean better than high viscosity muds. This study also reported the formation of unsteady beds and dunes, a problem that will be discussed further in the present study.

A similar study (Duan et al. 2008) conducted in highly deviated configurations examined the effect of rotation. The study was conducted in a flow loop with 30.48-m long annular test section (0.2032 m x 0.1143 m). Three different cutting sizes (0.45 to 3.3 mm) were used during the experiment. Besides the cuttings size, the authors investigated the effects of drill pipe rotation, fluid rheology, flow rate and hole inclination. Transporting smaller cuttings in highly inclined wells was more difficult than larger ones, and the result of these experiments were consistent with other studies (Parker (1987), Larsen (1990), Ahmed (2001)). Smaller cuttings resulted in higher cuttings concentration in the wellbore than larger cuttings in horizontal configurations. According to the results, the cleaning of large cuttings is sensitive to the flow rate, but pipe rotation and fluid rheology are the key factors to transport small cuttings. Another important finding of the study is the minor effect of the inclination angle on cuttings concentration within the range of 70°-90° from vertical.

2.1.1.3 Hole Cleaning with Fibrous Fluids

A number of studies (Karimi Rad et al. 2020; Ahmed et al. 2009; Ahmed and Takach 2009; Cheung et al. 2012; George et al. 2014; Elgaddafi and Ahmed 2020, Mahmoud et al. 2020; Aoki et al. 2020; Bulgachev and Pouget 2006) were conducted to investigate the cleaning performance of fibrous fluids. Ahmed et al. (2009) did an experimental study on fiber sweeps in horizontal and highly deviated configurations using two test fluids. The fluids included a base fluid consisting of 0.47% W/W Xanthan Gum and a fiber sweep with 0.47% W/W Xanthan Gum and 0.04% W/W synthetic fiber. Their results demonstrated that the addition of fiber has a negligible effect on the rheology of the fluid, while it improves the cleaning efficiency of the base fluid in horizontal configurations. At inclined configurations (68° from vertical), the enhanced cleaning efficiency of the fiber was moderated.

Mahmoud et al. (2020) ran some experiments to study the effects of polymer anionicity and fiber on the carrying capacity of polymer-based fluids. They focused on the settling behavior of fine cuttings in base fluids using polymers such as xanthan gum (XG), carboxymethyl cellulose (CMC), and polyanionic cellulose (PAC), with the addition of inert fibers. Their results showed that the increase in anionicity (solution's negative charge density) improves the carrying capacity of the solution. This is due to the increase in particle-particle and particle-polymer electrostatic repulsion forces. A small amount of fiber (0.08% W/W) improved the carrying capacity even more, with little impact on the rheology of the base fluid. The enhancement in carrying capacity caused by the fiber is due to the mechanical hindering effect of the formed fiber network and the hydrodynamic interactions between the cuttings and the fiber. It is important to mention that the performance of the fiber is directly related to the stability of its network within the polymer-based suspension. Also, the cutting size influences the carrying capacity of the fibrous fluid, where

smaller cuttings at lower flowrates are more difficult to be transported by the fiber network. Also, this means that larger cuttings are easier to be transported by the network. All of their results were obtained through measurements of the total suspended solids (TSS) of several mixture samples of base fluids and cuttings.

2.1.2 Steady Solids Transport

Steady solids transport studies represent steady-state drilling conditions at a constant rate of penetration in which an equilibrium bed height establishes in the wellbore. An earlier study (Sifferman and Becker 1992) evaluated the effects of ten operating variables (annular mud velocity, mud density, mud rheology, mud type, cuttings size, rate of penetration, drill pipe rotary speed, wellbore eccentricity, drill pipe diameter, and hole angle). They used a full scale 18.3-m long annular test section, with 0.076 m and 0.144 m OD drill pipes inside a 0.203 m ID wellbore. The inclination was varied from 45° to 90° from vertical. The results frequently showed a large buildup of cuttings in the annulus, which was very difficult to remove once the cuttings were deposited on the low side of the wellbore. The mud velocity and density showed the greatest effects on hole cleaning. It is important to notice that the experimental setup was not much different 30 years ago than most novel ones discussed so far, showing that there has not been much work done on the wellbore design, but mostly on the cleaning fluid. Another important takeaway from this experiment is that under normal drilling practices, up to 50% of the annular area may be filled with a cuttings bed. This verifies the importance of the studies related to improving the hole cleaning efficiency.

In more recent study (Allahvirdizadeh et al. 2016) experimentally studied the solid transport in a horizontal concentric annulus using water and drag-reducing polymer-based fluids. The focus was on the effects of drilling rate, mud flow rate, and polymer concentration on the cleaning

efficiency and pressure loss. The experiments were carried out using a 6.5-m long horizontal annulus in which the ID of the outer pipe was 0.074 m, and the OD of the inner pipe was 0.047 m. Using a solution of water and high molecular weight partially hydrolyzed polyacrylamide (PHPA), they observed a maximum drag reduction (38% reduction in frictional pressure drop) with a polymer concentration of 0.07% W/W. This fluid also resulted in the lowest accumulation of cuttings in the annuli.

2.2 Mechanistic Models

The mechanistic hole cleaning models developed to study solid transportation are based on mass and momentum balance equations (Naik 2015). According to Kelessidis and Mpandelis (2003), models vary principally in solid distribution in the solid-liquid layer, friction between the fluid and the pipe walls, and the interfacial friction between the fluid and the portion of the solids bed that is moving.

Clark and Bickman (1994) developed a mechanistic model to predict the minimum fluid velocity needed to transport solids at different wellbore inclinations. They discussed the impact of three mechanisms for solid transportation (rolling, settling, and lifting) depending on the inclination. They compared their predictions with experimental data. The predicted critical flow rate values were lower than the experimental data, possibly due to the uncertainties in critical flow rate criteria. A similar model (Ahmed et al. 2002) was later developed to predict the critical velocity required to initiate the movement of solid bed particles. The model considers a uniform bed of solid particles, resting on an inclined pipe wall, and fluid flowing over it. The model was tested by comparing its prediction with the results obtained from flow loop experiments. The movement of the bed particles was observed through a transparent pipe, with the flow rate of the

fluid controlled and changed over time. The study used two test fluids, water and aqueous solutions of Polyanionic cellulose. When comparing the model with the experimental data, the results showed a satisfactory agreement.

Elgaddafi et al. (2021) developed a more advanced mechanistic model for wellbore cleanout in horizontal and inclined wells. The model predicts the initiation of bed particle movement during cleanout operations with conventional muds and fluid containing fibers. The model introduced a fiber drag coefficient to account for the effect of fiber on the cleaning process. Also, the concept of the bed shear stress was introduced to predict the equilibrium bed height: critical fluid velocity. The existing wellbore cleanout models do not account for the variation of the bed shear stress. The use of bed shear stress makes this model's predictions more accurate. The predictions for fibrous and conventional fluids demonstrated good agreement with the experimental data.

2.3 Other Modeling Approaches

Becker (1987) developed an empirical correlation to determine the dependence of solid concentration to the fluid velocity, wellbore inclination, fluid density, well geometry, and initial gel strength. Inclinations of 0°-40°, 40°-45°, and 45°-90° and flow regimes were used to develop six correlations. They reported better solid transport in inclinations from vertical to 45° when the fluid was in laminar flow, and in higher inclinations when the flow was turbulent. They also observed high influence of rheology in laminar flow and little influence of it in turbulent flow.

Awad et al. (2020) developed a CFD modeling study of particle setting behavior during drilling operations, focusing on the impact of fluid rheology, flow regime, particle size and shape. The authors identified that the selection of a suitable rheological model and shape and size of the

particles are key factors when predicting the settling of solid particles in cleanout operations. Overall, their model showed an acceptable agreement with the experimental data.

2.4 Summary

Hole cleaning has been one of the main foci of study of engineers in the oil and gas industry around the world, where research related to it goes from decades ago to years and even months. There is a consensus that fluid rheology and drillstring rotation are the key factors affecting solid transport in horizontal wells, but parameters such as annular geometry, inclination angle, and solids properties are also taken into account. Studies related to the effect of fibers in the cleaning fluid are limited. The present work is aimed at helping to know fiber effects in horizontal hole cleaning.

Chapter 3: Theoretical Background and Modeling

This chapter provides a discussion on the theories and mathematical approaches used in this study, starting from basic definitions to more specific concepts related to hole cleaning. Adari et al (2010) presented a chart with the most relevant elements affecting hole cleaning, ranking them based on their influence and field control, as shown in Figure 3.1.

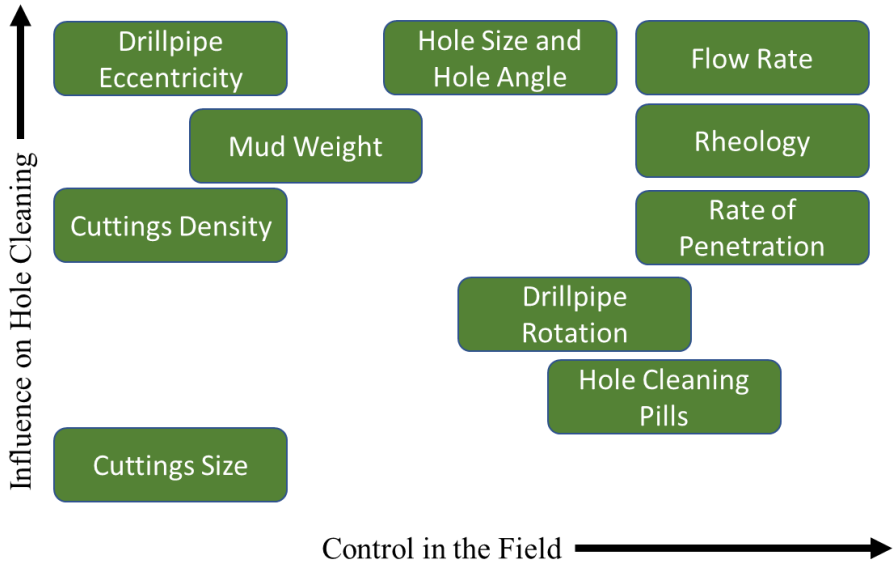

Figure 3.1 Important variables related to hole cleaning (adopted from Adari et al. 2000)

The variables presented in the chart are discussed in the previous chapter. Analysis of solid removal starts from the forces acting on an individual solid particle positioned on the surface of the bed. When circulating fluid to clean the wellbore, the solid particles are subjected to various forces including gravity, drag, buoyancy, and lift forces. The gravity force causes the solids settlement, and is given by:

$$F_g = \frac{\pi d_p^3 \rho_p g}{6}, \quad \text{Eq 3.1}$$

where F_g is the gravity force, d_p is the particle diameter, ρ_p is the particle density and g is the acceleration of gravity. The buoyancy force is one of the forces opposing the gravity, defined as:

$$F_b = \frac{\pi d_p^3 \rho_f g}{6}, \quad \text{Eq 3.2}$$

where F_b is the buoyancy force and ρ_f is the density of the fluid. The buoyancy force prevents the settling of the solids. Overall, the buoyancy force depends on the density of the fluid, which is why fluids with higher densities, that also have higher drag, can be more effective in hole cleaning operations. In addition, the drag and lift forces occur when a fluid flows over a solid body (deposited particles). The fluid's hydrodynamic drag and lift forces acting on the particles are defined using the following equations, respectively:

$$F_D = \frac{C_D \rho_f u^2 A_p}{2} \quad \text{Eq 3.3}$$

$$F_L = \frac{C_L \rho_f u^2 A_p}{2}, \quad \text{Eq 3.4}$$

where C_D and C_L are the drag and lift coefficients, u is the fluid's local velocity, and A_p is the flow projection area of the particle. The plastic force originated by the yielding behavior of the fluid opposes the particle motion. This force is defined as:

$$F_p = 0.5\pi d_p^2 \tau_y \left[\varphi + \left(\frac{\pi}{2} - \varphi\right) \sin^2\varphi - cos\varphi sin\varphi\right], \quad \text{Eq 3.5}$$

where φ is the angle of repose and τ_y is the yield stress of the fluid. Elgaddafi et al. (2012, 2016) developed a model to account for an additional drag force due to the presence of fiber in the fluid. This force which is known as fiber force, F_{Df}, is defined as:

$$F_{Df} = \frac{1}{2} C_{Df} (\rho_p - \rho_f) u^2 A_p, \quad \text{Eq 3.6}$$

where C_{Df} is the fiber drag coefficient. Figure 3.2 shows the analyzed forces acting on a solid bed particle.

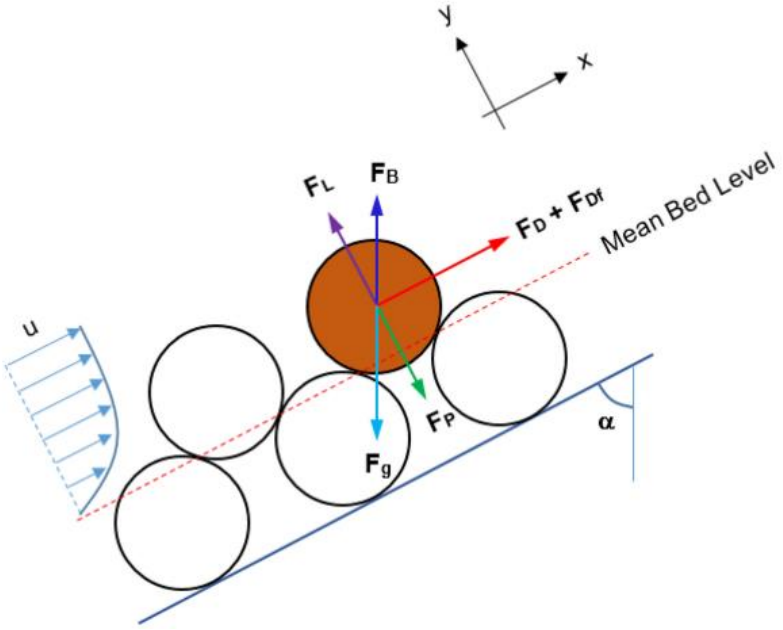

Figure 3.2 Forces acting on a solid bed particle (Elgaddafi et al. 2021)

In the present study, fluid viscosity (rheological behavior) is the property of most interest. The viscosity of fluid measures its resistance to continuous deformation (flow) and it depends on the nature of the fluid itself. Most of the fluids used for hole cleaning are non-Newtonian, which means that their viscosity is flow dependent. The process of calculating the rheological parameters for the fluids used in this study will be discussed in next chapters.

3.1 Geometrical Calculations

Figure 3.3 shows the eccentric configuration of a horizontal wellbore when a uniform bed height is considered. Two cases are considered in the schematic, a partially buried pipe case with the bed height less than the pipe diameter, and a fully buried pipe case with the bed height greater than the pipe diameter.

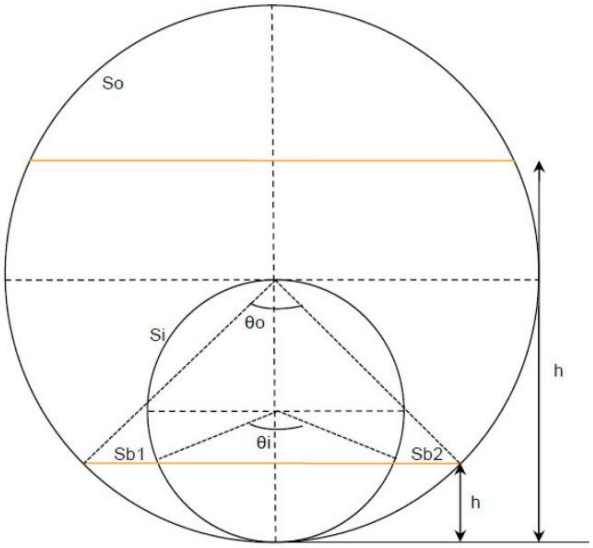

Figure 3.3 Wellbore geometric configuration for fully eccentric annulus (Elgaddafi et al. 2021)

Elgaddafi et al. (2021) presented a series of equations to describe the parameters shown in Figure 3.3. For any pipe configuration, the following two equations can be used to calculate the wetted perimeter (S) and flow area (A_f):

$$S = S_i + S_o + S_b \quad \text{Eq 3.7}$$

$$A_f = A_o - A_i, \quad \text{Eq 3.8}$$

where S_i, S_o, and S_b are the wetted perimeters of the drill-pipe (inner part of the annulus), the wellbore (outer part of the annulus), and the solids bed, respectively, and A_o and A_i are the areas of the outer part of the annulus and inner part of the annulus (drill-pipe), respectively.

When $h < D_i$ the bed height is lower than the diameter of the drill-pipe (partially covered drill-pipe). In this case, the following expressions can be derived from the flow configuration to determine various geometrical parameters. In all these equations, R_i and R_o are the radii of the inner and outer diameter of the annulus, respectively, and H_{bed} is the bed height.

$$\theta_o = 2 \times \cos^{-1}\left(\frac{R_o - H_{bed}}{R_o}\right) \quad \text{Eq 3.9}$$

$$\theta_i = 2 \times \cos^{-1}\left(\frac{R_i - H_{bed}}{R_i}\right) \quad \text{Eq 3.10}$$

$$S_o = \theta_o * R_o \quad \text{Eq 3.11}$$

$$S_i = \theta_i * R_i \quad \text{Eq 3.12}$$

$$S_b = \left(2 * \sqrt{R_o^2 - (R_o - H_{bed})^2}\right) - \left(2 * \sqrt{R_i^2 - (R_i - H_{bed})^2}\right) \quad \text{Eq 3.13}$$

$$A_o = R_o^2\left(\frac{\theta_o}{2}\right) + (R_o - H_{bed})\sqrt{R_o^2 - (R_o - H_{bed})^2} \quad \text{Eq 3.14}$$

$$A_i = R_i^2\left(\frac{\theta_i}{2}\right) + (R_i - H_{bed})\sqrt{R_i^2 - (R_i - H_{bed})^2} \quad \text{Eq 3.15}$$

$$A_f = Ao - A_i \quad \text{Eq 3.16}$$

Where θ_o and θ_i are the inner and outer angles of the general wellbore geometry shown in Figure 3.3.

When $h > D_i$, the bed height is higher than the inner pipe (fully covered drill-pipe). In this case, the equations to determine the geometric parameters are:

$$\theta_o = 2 \times \cos^{-1}\left(\frac{R_o - H_{bed}}{R_o}\right) \quad \text{Eq 3.17}$$

$$S_o = \theta_o * R_o \quad \text{Eq 3.18}$$

$$S_i = 0 \quad \text{Eq 3.19}$$

$$S_b = 2 * \sqrt{R_o^2 - (R_o - H_{bed})^2} \quad \text{Eq 3.20}$$

$$A_o = R_o^2\left(\frac{\theta_o}{2}\right) + (R_o - H_{bed})\sqrt{R_o^2 - (R_o - H_{bed})^2} \quad \text{Eq 3.21}$$

$$A_i = 0 \quad \text{Eq 3.22}$$

$$A_f = Ao - A_i \quad \text{Eq 3.23}$$

When a stationary uniform solids bed is formed, the hydraulic diameter, D_{hy}, can be calculated as:

$$D_{hy} = \frac{4A_f}{S_o + S_i + S_b} \quad \text{Eq 3.24}$$

3.2 Hydraulic Models

Two approaches will be used in this study to compute the average bed shear stress, which is correlated to the pressure drop and the bed height in the annulus. The first approach is the traditional (or existing) hydraulic model (Clark and Bickham 1994; Cho et al. 2002; Ahmed et al. 2003, 2005; Li et al. 2007; Duan et al. 2009). The second (new) approach is developed by Eldaddafi et al. (2021) based on previous CFD studies (Tang et al. 2016; Rojas et al. 2017; Singh 2019; Singh et al. 2021).

3.2.1 Traditional Hydraulic Model

Several of the existing wellbore hydraulic models (Clark and Bickham 1994; Cho et al. 2002; Ahmed et al. 2003, 2005; Li et al. 2007; Duan et al. 2009) obtain the bed shear stress directly from the overall wall shear stress. The wall shear stress is calculated as:

$$\tau_w = f\frac{\rho_f U^2}{2}, \quad \text{Eq 3.25}$$

where f is the Fanning friction factor, U is the average fluid velocity, and ρ_f is the fluid density. For laminar flow ($Re_{gn} < 2100$), the Fanning friction factor is expressed as:

$$f = \frac{16}{Re_{gn}}, \quad \text{Eq 3.26}$$

where Re_{gn} is a general Reynolds number given by (Whitaker, *Theory and Applications of Drilling Fluid Hydraulics*.; Chen, "Cuttings Transport with Foam in Horizontal Concentric Annulus under Elevated Pressure and Temperature Conditions."):

$$\mathrm{Re_{gn}} = \frac{8\mathrm{U}^2\rho_\mathrm{f}}{\mathrm{K}\left(\frac{8\mathrm{U}}{\mathrm{D_{eff}}}\right)^\mathrm{n}}, \quad \text{Eq 3.27}$$

where K is the flow consistency index and n is the flow behavior index. The effective diameter shown in Eq 3.27 is defined as: $\mathrm{D_{eff}} = \mathrm{D_{hy}}/\mathrm{G}$, where $\mathrm{D_{hy}}$ is the hydraulic diameter. G is a dimensionless parameter, defined as:

$$\mathrm{G} = \frac{(3-\mathrm{Z})\mathrm{n}+1}{(4-\mathrm{Z})\mathrm{n}}\left(1+\frac{\mathrm{Z}}{2}\right), \quad \text{Eq 3.28}$$

where Z is a dimensionless parameter, defined as:

$$\mathrm{Z} = 1-(1-\mathrm{k}^Y)^{1/\mathrm{Y}} \quad \text{Eq 3.29}$$

where k is the diameter ratio ($\mathrm{k} = \mathrm{D}_i/\mathrm{D}_o$) and $Y = 0.37n^{-0.14}$.

For turbulent flows ($\mathrm{Re_{gn}} > 2100$), several implicit correlations (Dodge & Metzner, 1959; Colebrook et al. 1939) were developed to compute friction factors of Newtonian and non-Newtonian fluids. Enfis et al. (2013) introduced an explicit correlation for power-law fluids, and is a correlation is used in this study. Thus:

$$f = 0.0918 * \mathrm{n}^{-0.364} * \mathrm{Re_{gn}}^{(0.12\mathrm{Ln(n)}-0.27)} \quad \text{Eq 3.30}$$

Once the wall shear stress is calculated, regardless of the flow regime, the pressure drop can be calculated as:

$$\frac{\Delta P}{\Delta L} = \frac{4\tau_w}{D_{hy}} \quad \text{Eq 3.31}$$

3.2.2 New Hydraulic Model

The new hydraulic model (Elgaddafi et al. 2021) is different from the existing ones by considering the bed shear stress, which is different from the overall shear stress. To calculate the

bed shear stress, different formulations are used for fully buried pipe and partially buried pipe cases.

3.2.2.1 Fully buried pipe

The normalized bed shear stress is defined as the ratio of average bed shear stress to the overall wall shear stress. Under laminar flow conditions, for a fully buried inner pipe ($H_{bed} > D_i$), the normalized bed shear stress is determined as (Tang et al. 2016):

$$\frac{\tau_b}{\tau_w} = a_1 + b_1\left(\frac{H_{bed} - H}{2R_o}\right) + c_1\left(\frac{H_{bed} - H}{2R_o}\right)^2 + d_1\left(\frac{H_{bed} - H}{2R_o}\right)^3 \quad \text{Eq 3.32}$$

Where τ_b is the bed shear stress, H is the annular clearance ($H = R_o - R_i$). The empirical coefficients a_1 to d_1 are calculated from the diameter ratio as described in Table 3.1. In Eq 3.32, the overall wall shear stress is calculated as:

$$\tau_w = K\left(\frac{8U}{D^*_{eff}}\right)^n \quad \text{Eq 3.33}$$

D^*_{eff} is known as the modified effective diameter, and can be calculated using:

$$D^*_{eff} = 4A_f/(S_i + S_b + S_o) \quad \text{When } 0 \le H_{bed} \le 0.5x \quad \text{Eq 3.34a}$$

$$D^*_{eff} = S_i.H_{bed} + I_n \quad \text{When } 0.5x \le H_{bed} \le 1.5x \quad \text{Eq 3.34b}$$

$$D^*_{eff} = 1.07 \times 4A_f/(S_i + S_b + S_o) \quad \text{When } 1.5x \le H_{bed} \le D_h, \quad \text{Eq 3.34c}$$

where A_f, S_i, S_b, and S_o are computed from the geometric calculations shown in chapter 3.1. x is defined as the hydraulic radius of a concentric annulus with no cuttings bed, and it is calculated as $x = 0.5(D_o - D_i)$. I_n is an empirical coefficient determined by the following correlation (Tang et al. 2016):

$$I_n = D_{hy}(0.5x) - 0.5x.S_l, \quad \text{Eq 3.35}$$

where S_l is another empirical coefficient, calculated by:

$$S_l = \left[1.07D_{hy}(1.5x) - D_{hy}(0.5x)\right]/x \qquad \text{Eq 3.36}$$

Table 3.1. Empirical coefficient values to use in Eq 3.32

Empirical coefficient	Value
a_1	$0.85998 - 0.75366k + 0.40328\mathrm{k}^2$
b_1	$0.12922 + 1.6713k - 1.71512\mathrm{k}^2$
c_1	$-0.27887 - 4.01044k + 4.81040\mathrm{k}^2$
d_1	$2.20354 - 3.43634k + 1.20312\mathrm{k}^2$

Under turbulent flow conditions, the traditional hydraulic model, using frictional pressure loss to calculate the average bed shear stress, is applied. In fully buried pipe situations, the average bed shear stress computed from the frictional pressure loss provides the closest prediction to the actual bed shear stress.

3.2.2.2 Partially buried pipe

A partially buried pipe happens when the bed height is lower than the inner pipe diameter ($H_{bed}<D_i$). In this situation, the normalized bed shear stress depends on the flow regime. For laminar flows ($Re_k < 2100$), the normalized bed shear stress can be calculated using the following equation (Rojas et al. 2017):

$$\left(\frac{\tau_b}{\tau_w}\right)^n = \mathrm{A_1 H_b^{4.511}} + \mathrm{B_1 H_b^{2.51}} + \mathrm{C_1 H_b^{0.51}} + \mathrm{D_1 n}k^{0.51} + \mathrm{E_1(nH_b)^{1.431}} + \mathrm{F_1 n} + \mathrm{G_1} \qquad \text{Eq 3.39}$$

Where $\mathrm{H_b}$ is the dimensionless bed height ($H_b = H_{bed}/D_i$). Under turbulent flow conditions, the normalized bed shear stress can be calculated using the formula provided by Singh (2019):

$$\left(\frac{\tau_b}{\tau_w}\right)^n = \mathrm{A_2 H_b^{4.5}} + \mathrm{B_2 H_b^{2.5}} + \mathrm{C_2 H_b^{0.51}} + \mathrm{D_2 n}k^{0.51} + \mathrm{E_2(nH_b)^{1.4}} + \mathrm{F_2 n} + \mathrm{G_2} \qquad \text{Eq 3.40}$$

In Eqs 3.39 and 3.40, $A_1 - G_1$ and $A_2 - G_2$ are empirical coefficients for laminar and turbulent bed shear stress correlations, presented in Table 3.2. To determine the flow regime, the generalized Kozicki Reynolds number is expressed as Kozicki, Chou, and Tiu, "Non-Newtonian Flow in Ducts of Arbitrary Cross-Sectional Shape.":

$$\mathrm{Re_k} = \frac{\mathrm{D_{hy}^n U^{2-n} \rho_f}}{8^{n-1} \mathrm{K} \left(\frac{a}{n} + b\right)^n} \quad \text{Eq 3.41}$$

Table 3.2 Empirical coefficients for Equations 3.39 and 3.40

Empirical coefficient	Value	Empirical coefficient	Value
A_1	0.4668	A_2	0.4930
B_1	-0.7470	B_2	-.7909
C_1	0.8957	C_2	0.8590
D_1	-0.5166	D_2	-.5004
E_1	0.6366	E_2	0.4878
F_1	-0.4077	F_2	-.2851
G_1	0.5250	G_2	0.5559

The constants *a* and *b* are then calculated from the dimensionless bed height:

$$a = \lambda_0 H_b^3 + \lambda_1 H_b^2 + \lambda_2 H_b + \lambda_3 \quad \text{Eq 3.42}$$

$$b = b_0 H_b^3 + b_1 H_b^2 + b_2 H_b + b_3, \quad \text{Eq 3.43}$$

where λ_0, λ_1, λ_2, λ_3, b_0, b_1, b_2, and b_3 are dimensionless coefficients computed using the correlations provided in Table 3.3.

Table 3.3. Empirical coefficients for Eq 3.42 and 3.43 (Rojas et al. 2017)

$\lambda_0 = -6.2328k^2 + 4.1994k - 0.845$	$b_0 = -0.964k^2 + 5.425k - 1.321700$
$\lambda_1 = 9.152k^2 - 6.7796k + 1.10960$	$b_1 = -0.1792k^2 - 8.1756k + 2.0884$
$\lambda_2 = -3.236k^2 + 2.7778k - 0.0881$	$b_2 = 0.836k^2 + 3.4122k - 0.932500$
$\lambda_3 = 0.284k^2 - 0.4266k + 0.06684$	$b_3 = 0.2456k^2 - 0.2934k + 0.87610$

In this approach, the prediction of the bed shear stress depends on the calculation of the overall wall shear stress using the traditional approach (Eq 3.25). However, the fanning friction factor is now calculated from geometric parameters as (Rojas et al. 2017).

$$f = \frac{\left(\frac{a}{n}+b\right)^{n}\left(2^{3n+1}\right)}{Re}, \qquad \text{Eq 3.44}$$

where the Reynolds number (Re) is calculated from:

$$Re = \frac{\rho_f U^{2-n} D_{hy}^{n}}{K} \qquad \text{Eq 3.45}$$

The previous equations are valid for laminar flow conditions. Under turbulent flow, the fanning friction factor is calculated using Eq 3.30. The coefficients *a* and *b* used in Eq 3.44 are the same as the ones presented in Eqs 3.42 and 3.43. The numerical procedures to calculate the bed shear stress and the predicted bed height are described in the mechanistic model developed by Elgaddafi et al (2021).

Chapter 4: Experimental Study

The purpose of this chapter is to describe the experiment carried out in this study, starting with the test setup where the experiments were performed, followed by a description of the test procedure, and finalizing with the descriptions of the materials utilized.

4.1 Facility Setup

A schematic of the flow loop utilized to carry out the hole cleaning and hydraulic tests is shown in Fig 4.1. The main components of the setup are as follows:

- The annular and pipe sections, where the experimental investigation were carried out.
- The mixing tank, where the polymers and fiber were mixed with water to prepare test fluids; it also serves as a re-circulation tank.
- The solids injection tank, where the proppant was introduced into the system to build the bed in the horizontal test section.
- Two hydrocyclones, which were utilized to separate the solids from the cleaning fluid.
- The solids collection tank, where the solids were collected after being separated from the cleaning fluid using the hydrocyclones.
- Centrifugal pumps, which were used to circulate the cleaning fluid at different flowrates.
- Measuring instrumentation such as Coriolis flowmeters, differential pressure transducers, and transmitters for measuring pressure loss, static pressure, and temperature.

- Data acquisition (DAQ) system, which displays and records several experimental parameters.

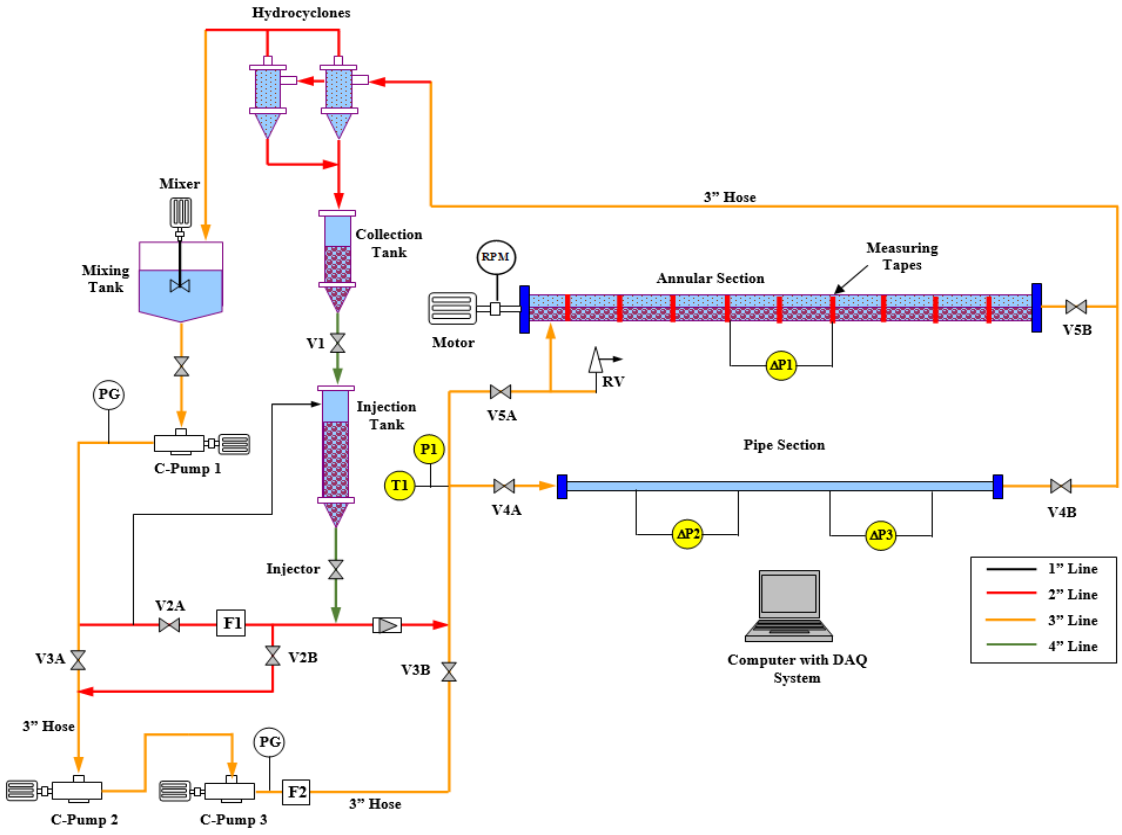

Figure 4.1 Schematic of the experimental setup (Mendez et al. 2022)

4.2 Test procedure

The testing procedure can be divided into three major steps that summarize the experiment: preparation of the cleaning fluid, formation of the solids bed in the annular test section, and bed erosion.

4.2.1 Fluid preparation

The base fluid was prepared by mixing water, polyanionic cellulose (PAC), and xanthan gum (XG). The concentrations of PAC and XG were 1.75 and 2.12 g/L, respectively. The fibrous fluid was prepared by adding fiber to the base fluid at a concentration of 0.4 g/L. The flow loop

volume is estimated to determine the amount of PAC, XG, and fiber needed to prepare a given volume of base fluid. Table 4.1 shows the worksheets used to approximate volume of the flow loop.

Table 4.1 Approximate volume of the flow loop

Loop Element	Length (ft)	Vol (gal)
Fittings		40.00
3" Pipe/hose	150	55.08
Test Section	50	39.49
C-Pumps		15
2" pipe/hose	20	3.26
Mixing Tank		80.00
Total volume		**232.84**

The volume of test fluid in the mixing tank can be adjusted. However, after several tests, it was determined that 80 gallons (302.83 L) of test fluid in the mixing tank leads to an optimum mixing efficiency with the polymers.

Figure 4.2 Mixing tank of the flow loop

Once the fluids volume in the tank is known, the total flow loop volume is calculated and used to determine the mass of PAC and XG needed to achieve the desired concentration in the test fluid. The viscosifying polymers were placed inside buckets and they were slowly added into the tank while a high-speed agitator mixed the polymers with water placed in the tank. It is important to mention that the flow loop was kept running at a flowrate of 200 GPM (757.08 L/m) during the mixing of the testing fluid. After 30 minutes, the agitator and fluid circulation were stopped, and the fluid is left overnight to hydrate. The hydration of the fluid plays a major role in the experiment; without hydration, the rheological properties will not be stable enough to carry out the test and the fiber do not form a stable network. After the proper hydration, the rheological properties (consistency index, fluid behavior index, yield stress, and gel strength) were measured using a rotational viscometer.

Figure 4.3 Scale and bucket utilized to measure the polymers and fiber

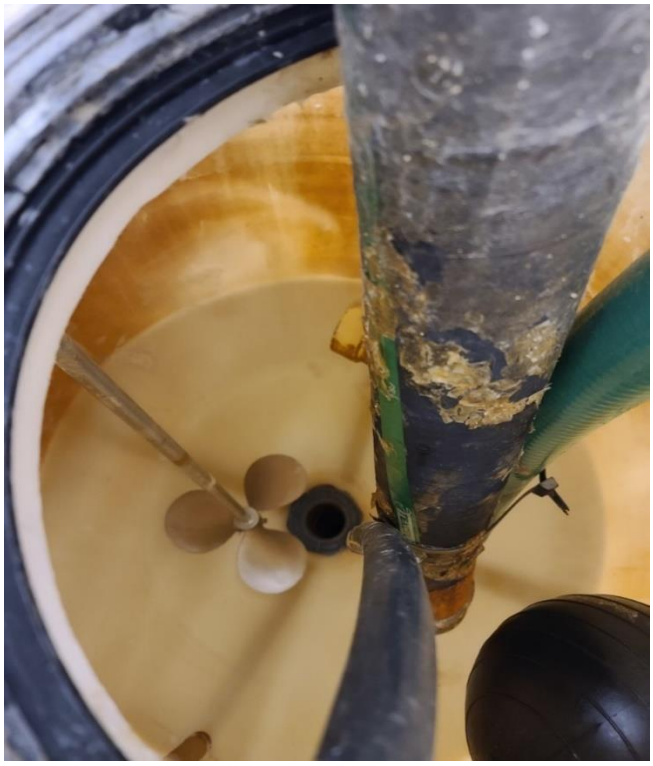

Figure 4.4 Top view of the tank showing the agitator

4.2.2 Formation of a solids bed in the horizontal annular section

After the testing fluid was prepared and ready for testing, a solids bed was formed in the annular section to perform the erosion test. The steps to form a solids bed in the test section were as follows:

1. Close the bypass valves (V_{4A} and V_{4B} in Fig 4.1) and open the inlet and outlet valves of the annular test section (V_{5A} and V_{5B} in Fig 4.1).
2. Only one of the three pumps was necessary to inject the solids, so valves (V_{3A}, V_{3B}, and V_{2B} in Fig 4.1) were kept close as well.
3. The flow rate was set and maintained at 30 GPM.
4. After the flowrate was stabilized, the injection of solids was started by opening the injection valve (shown as “Injector” in Fig 4.1). A mixture of test fluids and solid

started flowing, and the solids begun accumulating in the annular test section due to the reduced annular velocity.

5. The return fluid kept flowing with some undeposited solids that were recovered by the hydrocyclones and then accumulated in the collection tank. After some time (usually between 10 to 20 minutes), a thick uniform bed was formed, then circulation was stopped, and the injection valve was closed.

Figure 4.5 Solids depositing on the horizontal annular test section

4.2.3 Bed Erosion

Once a stationary thick uniform bed was formed, the erosion process (cleaning process using either the base test fluid or the fibrous test fluid) started. The test was started at the lowest flowrate (35 GPM), which was kept at constant rate for 45 minutes; after 45 minutes (sometimes even at 30 minutes) the solids bed height reached its equilibrium value and the pressure loss across the horizontal test section was approximately stable.

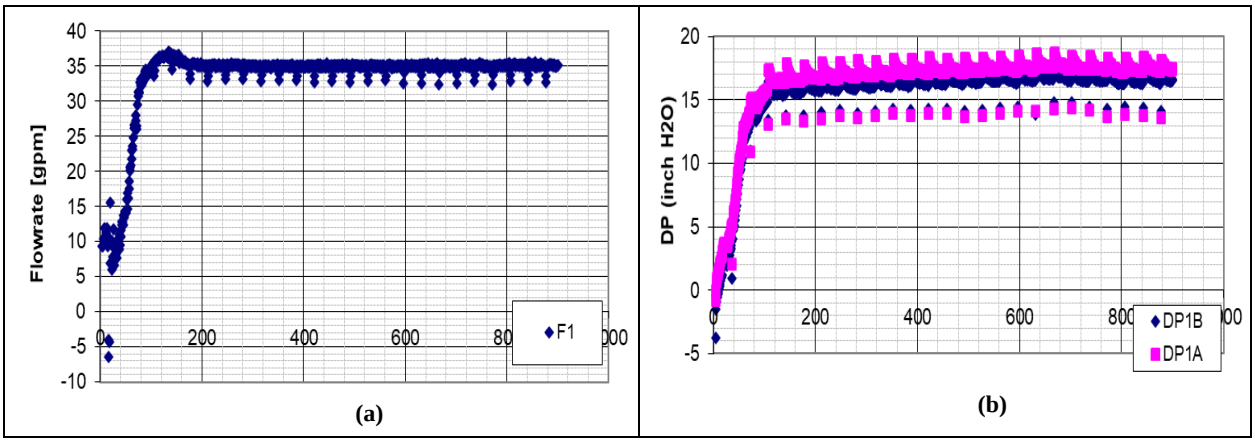

Figure 4.6 a) Stabilized flow rate of the test **b)** Stabilized pressure of the test

The flow rate was stopped when equilibrium was reached. Then, the bed height was measured along the right and left sides of the horizontal test section, as shown in Figure 4.7.

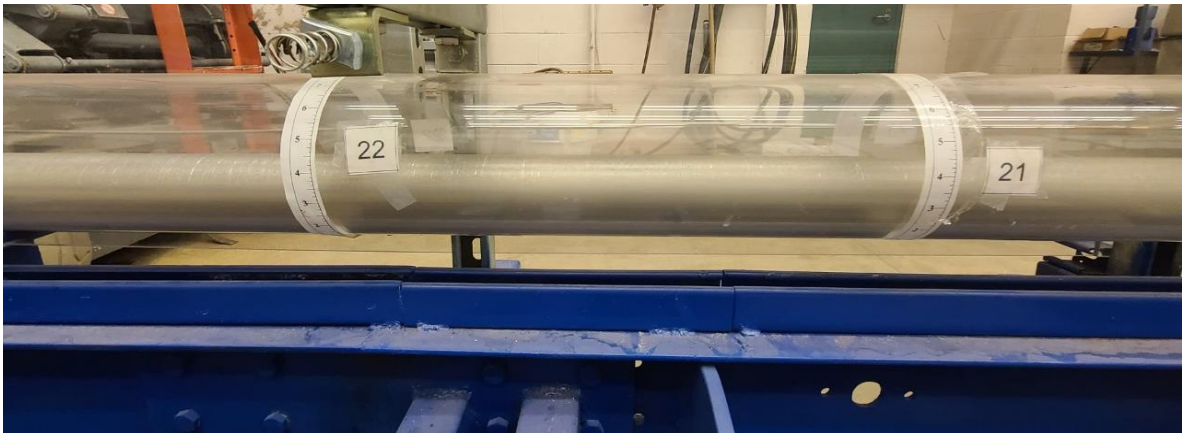

Figure 4.7 Bed height measuring points of the horizontal annular test section

After measuring and recording the bed height, the flow rate was increased and maintained until another equilibrium condition was achieved. After that, new bed height measurements were taken, and the process was repeated at a higher flow rate. Step by step, the process continued until the entire bed was cleaned. Measurements of bed height and flowrate are presented in Chapter 5. During the experiment, all test parameters, including flow rate, average bed height, and pressure loss across the annulus, were monitored and recorded using the data acquisition system. The rheology of the fluids was measured at the end of the experiment.

Figure 4.8 OFITE model 900 rotational viscometer

4.3 Properties of the Test Materials

The materials utilized in the experiment are base fluid, natural sand used to represent cuttings, and the fiber added to the base fluid to create the fibrous fluid.

4.3.1 Base Fluid

The most relevant base fluid property is it is rheology which was measured after it was prepared and properly hydrated. A rotational viscometer was used to measure the resulting shear stress of the fluid at several shear rates. Table 4.2 shows the values obtained from the rotational viscometer.

Table 4.2 Rheology of base fluid

Hydration time = 23 hours			**T=74.4°F**
Shear Rate	**Shear stress (Pa)**	**Shear stress (lbfS^2/100 ft2)**	**Apparent viscosity (cp)**
1.7	0.9	1.9	519.4
3.4	1.1	2.3	326.3
5.11	1.3	2.7	259.4
10.21	1.8	3.8	171.5
17.02	2.2	4.6	127.4
34.05	2.9	6.1	84.9
51.07	3.4	7.1	67.0
102.14	4.6	9.6	45.1
170.23	5.8	12.1	34.3
340.46	8.2	17.1	24.2
510.69	10.1	21.1	19.7
1021.38	14.1	29.4	13.8

The shear rate shown in Table 4.2 is obtained by assuming Newtonian fluid. However, the base fluid is non-Newtonian fluid as indicated by the decreasing apparent viscosity with shear rate; therefore, the shear rate needs to be corrected. Bourgoyne Jr et al. (1991) presented a formula to calculate the corrected shear rate for power law fluid. Thus:

$$\dot{\gamma} = 0.2094\mathrm{N}\frac{\frac{1}{r_1^{2/n}}}{n\left(\frac{1}{r_1^{\frac{2}{n}}} - \frac{1}{r_2^{\frac{2}{n}}}\right)} \qquad \text{Eq 4.1}$$

where N is the revolutions per minute (RPM) of the rotational viscometer, $r_1$and r_2 are the radius of the bob and the rotor of the rotational viscometer, respectively, and n is the flow behavior index of the power law cleaning fluid. Table 4.3 shows the final result of the rotational viscometer test after adjusting the shear rate.

Table 4.3 Results of the rotational viscometer test adjusting the shear rate

Hydration time = 23 hours			T=74.4°F
Shear Rate	**Shear stress (Pa)**	**Shear stress (lbfS^2/100 ft2)**	**Apparent viscosity (cp)**
1.87	0.9	1.9	519.4
3.73	1.1	2.3	326.3
5.60	1.3	2.7	259.4
11.20	1.8	3.8	171.5
18.67	2.2	4.6	127.4
37.33	2.9	6.1	84.9
56.00	3.4	7.1	67.0
112.00	4.6	9.6	45.1
186.66	5.8	12.1	34.3
373.32	8.2	17.1	24.2
559.98	10.1	21.1	19.7
1119.96	14.1	29.4	13.8

Figure 4.9 shows a log-log plot of the shear stress versus the shear rate, which we can use to obtain the flow behavior index and the flow consistency index of the fluid.

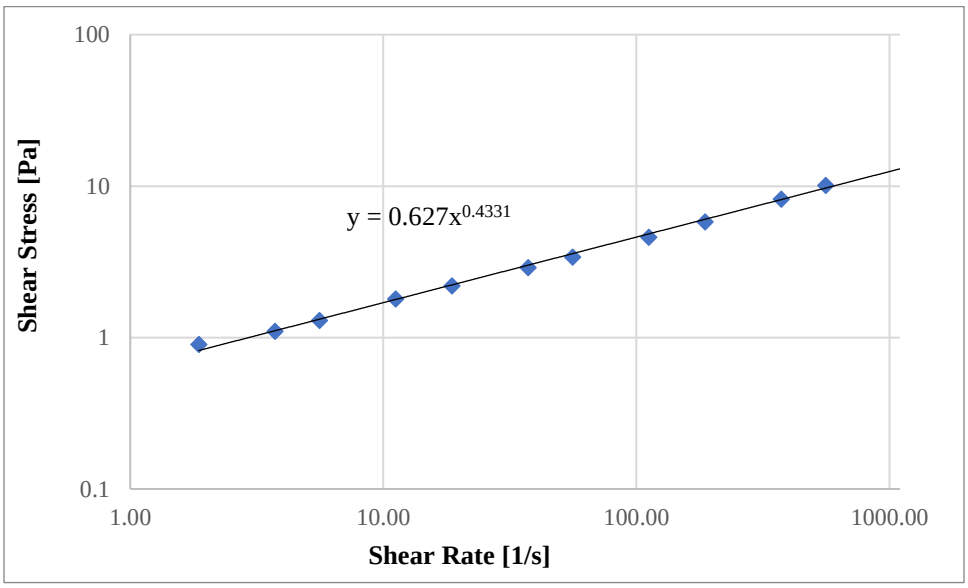

Figure 4.9 Shear Stress vs Shear Rate plot of cleaning fluid prepared in the lab

Applying a power law regression, we can obtain a formula in which the coefficient of "x" is the fluid consistency index and the exponent of "x" is the fluid behavior index, which is

dimensionless. A rotational viscometer test was conducted after each experiment in order to verify the rheological properties of the fluid is within a range of 10% from the ones measured at the lab.

4.3.2 Sand properties

The properties of solids (sand) play a very important role in the cleaning process. The properties of the sand relevant for this study are the grain size distribution, bulk density, and angle of repose. The grain size distribution was determined using a grain size analyzer, Table 4.4 shows a summary of the data obtained in the experiment.

Table 4.4 Grain size distribution of the proppant

Particle size [µm]	**%**	**Particle size [µm]**	**%**
449.67	0.16	948.34	10.36
493.63	0.15	1041.05	16.73
541.89	0.11	1142.83	20.15
594.87	0.27	1254.55	18.18
653.03	0.55	1377.2	12.34
716.87	0.86	1511.84	6.74
786.95	1.83	1659.64	3.83
863.88	4.77	1821.89	2.98
Mean [µm]	1246.18	**SD**	250.51
Median [µm]	1221.65	**CV**	20.1

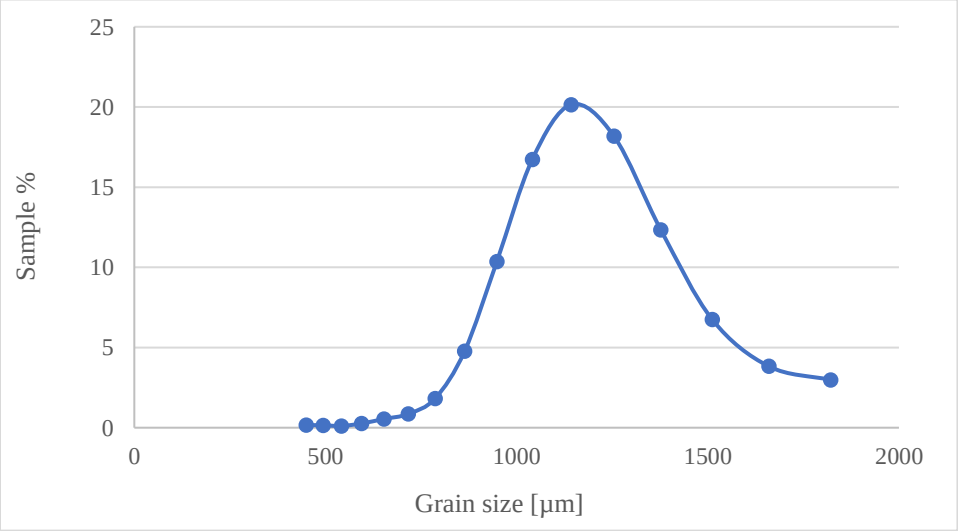

Figure 4.10 Distribution of the grain sizes of the sand

The particle size plot shown in Figure 4.10, indicates a normal distribution with a mean value very close to the median. The grain size to be used in the calculations is the average grain size of 1246.18 µm. The bulk density is determined in the lab using a scale and a volumetric flask. After several tests, the average bulk density is found to be 2.19 g/ml.

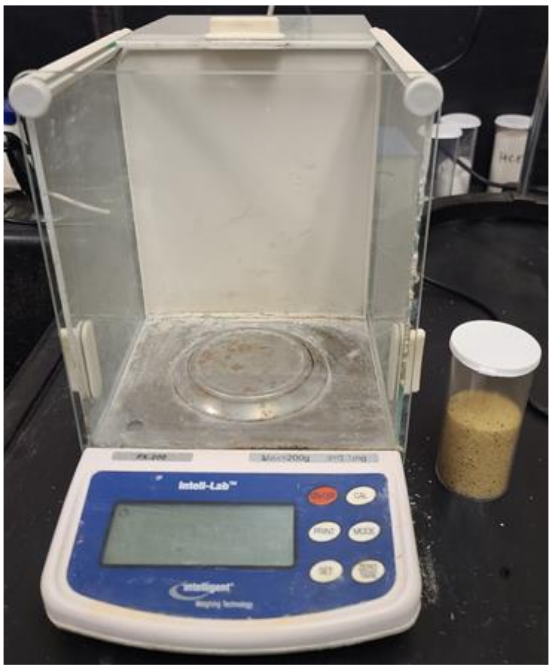

Figure 4.11 Scale and volumetric flask

Another important sand parameter is the angle of repose, which is the highest angle at which a pile of sand remains without slumping. The angle of repose is an indirect measure of the friction force between the sand particles. Figure 4.12 shows a schematic of the angle of repose for a pile of sand:

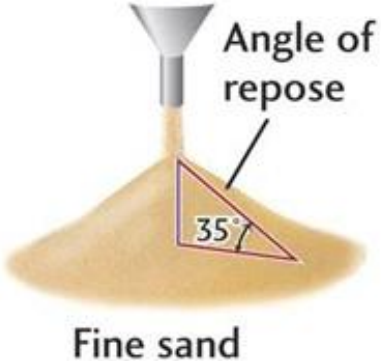

Figure 4.12 Angle of repose (adopted from knowledge of pharma blog)

For the present study, the angle of repose was measured for the wet sand, which is representative of the angle of the pile of sand underwater. After several measurements, the average angle of repose was found to be 35°.

4.3.3 Fiber properties

The fiber utilized to create the fibrous fluid is known as FORTA super sweep® fiber, manufactured by FORTA drilling products. It is a white odorless polypropylene fiber with a specific gravity of approximately 1.0. The fiber is an inert material. So, it does not react with the polymeric base fluid. The fiber particles have an average length of 0.5 inches and diameter of 100 micrometers.

Chapter 5: Experimental Results

This chapter covers the results obtained from the tests performed in the laboratory. The bed height calculations to evaluate the cleaning performance and the pressure drop of the horizontal section are presented for the base and fibrous cleaning fluids, with and without rotation of the drill pipe. The input parameters of the control system are flowrate, varied from 35 to 195 GPM, and inner drill pipe rotation velocity, set at 0, 50, 100, and 150 RPM.

For all the experiments, the average bed height is calculated from the observations taken at measuring points shown in Figure 4.7. There are 29 measuring points on the left and the right sides of the annulus. Each bed perimeter is recorded and used to calculate the average height of the annulus covered by the bed. Table 5.1 shows a sample of the readings for the first 5 stations after a test with fibrous fluid at a flowrate of 35 gpm.

Table 5.1 Sample of recorded bed perimeters

Station Number	**1**	**2**	**3**	**4**	**5**
Bed Height - Left (in)	4 3/4	5 1/2	5 7/8	5 7/8	6
Bed Right - Right (in)	4 3/4	5 1/2	5 1/2	5 3/4	5 3/4

At the end of each experiment, a total of 29 bed perimeter measurements were collected from both sides of the annulus. The measurements are then averaged to obtain mean bed perimeters for the left and the right side of the annulus. Once the average bed perimeter of each side is computed, the following equation, which is based on annular geometry, is utilized to calculate the average equilibrium bed height of the experiment.

$$H_{bed} = \frac{1}{2} D_o * \left(\cos\left(\pi - \frac{H_{bed-right} + H_{bed-left}}{D_o} \right) + 1 \right) - 0.25 \qquad \text{Eq 5.1}$$

where D_o is the inner diameter of the acrylic horizontal annulus, $H_{bed-right}$ and $H_{bed-left}$ are the average of the measurements from the right and left sides of the annulus. The dimensionless bed height can be defined as the bed height divided by the inner diameter of the annulus.

5.1 Water Test Results

The base and fibrous cleaning fluids are both water-based muds. Initially, tests were carried out with only water to serve as a basis for the performance evaluation of the fluids. The results obtained from the water tests are shown in Table 5.2.

Table 5.2 Water test results

Water tests (0 RPM)		
Q [GPM]	H_{bed} [in]	DP [inH_2O]
Initial	4.32	N/A
40	3.37	2.52
75	1.17	2.25
115	0	2.95
Water tests (50 RPM)		
Q [GPM]	H_{bed} [in]	DP [inH_2O]
Initial	4.32	N/A
40	0.93	1.26
75	0	1.62
Water tests (100 RPM)		
Q [GPM]	H_{bed} [in]	DP [inH_2O]
Initial	4.32	N/A
35	0.14	0.75
75	0	1.55
Water tests (150 RPM)		
Q [GPM]	H_{bed} [in]	DP [inH_2O]
Initial	4.32	N/A
35	0	0.95

It is essential to notice the effect of the inner pipe rotation on the cleaning efficiency of the fluid. With the increase in the rotation speed, more solids were removed by circulating water. The best way to interpret the results is by introducing the concept of bed coverage, which is defined as

the average cross-sectional area of the bed divided by the total cross-sectional area of the annulus. The bed coverage can be calculated from the wellbore geometry presented in Chapter 3.1. Figure 5.1 shows the bed coverage plot of the tests conducted with water without pipe rotation, illustrating the changes in the cleaning efficiency of water. It can be seen that a significant part of the solids bed was cleaned at 75 GPM.

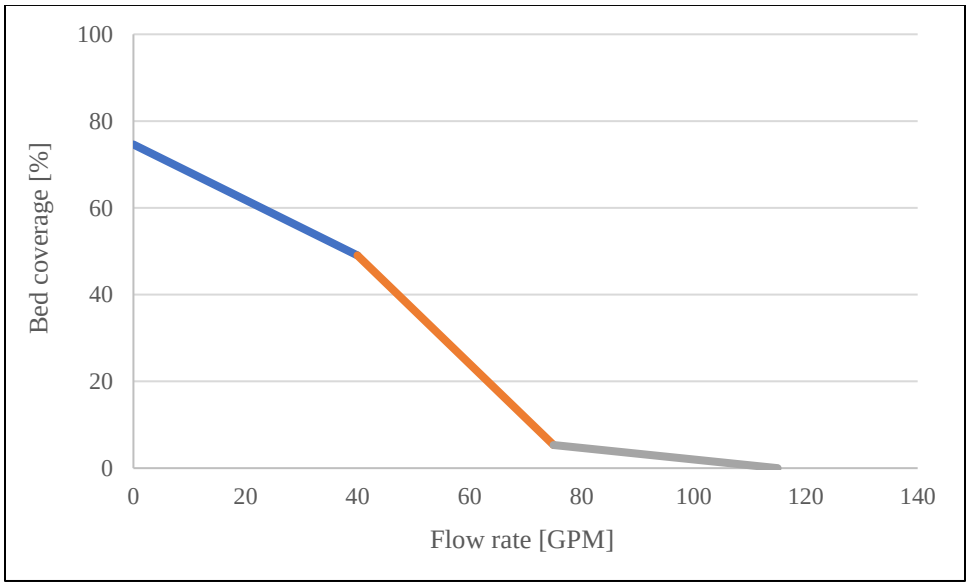

Figure 5.1 Water test cleaning efficiency plot at 0 RPM drill pipe rotation

Figure 5.2 shows the cleaning efficiency plot for the tests with water and varying drill pipe rotation speeds. As mentioned before, rotating the inner pipe improves the removal of the sand particles, increasing the cleaning efficiency of the water. As a result, a smaller flowrate is enough to clean thick solids beds formed in the horizontal annulus regardless of the rotation speed. Therefore, the effect of increasing the rotational speed from 50 to 150 RPM on hole cleaning efficiency is negligible.

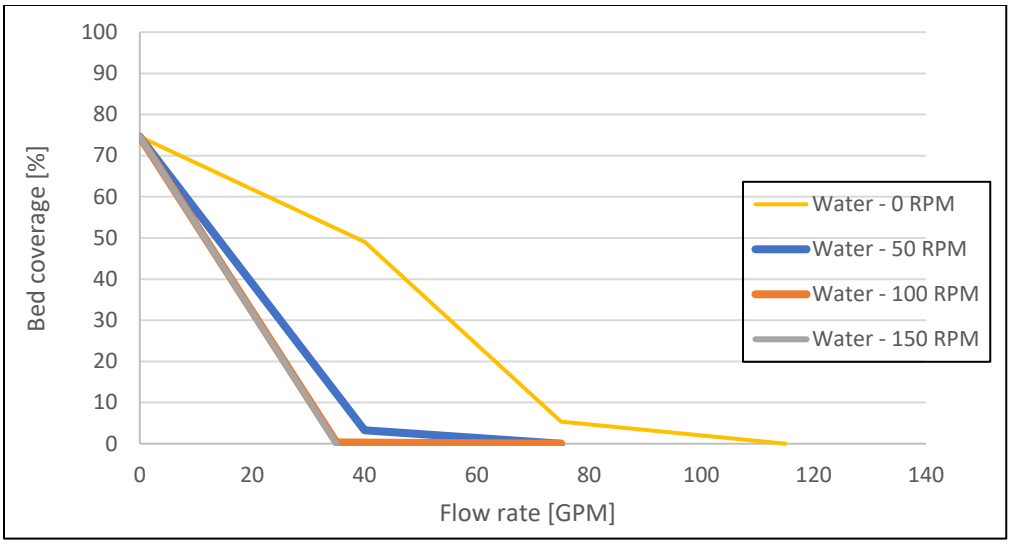

Figure 5.2 Water tests cleaning efficiency comparison for varying pipe rotations

The pressure drop is another key parameter that needs to be considered in the hole cleaning analysis. The relevance of this parameter is mainly due to the strong relationship between the bed height and the hydraulic resistance of the annulus and its effect on the downhole pressure. Therefore, for each test, the data acquisition system recorded flow rate and the corresponding pressure drop with time, as shown in Figure 5.3 for the case of 40 gpm flow rate and no pipe rotation.

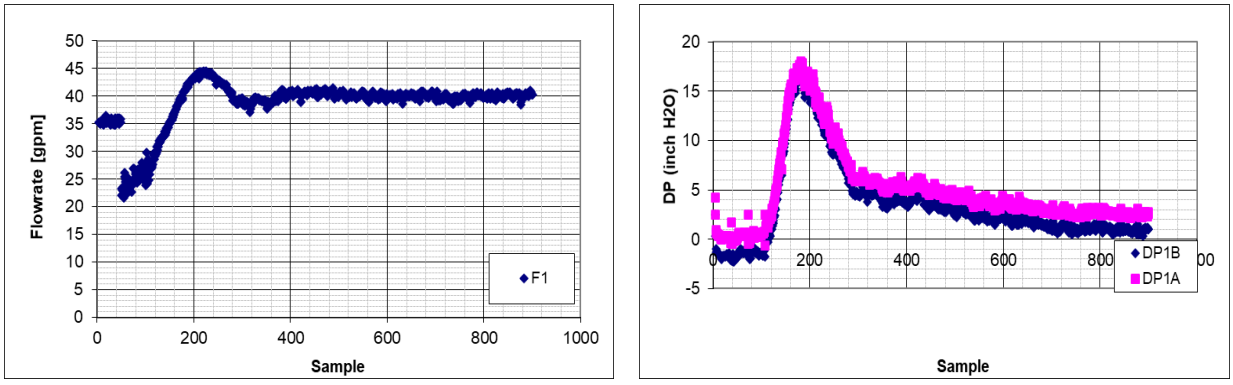

a) Stabilized flowrate (40 GPM) @0 RPM **b) Pressure during the test at 40 GPM @0 RPM**

Figure 5.3 Sample of flowrate and pressure drop plots with time for a water test

The critical part of each experiment (equilibrium or steady-state condition) happens when the bed becomes stable at the desired flow conditions. Under equilibrium conditions, the bed

erosion stops, and the pressure drop becomes stable with minimal changes with time. When the pressure drop stabilizes, the test is considered under equilibrium conditions, and the bed height measurements are taken. Then, the flow rate is increased for the next test.

Besides the pressure loss measurements and the cleaning efficiency plots, another way to interpret the experimental results is through the bed profile that shows the bed heights at various measuring stations of the annulus. The created plot shows the non-uniformity of the bed height along the annulus caused by the development of dunes and ripples that are caused by the various transport mechanisms involved in the cleaning process such as rolling and saltation of the particles on the bed surface. A sample of a bed profile is shown in Figure 5.4 for a water test with 40 gpm flowrate and no pipe rotation.

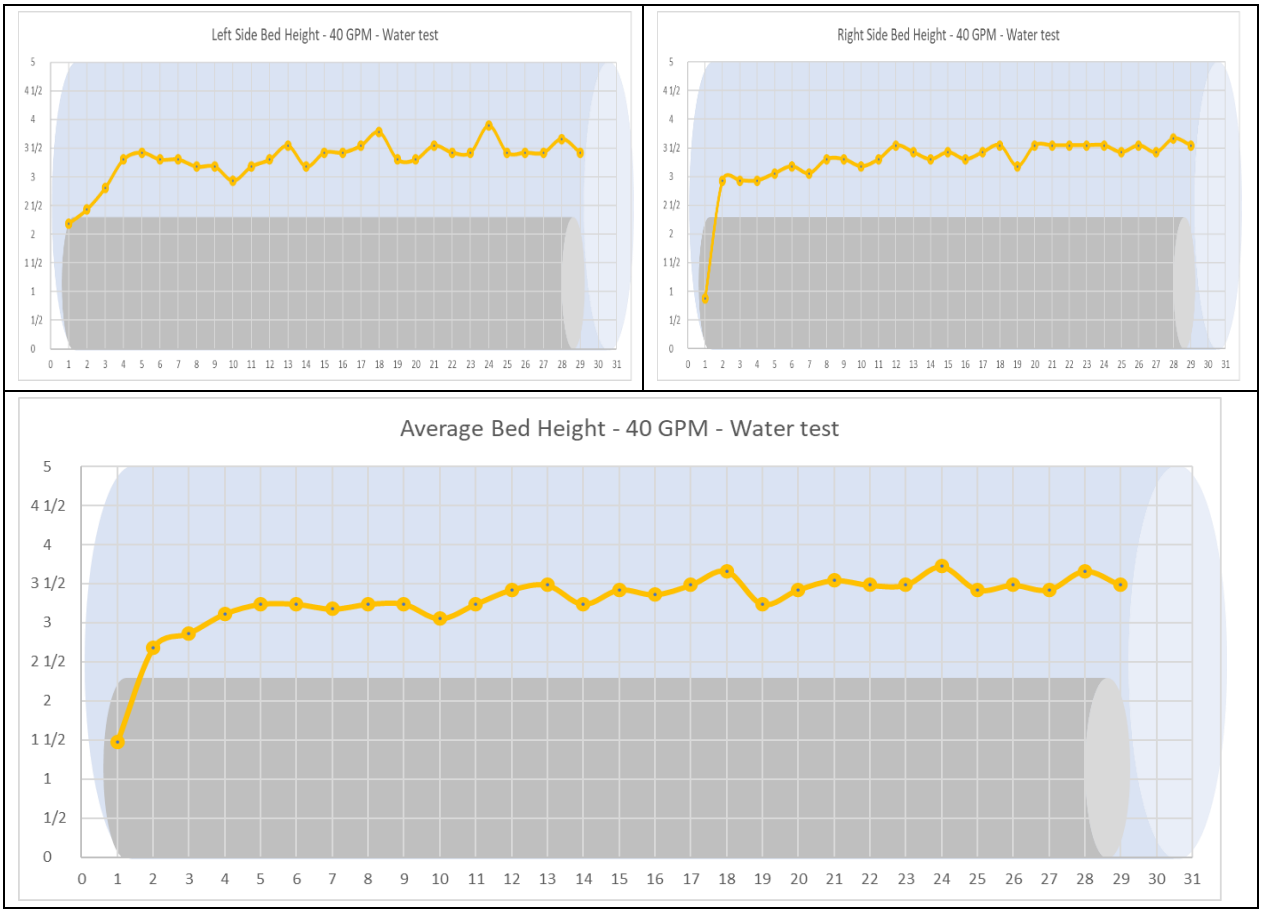

Figure 5.4 Left-side, right-side, and average bed profiles with water (40 GPM, 0 RPM)

Examining the bed profile plots, the shape of the bed in the horizontal annulus can be seen. As discussed in the modeling chapter, whether the bed is higher or lower than the top of the inner pipe is a critical parameter. In addition, the non-uniformity of the bed profile across the horizontal section is an essential factor. In the case of the water tests, we can notice some waving behavior due to the cleaning process's transport mechanisms that involves the formation and movement of dunes and ripples along the axial direction of the annulus. A complete report of the pressure drop and the bed profile for each water test is shown in the appendix section.

5.2 Base Cleaning Fluid Test Results

The base fluid (polymer-based fluid without fiber) was prepared 24 hours prior to each experiment. The rheological characterization was done following the procedure discussed in Section 4.3.1. The results obtained using the data from the viscometer are shown in Table 5.3.

Table 5.3 Flow consistency index and flow behavior index for base cleaning fluid

Test	**n**	**K** $[\boldsymbol{Pa} * \boldsymbol{s^n}]$
0 RPM	0.41	0.65
50 RPM	0.42	0.70
100 RPM	0.42	0.70
150 RPM	0.42	0.70

The rheological parameters n and K were kept within a 10% range from the measurement of the laboratory sample to keep the consistency between the experiments. The results obtained from the base cleaning fluid experiments are shown in Table 5.4.

Table 5.4 Base cleaning fluid test results

Base fluid test 0 RPM			**Base fluid test 50 RPM**		
Q [GPM]	H_{bed} [in]	DP [inH_2O]	Q [GPM]	H_{bed} [in]	DP [inH_2O]
Initial	4.32	N/A	Initial	4.32	N/A
35	4.23	22.84	10	2.49	9.68
75	3.60	14.34	35	1.61	6.58
115	2.82	11.43	75	0.25	7.00
155	2.42	7.11			
195	2.41	11.77			
Base fluid test 100 RPM			**Base fluid test 150 RPM**		
Q [GPM]	H_{bed} [in]	DP [inH_2O]	Q [GPM]	H_{bed} [in]	DP [inH_2O]
Initial	4.32	N/A	Initial	4.32	N/A
10	0.24	3.09	10	0.00	2.48
35	0.09	5.11			

Similar to the bed removal experiment with water, higher cleaning efficiencies were observed with inner pipe rotation. This demonstrates that the efficiency improvement with rotation remains consistent regardless of the fluid type used. Figure 5.5 shows the cleaning efficiency plot for the base fluid.

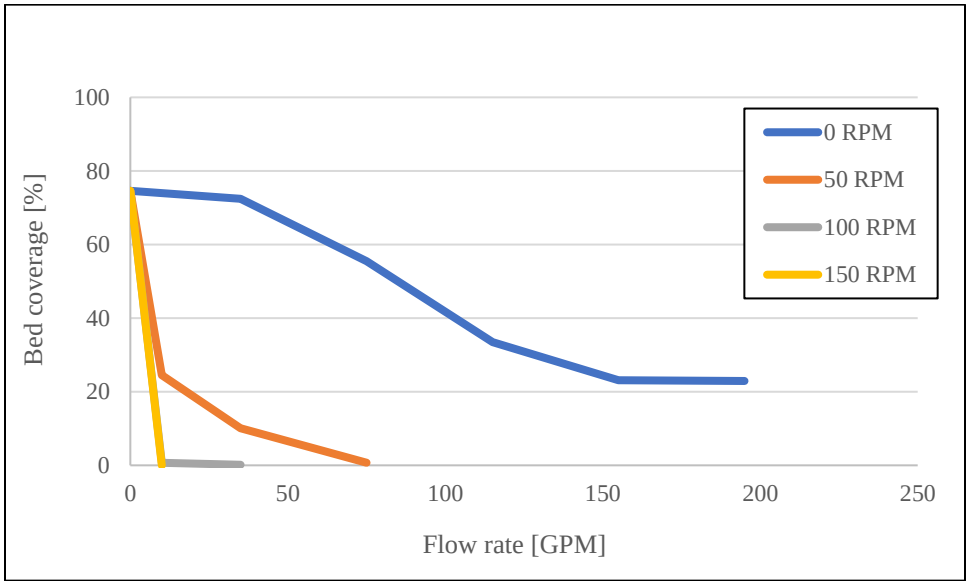

Figure 5.5 Base fluid test cleaning efficiency plot

There are situations in the field where it is impossible to utilize rotation to prevent the settling of the particles. This condition is the case the analysis from the tests without rotation

becomes essential. A comparison of the cleaning efficiencies of the water and base fluid without rotation is shown in Figure 5.6. It is apparent from the plot that most of the bed removal occurs between 35 and 115 GPM (the region of the plot with the higher slopes). Water has a better cleaning performance than the base fluid in the horizontal annulus due to the flow turbulence and its unique velocity profile. However, as discussed in Chapter 2, its weak performance in carrying the cuttings in the vertical section of the well makes it a wrong choice as a cleaning fluid. On the other hand, the base fluid is viscous fluid with a higher carrying capacity than water in the vertical section.

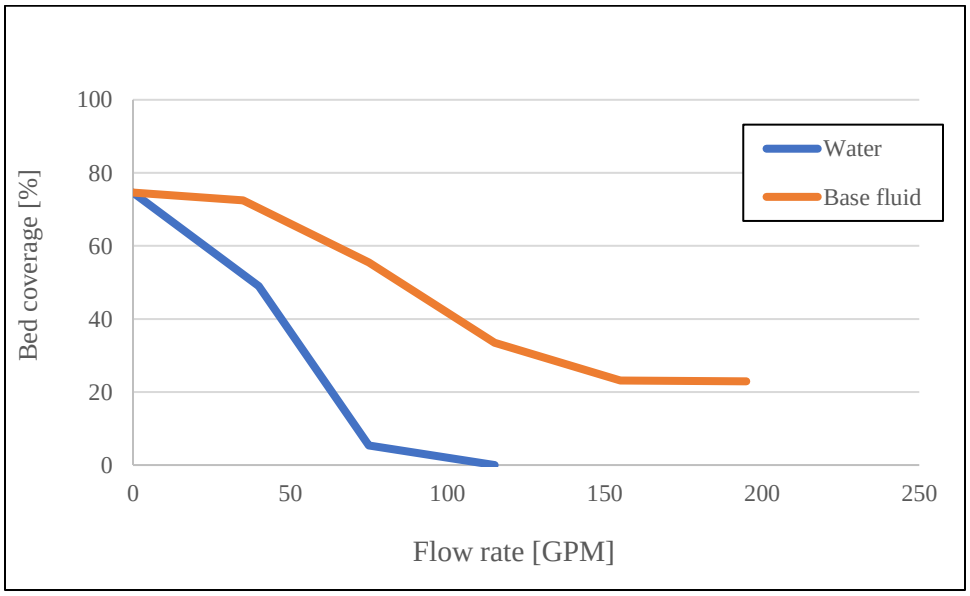

Figure 5.6 Cleaning efficiency comparison between base fluid and water

A sample of the bed profile for the base fluid test without rotation is shown in Figure 5.7. At 35 GPM, it is evident that the bed profile is more uniform than the one observed in the water test (Figure 5.4). This is due to the laminar nature of the flow at this flowrate. A complete report of the pressure drop and bed profile for all of the base fluid tests is shown in the appendix.

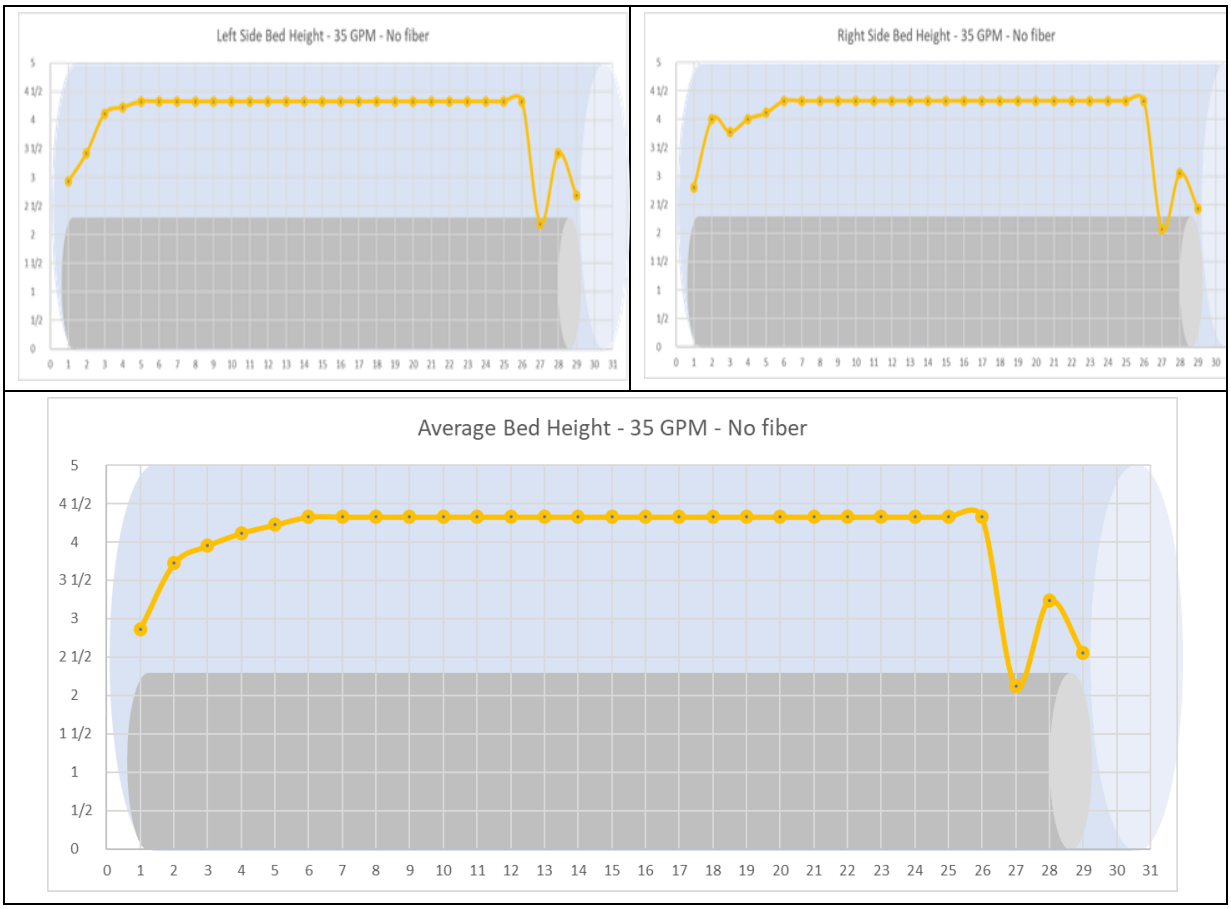

Figure 5.7 Left-side, right-side, and average bed profiles with base fluid (35 GPM, 0 RPM)

5.3 Fibrous Fluid Test Results

The fibrous fluid consists of the base cleaning fluid and fiber at a concentration of 0.14 [lb/bbl]. The fiber was added right after preparing the base fluid. After the fiber addition, the fluid was left to hydrate for 24 hours. The results obtained from the rheometer are shown in Table 5.5. Fibrous fluid with concentration of 0.28 [lb/bbl] was also tested; however, the tests were not completed due to the plugging of hydrocyclones and solids injection line.

Table 5.5 Flow consistency index and flow behavior index for fibrous cleaning fluid

Test	**n**	**K** $[Pa * s^n]$
0 RPM	0.42	0.70
50 RPM	0.41	0.70
100 RPM	0.40	0.70
150 RPM	0.40	0.70

The rheological parameters n and K were kept within a 10% range from the measurement of the laboratory sample to keep consistency between the experiments. It is important to mention that at this concentration the fiber does not have a noticeable effect on the rheological parameters. The minor differences with the results of the base cleaning fluid could be attributed to the measurement uncertainty. The results obtained from the fibrous cleaning fluid experiments are shown in Table 5.6.

Table 5.6 Fibrous cleaning fluid test results

Fibrous fluid test - 0 RPM		
Q [GPM]	H_{bed} [in]	DP [inH_2O]
Initial	4.32	N/A
35	3.98	20.22
65	3.65	18.94
115	1.25	16.29
155	0.85	14.08
195	0.70	15.03
Fibrous fluid test - 50 RPM		
Q [GPM]	H_{bed} [in]	DP [inH_2O]
Initial	4.32	N/A
35	2.83	12.79
75	1.32	8.95
115	0.15	9.09
155	0.00	7.53
Fibrous fluid test - 100 RPM		
Q [GPM]	H_{bed} [in]	DP [inH_2O]
Initial	4.32	N/A
35	1.95	6.77
75	0.01	6.40

Even though the fiber does not change the viscous properties of the fluid, it is evident that the cleaning efficiency is significantly improved. The cleaning efficiency plot of the fibrous fluid with varying pipe rotations is shown in Figure 5.8. The presence of fiber has a great impact on the performance of the fluid without rotation. The bed is almost fully removed at 115 GPM. The extra

drag force created by the fiber network in the fluid hindered the settling of the cuttings in the low viscosity fluid and subsequently helped the transportation of the particles.

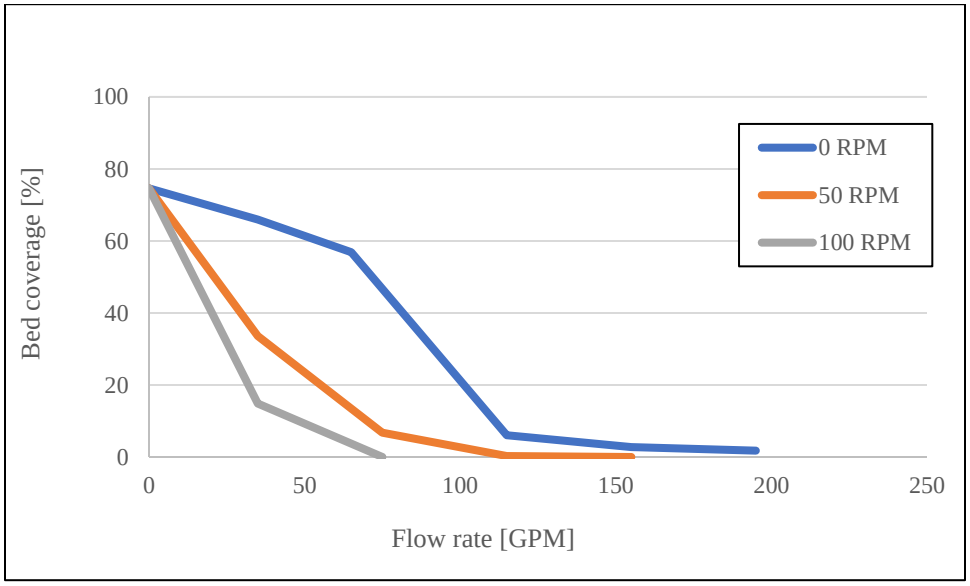

Figure 5.8 Fibrous fluid cleaning efficiency plot

A comparison between the base and fibrous fluid cleaning efficiencies without the pipe rotation is shown in Figure 5.9. At low flowrates, the cleaning efficiencies of the base and fibrous fluids were similar. However, the effect of the fiber became evident at 115 GPM, causing an enormous improvement in the bed removal. The objective of the experiments is to find a fluid that has a similar cleaning efficiency as water in the horizontal section, with a better performance in solid transportation in the vertical section of the wellbore. The fibrous fluid accomplishes both tasks satisfactorily.

Figure 5.10 presents a sample of bed profile in the annulus with the fibrous fluid without pipe rotation. One of the main effects of the fiber is the formation of non-uniform bed profiles such as dunes and ripples, as seen in Figure 5.10. The modeling chapter will discuss the hydraulic effects caused by the dunes and ripples. Complete sets of pressure drop and bed profile measurements for all fibrous fluid tests are shown in the appendix.

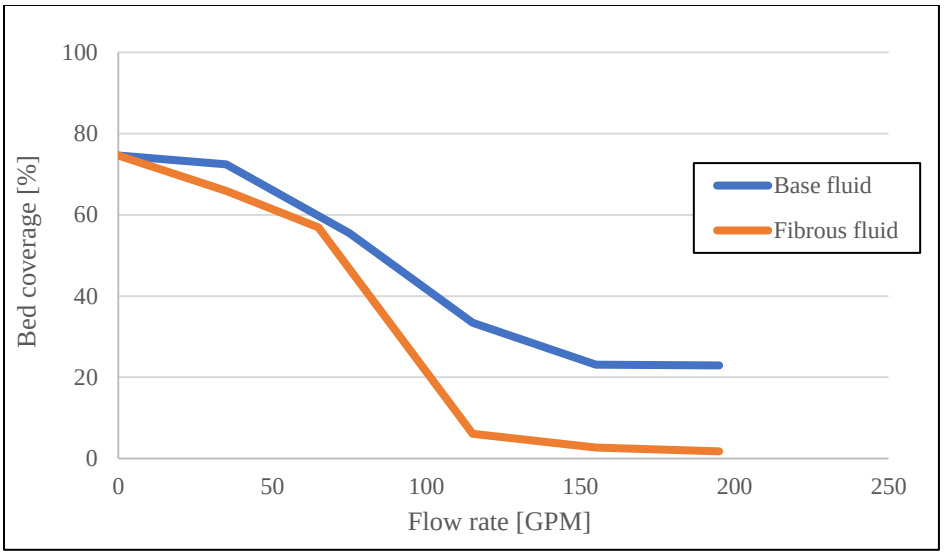

Figure 5.9 Cleaning efficiency comparison between the base fluid and the fibrous fluid

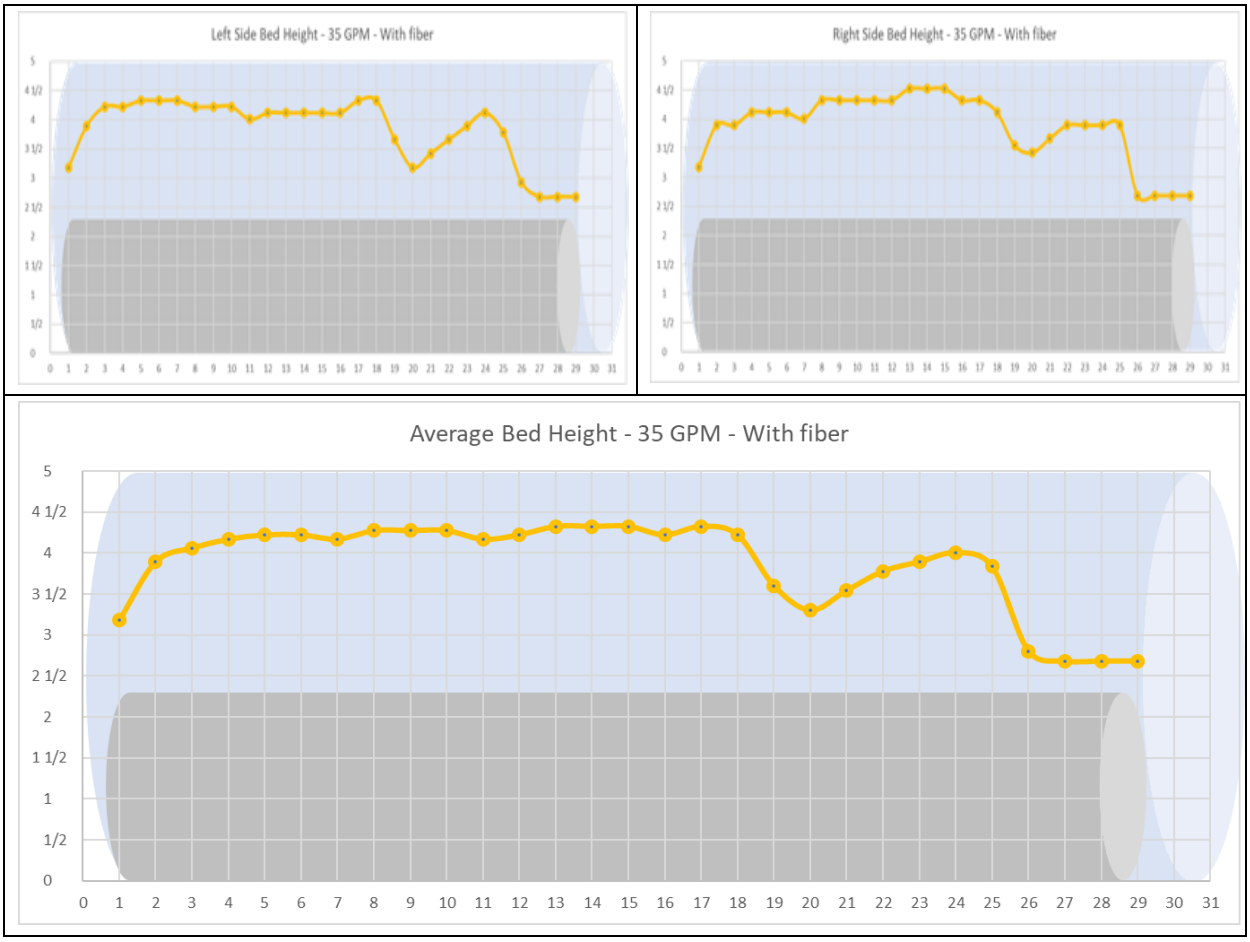

Figure 5.10 Left-side, right-side, and average bed profiles with fibrous fluid (35 GPM, 0 RPM)

Chapter 6: Model Predictions

In this chapter, the traditional and new hydraulic models discussed and presented by Elgaddafi et al. (2021), are evaluated. The model predictions are compared to the pressure drop measurements obtained from the flow loop experiments. In addition, the new model (Elgaddafi's model) is utilized to reproduce the bed height measurements collected during flow loop experiments.

6.1 Pressure Loss Predictions

The pressure drop across the annulus was evaluated at different flowrates in absence of bed for both base and fibrous fluids. Table 6.1 shows the experimental and predicted pressure drops for the base fluid without bed formation.

Table 6.1 Pressure drop prediction: base fluid with no bed

Measurements		Existing model			Elgaddafi's model		
q [GPM]	DP [inH2O]	Re_{gen}	Theory DP [inH2O]	%Error	Re	Theory DP [inH2O]	% Error
14	2.61	27	6.12	134%	11	3.65	40%
23	4.88	59	7.48	53%	24	4.47	-8%
36	4.95	121	8.98	81%	48	5.36	8%
52	5.2	217	10.43	100%	87	6.23	20%
65	6.06	309	11.41	88%	124	6.82	13%
85	6.52	474	12.73	95%	190	7.60	17%
113	7.76	746	14.29	84%	298	8.54	10%
136	8.32	1003	15.41	85%	401	9.20	11%
160	10.06	1299	16.46	64%	519	9.83	-2%
183	10.68	1609	17.38	63%	643	10.38	-3%
206	11.6	1943	18.24	57%	777	10.89	-6%
230	11.81	2317	18.80	59%	926	11.39	-4%
252	13.77	2680	21.36	55%	1071	11.82	-14%
275	14.21	3080	24.13	70%	1231	12.25	-14%
295	14.73	3444	26.62	81%	1377	12.61	-14%

Re_{gen} is the general Reynolds number presented in equation 3.27 and Re is the Reynolds number presented in equation 3.45. As a general rule, when Re_{gen} is lower than 2100 the flow is considered to be laminar, otherwise the flow is turbulent.

The error for both existing and new models was calculated using the following equation:

$$\%Error = \left(\frac{DP_{model} - DP_{exp}}{DP_{exp}}\right) * 100 \qquad \text{Eq 6.1}$$

where DP_{exp} is the experimental value, and DP_{model} is the value obtained from the model. The sign of the percentage error is presented as negative when the prediction is lower than the measured value, and positive when the prediction is higher than the measured value. It is important to notice that the existing model excessively over predicts the pressure drop for all flow rates. This is because it does not consider the eccentricity of the inner pipe and uses simplified correlations to determine the differential pressure drop. On the other hand, the new model shows a better overall prediction of the pressure drop by considering the eccentricity of the pipe and a more accurate Computational Fluid Dynamics (CFD) based dimensionless correlations to calculate the pressure drop and bed shear stress.

Table 6.2 shows the performances of the models in predicting the pressure drop for the fibrous fluid in the absence of a bed. It is important to notice that the fiber creates a network in the fluid that directly impacts its behavior, causing some changes in the differential pressure drop.

It can be noticed that the overall error in the existing model is slightly higher than the one calculated for the base fluid. Evaluating the pressure drop in the absence of a bed provides a good baseline to analyze if the model captures the flow hydraulics well. The presence of a bed adds extra assumptions that are not fulfilled in some cases. The assumptions increase the uncertainty of

the model. According to Elgaddafi et al. (2021), the main assumptions made to develop the new model includes:

- The solids bed is flat and uniform in thickness.
- The wellbore is highly eccentric (80 to 100%).
- Solid particles are considered spherical and uniform in size and density.
- The flow is steady and isothermal.
- The fluid is homogeneous and incompressible.
- There solids concentration in the upper clear layer is negligible.
- The contribution of particle collision on solid transport is minor.

Table 6.2 Pressure drop prediction: Fibrous fluid no bed

Measurements		Existing model			Elgaddafi's model		
q [GPM]	DP_{exp} [inH2O]	Re_{gen}	DP_{model} [inH2O]	%Error	Re	DP_{model} [inH2O]	% Error
15	2.27	30	6.26	176%	12	3.75	65%
23	2.35	59	7.44	216%	24	4.45	89%
35	3.74	116	8.81	135%	46	5.27	41%
40	4.23	144	9.29	120%	57	5.56	31%
61	5.4	282	11.02	104%	112	6.59	22%
84	6.27	470	12.53	100%	187	7.50	20%
111	7.29	734	14.02	92%	291	8.39	15%
135	8.09	1003	15.17	88%	398	9.08	12%
158	9.16	1290	16.16	76%	512	9.67	6%
182	10.39	1617	17.11	65%	641	10.24	-1%
206	11.16	1971	17.98	61%	782	10.76	-4%
228	12.28	2317	18.38	50%	919	11.21	-9%
261	13.3	2876	22.19	67%	1141	11.84	-11%
273	13.46	3090	23.63	76%	1226	12.05	-10%
290	14.59	3403	25.71	76%	1350	12.35	-15%

Table 6.3 shows the pressure drop predictions of the base fluid experiments with a bed. The pressure loss trends are similar to those observed in experiments conducted in the absence of solids beds. The new model offers a lower error and better overall prediction than the existing one.

An acceptable error for pressure drop prediction is up to 20%, at this particular scenario. The trip margin in real life scenarios can have more sensitivity to other variables. The new model underestimates the pressure drop because of the simplifying assumptions that are not satisfied with the experimental conditions. However, at a flow rate of 155 GPM, the model over predicts the pressure drop. The formation of dunes and ripples normally generate additional hydraulic resistance due to the formation complex flow structures and eddies. This outlying data point showed very low-pressure loss measurements contrary to the bed profile observation, which indicates significant bed height variation (Figure 6.1).

Table 6.3 Pressure drop prediction: Base fluid with bed

Test Results					Existing model		Elgaddafi's model	
Q [GPM]	H bed [in]	CV	Re_Gen	Experimental ΔP [inH2O]	Theoretical ΔP [inH2O]	Error [%]	Theoretical ΔP [inH2O]	Error [%]
35	3.985	0.11	87.805	22.842	23.277	2%	16.436	-28%
75	3.351	0.06	356.235	14.339	16.582	16%	11.709	-18%
115	2.571	0.18	812.908	11.426	11.976	5%	8.457	-26%
155	2.171	0.30	1366.489	7.112	11.583	63%	9.135	28%
195	2.160	0.26	1967.994	11.774	12.711	8%	10.030	-15%

It is evident that the left-side and right-side views of the bed profile are different, and both varying significantly along the length of the horizontal section. This can be attributed to the presence of sand dunes in the annulus. The presence of high-amplitude dunes violates one of the main assumptions of the model that considers the formation of a flat uniform bed, resulting in the under-prediction of the pressure drop.

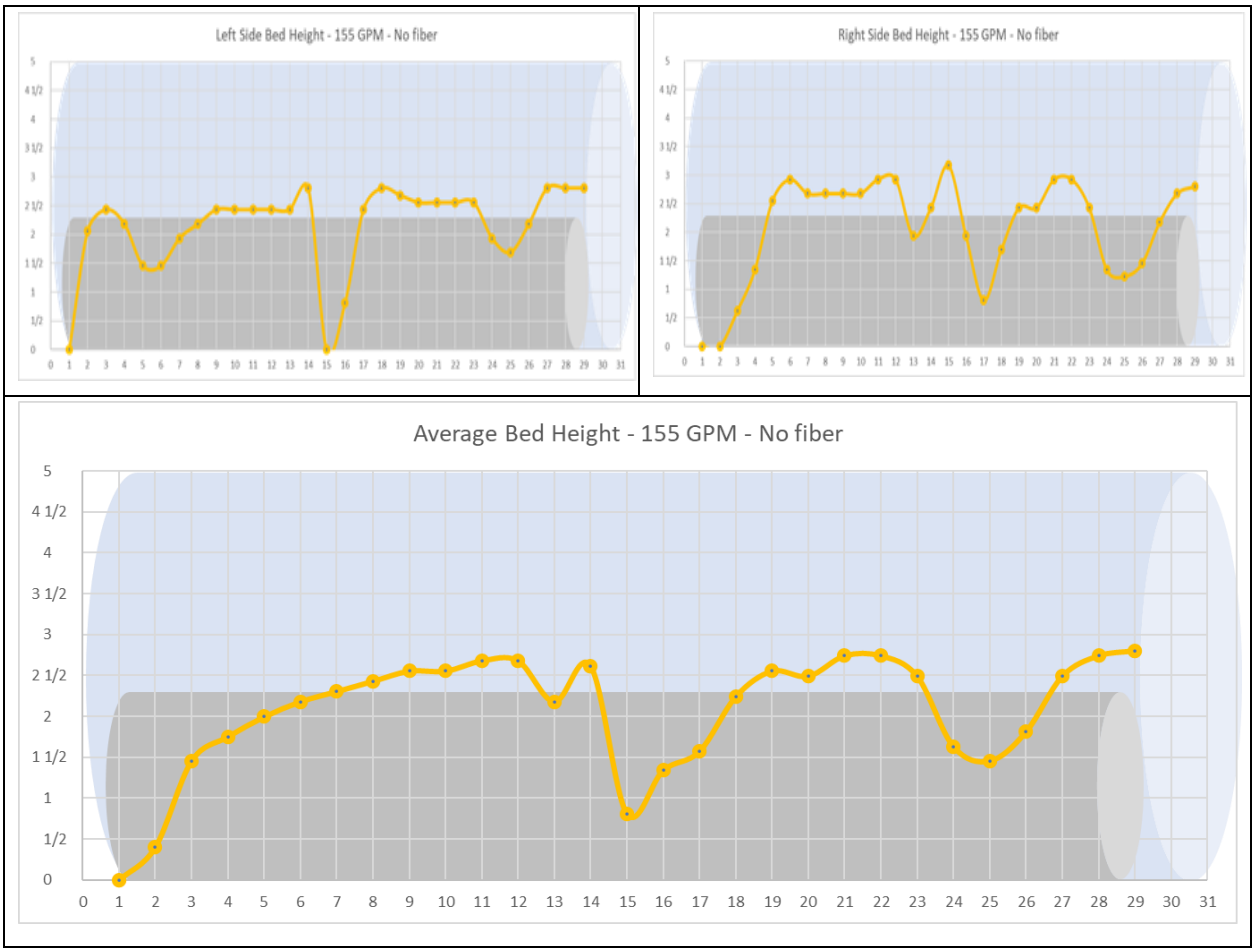

Figure 6.1 Left-side, right-side, and average bed profiles with base fluid (155 GPM, 0 RPM)

The variability of the bed profile is observed in all of the experiments at different levels. Sometimes it is barely noticeable and sometimes, like in Figure 6.1, it is more evident. A statistical concept known as the coefficient of variation (CV) was introduced to analyze the effect of variations in the bed profile on the prediction errors of the new model. CV is defined as:

$$CV = \frac{Standard\ deviation\ of\ the\ bed\ height}{Average\ bed\ height} \qquad \text{Eq 6.2}$$

The coefficient of variation is related to the variation in bed height values obtained throughout the measuring stations in the annulus. Overall, the higher the coefficient of variation is, the less uniform the bed profile becomes, causing higher errors (i.e. significantly lower model

predictions than measurements) in the model's prediction. For example, the model under predicts the pressure drop at a flow rate of 75 GPM. The bed profile of this test is shown in Figure 6.2. We can notice the bed was not completely flat, and its variability resulted in a higher pressure drop measurement.

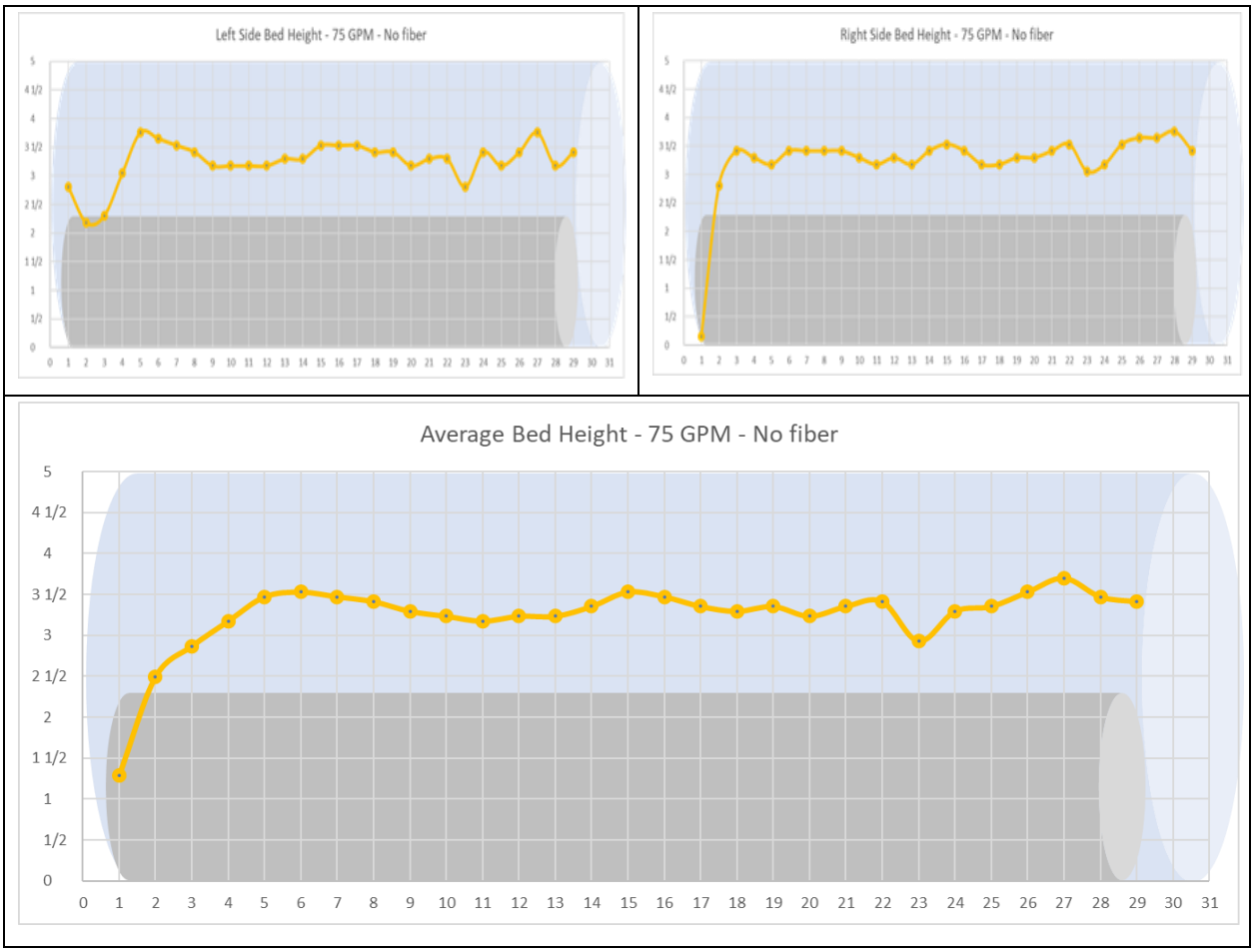

Figure 6.2 Base cleaning fluid left-side, right-side, and average bed profiles (75 GPM, 0 RPM)

The CV helps explain the errors in the prediction of the new model. However, we can see that the CV varies with flow rates. As a result, the CV at 35 GPM was higher than that observed at 75 GPM. To better understand the CV at 35 GPM, the bed profile is shown in Figure 6.3. The bed profile was almost uniform except at the bed measuring stations close to the exit. Consequently, the coefficient of variation is high, resulting in increased pressure loss

measurement. Therefore, even though the CV is a good way of understanding the model's performance, it is important to analyze all the measurements before concluding.

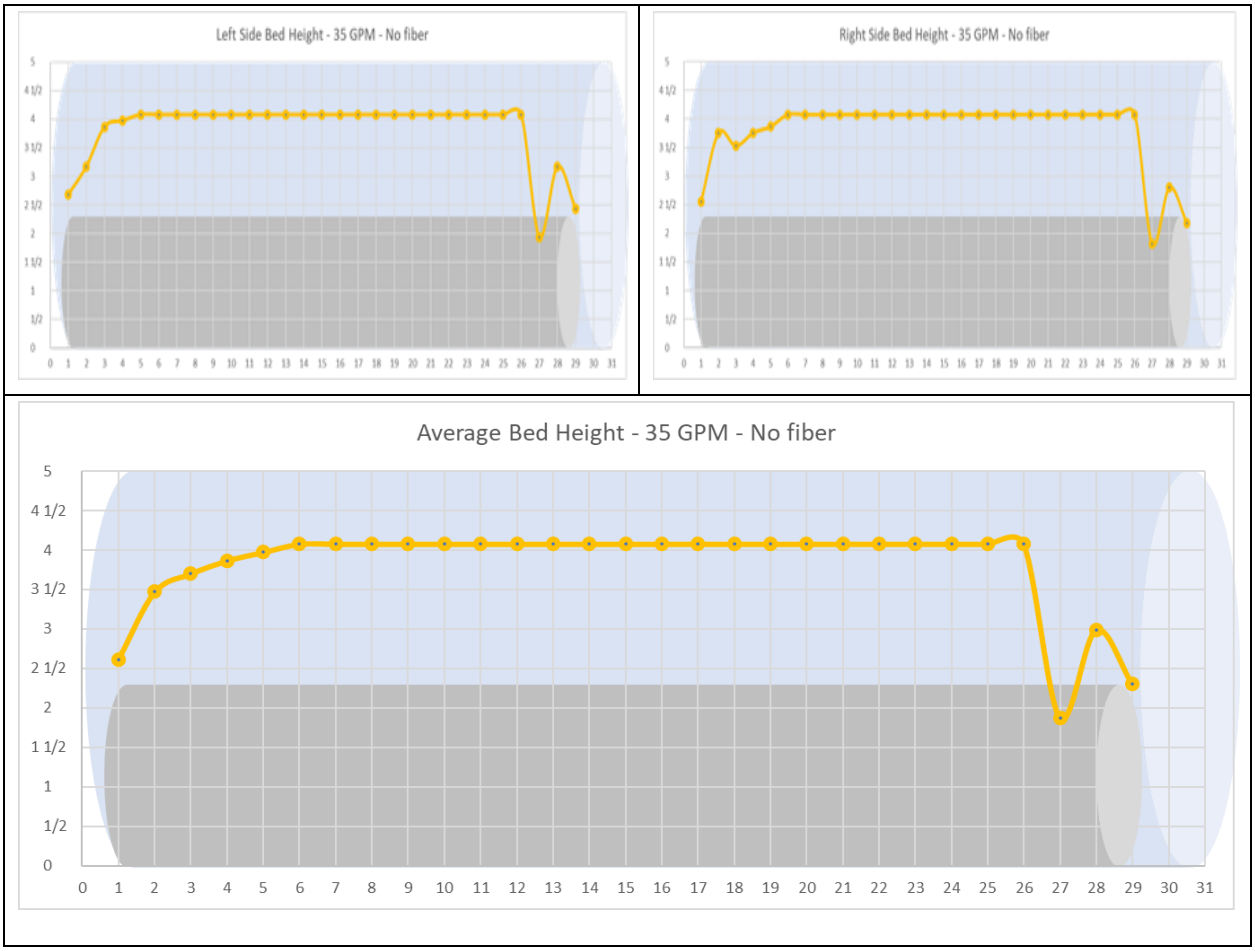

Figure 6.3 Base cleaning fluid left-side, right-side, and average bed profiles (35 GPM, 0 RPM)

Overall, the new model is a good predictor of the pressure drop for the base fluid experiments. The next section presents the analysis for the fibrous fluid experiments. Table 6.4 shows the pressure drop predictions for the fibrous fluid tests.

Table 6.4 Pressure drop prediction with CV: Fibrous fluid with bed

Test Results					Existing model		Elgaddafi's model	
Q [GPM]	H bed [in]	CV	Re_Gen	Experimental ΔP [inH2O]	Theoretical ΔP [inH20]	Error (%)	Theoretical ΔP [inH2O]	Error [%]
35	3.734	0.13	88	20.216	18.727	-7%	13.213	-35%
65	3.400	0.14	258	18.941	17.701	-7%	12.489	-34%
115	0.997	0.77	786	16.294	10.945	-33%	8.515	-48%
155	0.601	1.05	1238	14.075	13.203	-6%	9.696	-31%
195	0.454	0.96	1763	15.029	15.032	0%	10.677	-29%

Unlike the base fluid tests, where the new model provides a more accurate prediction compared to the existing model, the presence of fiber changes the trend. A decrement is observed in the prediction performance of the new model with fiber.

Figure 6.4 shows the bed profile at 115 GPM with fiber, where the prediction error is the highest for both models. Table 6.5 shows that the coefficient of variation for this test is very high, and analyzing Figure 6.4 reveals the reason for it. The absence of bed height in the middle of the test section indicates two large dunes. The lack of bed uniformity in this test violates one of the assumptions of the new model, causing the error to increase. The pressure drop sensors of the experiments are located at stations number 3 and number 27, where sharp changes are observed in the bed height. This situation creates a choke effect, increasing the pressure drop measurement in the experiment. The lack of bed uniformity is amplified in the presence of fiber, resulting in the formation of large dunes. Therefore, the predictions made by the new model have a higher level of error.

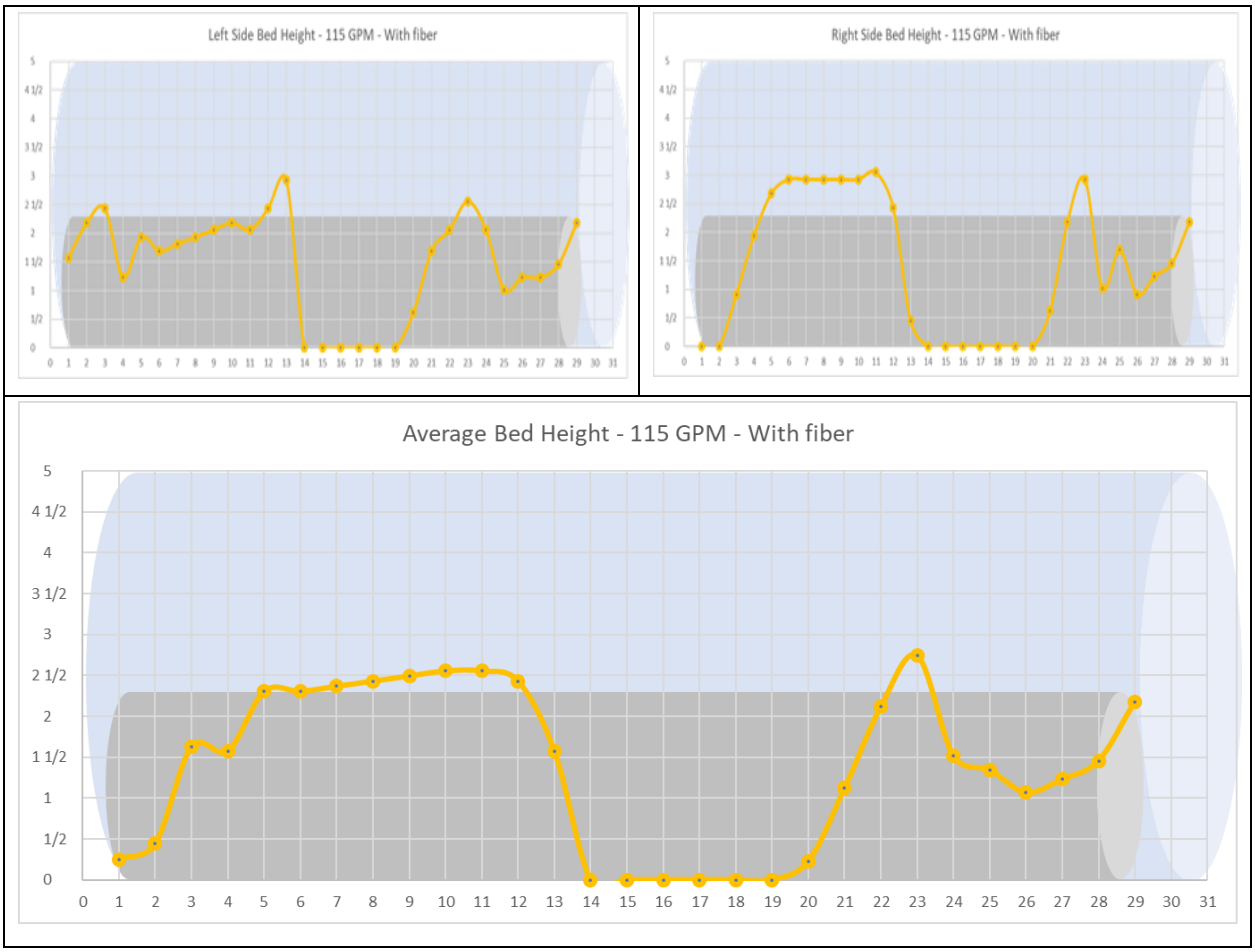

Figure 6.4 Fibrous fluid left-side, right-side, and average bed profiles (115 GPM, 0 RPM)

At 65 GPM, the coefficient of variation is low, but the model's prediction error is still high. Figure 6.5 shows the bed profile for this flowrate. The average bed height seems to be consistent and homogeneous, but it is evident that the right side and left side have high variability. The variation of the bed profile is significant when looking separately from each side of the annulus. This can be the reason for large prediction errors.

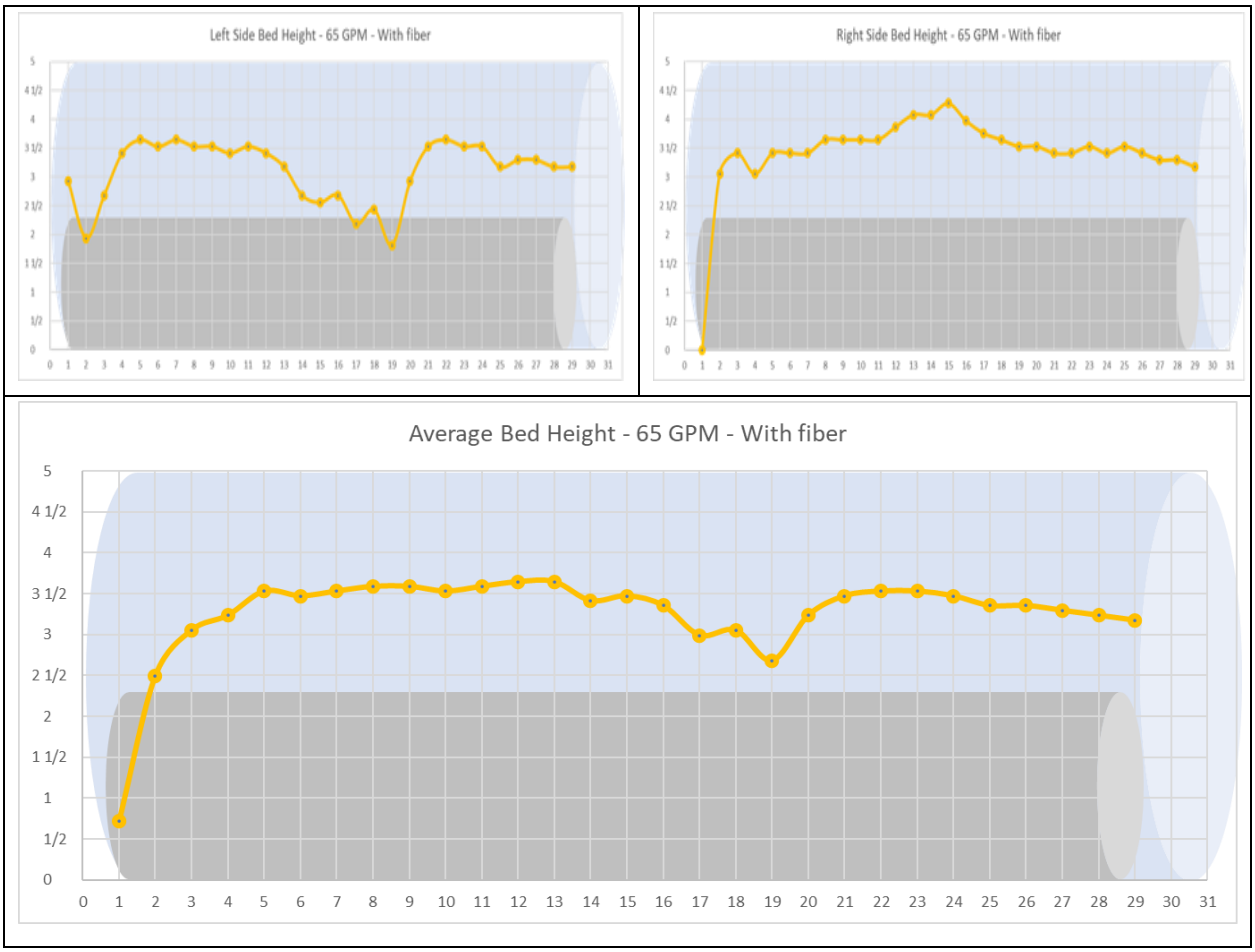

Figure 6.5 Fibrous fluid left-side, right-side, and average bed profiles (65 GPM, 0 RPM)

Higher bed thickness variability and more dune formation are present in the fibrous fluid experiments. This could be explained by considering the increase in the drag force exerted by the fiber network, which is capable of displacing larger masses of sand particles. In the ideal conditions (conditions where the assumptions are fulfilled), the new model is expected to provide reasonable predictions for the fibrous fluid tests. If the fluid were more viscous, the dunes might be reduced, improving the predictions. The dunes are practically inexistent when pipe rotation is used. Plots of the bed profiles for the fibrous fluid with rotation can be found in the appendix section.

An improvement for the pressure drop prediction model can be introduced using the coefficient of variation (CV) concept to account for the lack of homogeneity in the bed profile.

Figure 6.6 shows the relationship between the CV and the prediction error, and Figure 6.7 shows relationship between the CV and the normalized bed shear stress (τb) for each experiment.

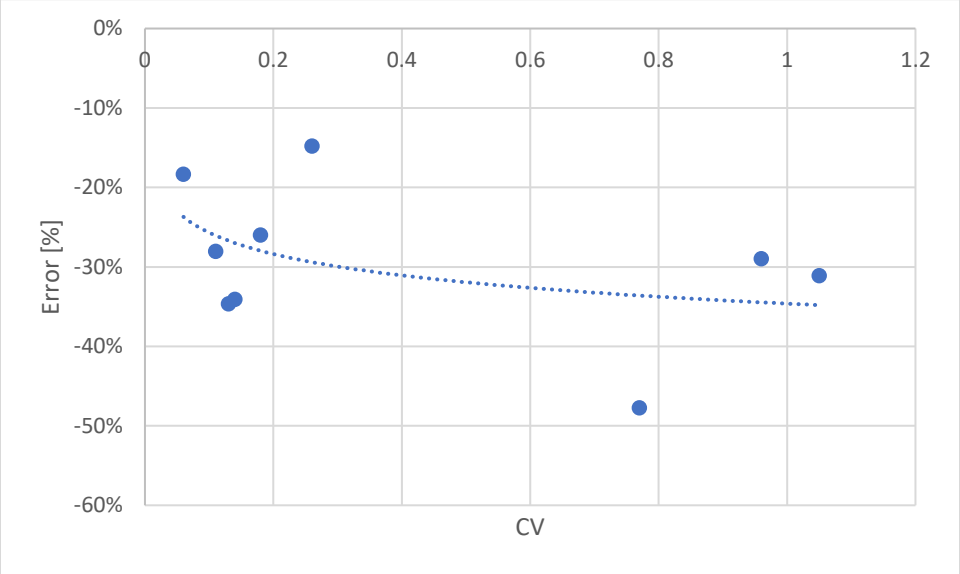

Figure 6.6 Prediction error vs. the bed profile CV of the tests

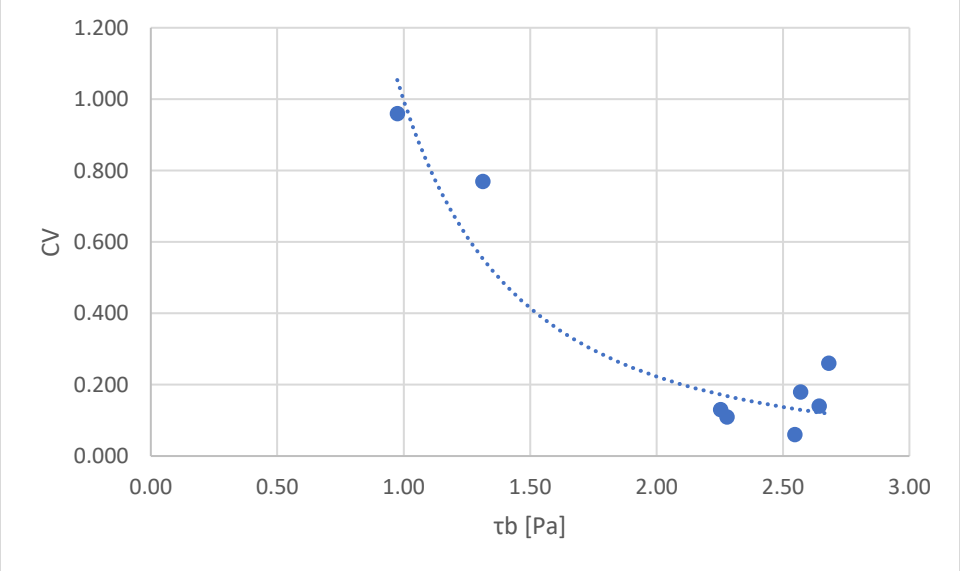

Figure 6.7 Bed profile CV vs Normalized Bed Shear Stress of the tests

The correlation between the normalized bed shear stress and the coefficient of variation is defined by:

$$CV = 0.997 * (\tau b^{-2.162}) \qquad \text{Eq 6.1}$$

The correlation between the coefficient of variation and the prediction error is defined by:

$$\%Error = -35.958 + \frac{36.049}{1 + (x/0.0344)\text{^}0.852)} \quad \text{Eq 6.2}$$

The bed shear stress of each experiment can be calculated. Using the calculated bed shear stress, CV can be calculated using Equation 6.1. The calculated CV can be utilized in Equation 6.2 to obtain a new %Error which can be used as a correction factor for the predicted bed height. Table 6.5 shows the pressure drop predictions of the improved model for the base fluid.

Table 6.4 Pressure drop prediction of improved model: Base fluid

Test Results				Improved model no fiber			
Q (GPM)	H bed [in]	Experimental ΔP [inH2O]	τb [Pa]	Calculated CV	Correction factor	New ΔP	Model error
35	3.985	22.842	2.278	0.168	-0.285	21.127	-8%
75	3.351	14.339	2.548	0.132	-0.273	14.901	4%
115	2.571	11.426	2.570	0.129	-0.272	10.753	-6%
155	2.171	7.112	2.445	0.144	-0.277	11.670	64%
195	2.160	11.774	2.681	0.118	-0.266	12.700	8%

The pressure drop predictions of the improved model are more accurate, where the experimental pressure obtained at a flowrate of 155 GPM is an outlier. Table 6.5 shows the pressure drop predictions of the improved model for the fibrous fluid.

Table 6.5 Pressure drop prediction of improved model: Fibrous fluid

Test Results				Improved model with fiber			
Q (GPM)	H bed [in]	Experimental ΔP [inH2O]	τb [Pa]	Calculated CV	Correction factor	New ΔP	Model error
35	3.734	20.216	2.25	0.172	-0.287	17.000	-16%
75	3.400	18.941	2.64	0.122	-0.268	15.836	-16%
115	0.997	16.294	1.31	0.553	-0.329	11.313	-31%
155	0.601	14.075	0.97	1.054	-0.341	13.003	-8%
195	0.454	15.029	0.86	1.392	-0.345	14.358	-4%

Similar to the base fluid, the pressure drop predictions for the fibrous fluid are better with the improved model. A relationship between the measured pressure drop and the pressure drop calculated by the model for the base fluid and fibrous fluid is shown in Figure 6.8 and Figure 6.9

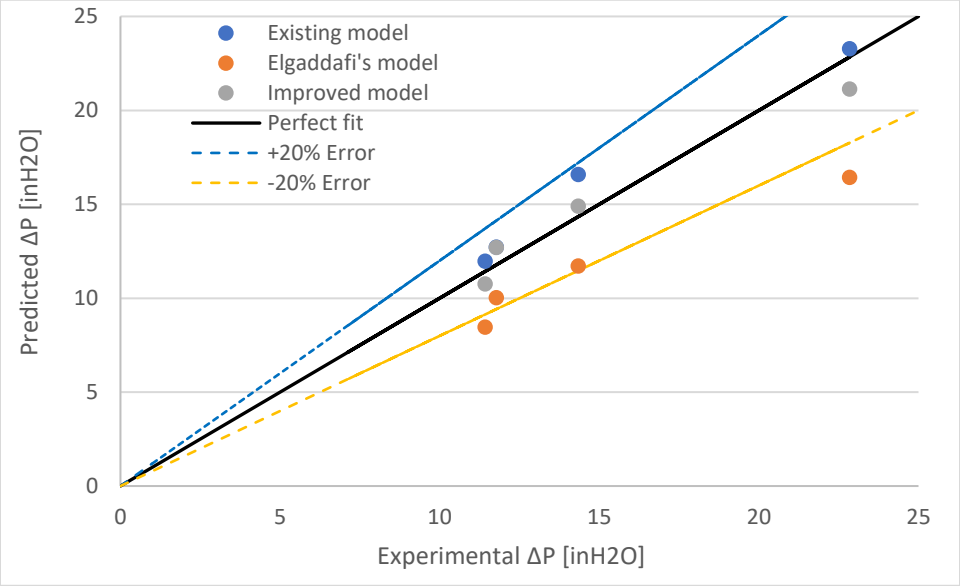

Figure 6.8 Predicted vs experimental pressure drop for the base fluid

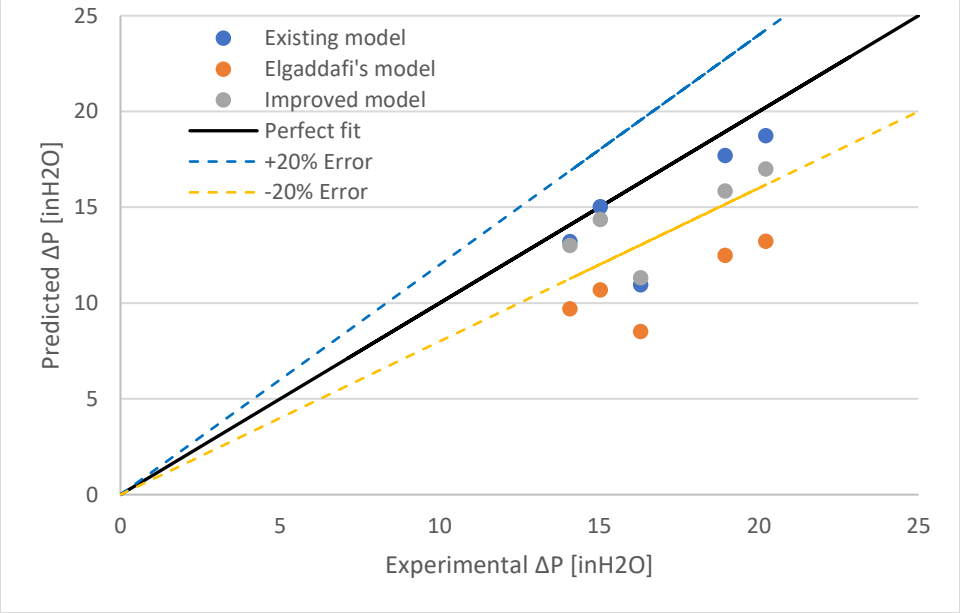

Figure 6.9 Predicted vs experimental pressure drop for the fibrous fluid

6.2 Bed Height Prediction

One of the virtues of Elgaddafi's model, introducing the bed shear stress concept, is developing an approach to predict the bed height using a mechanistic hole cleaning model. The detailed formulation of the most recent mechanistic model is presented by Elgaddafi et al. (2021), including its step-by-step calculation procedure. The bed height predictions of the model for the base fluid tests are shown in Table 6.6.

Table 6.6 Bed height predictions and measurements: Base fluid

Test Results			Mechanistic model prediction	
Q [GPM]	H_bed [in]	CV	H_bed [in]	Error (%)
35	3.985	0.113	3.940	-1%
75	3.351	0.047	3.572	7%
115	2.571	0.165	2.830	10%
155	2.171	0.239	2.375	9%
195	2.160	0.124	2.192	1%

The bed height predictions of the mechanistic model are relatively accurate for the base fluid. The highest errors occur for tests with higher coefficients of variation. At 155 GPM, the bed profile is far from being uniform, as shown in Figure 6.1, explaining the error in prediction. Overall, the errors in the prediction of the bed height can be explained using the same criteria established for the prediction of the pressure drop because the mechanistic model also assumes the presence of a uniform bed in the annulus.

The bed height predictions for the fibrous fluid are shown in Table 6.7. Unlike the base fluid, the bed height prediction errors for the fibrous fluid are considerably, especially the bed height measurements are very low (i.e. when the bed heights are in the order of accuracy level of the measuring methods). The accuracy in bed height measurement is approximately ± 0.25 inches. At lower flowrates, the model is underpredicting the bed height, while it is overpredicting the bed height at higher flowrates. The best prediction is obtained at 115 GPM, which is where the best

cleanout performance is obtained, as shown in Figure 5.8. The explanation for this behavior is related to the presence of the fiber network, which may affect the velocity profile of the fibrous fluid in the flow stagnant zones of the annulus.

Table 6.7 Bed height predictions and measurements: Fibrous fluid

Test Results			Mechanistic model prediction	
Q [GPM]	H bed [in]	CV	H bed [in]	Error [%]
35	3.734	0.126	2.258	-40%
75	3.400	0.067	1.536	-55%
115	0.997	0.727	1.137	14%
155	0.601	0.853	0.979	63%
195	0.454	0.914	0.874	92%

6.3 Sensitivity Analysis

Both pressure drop and bed height depend on various factors including fluid and solids characteristics and field operating parameters. Therefore, optimizing hole cleanout operations is critical to reduce unproductive time and associated operating expenses. A sensitivity analysis is a good way to determine which factors are relevant (influential) in improving hole cleaning. After knowing the most important parameters, decisions can be made to optimize a cleanout operation. The sensitivity of a variable can be defined as the change in the output of the model caused by a change in a single input parameter, while keeping the other variables constant.

6.3.1 Sensitivity Analysis for Pressure Drop

Figure 6.10 shows the sensitivity of the new hydraulic model's pressure drop prediction for the base fluid. The blue and orange bars represent the variation of each input. The blue bars mean that the input is increased by 10%, while the orange bars represent a 10% decrease in the input variable. D_i is the outer diameter of the pipe, D_o is the inner diameter of the annulus, K and n are the flow consistency index and the fluid behavior index, respectively, ρ is the density of the fluid, q is the flowrate, and H_{bed} is the bed height.

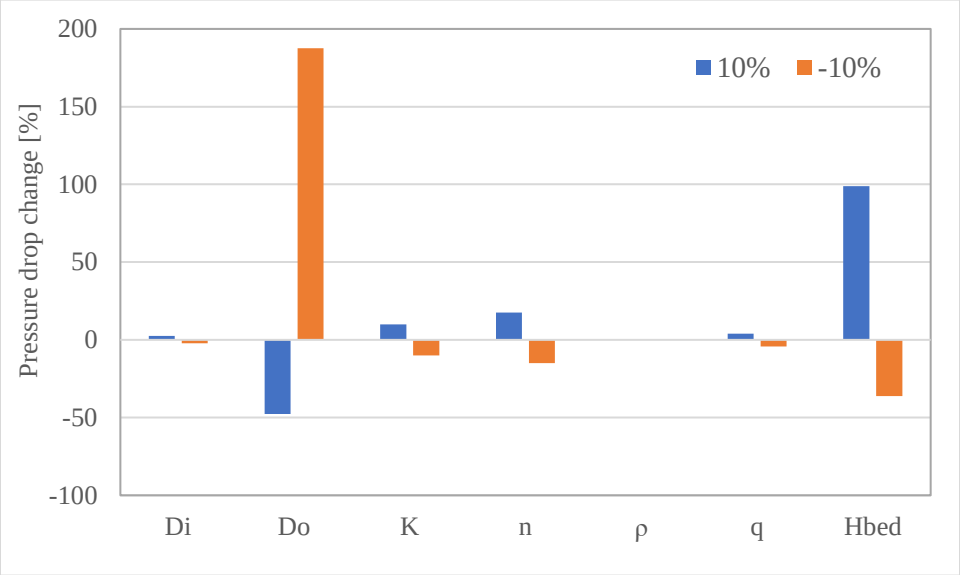

Figure 6.10 Sensitivity plot for base fluid pressure drop (q=35 GPM, H_{bed}=3.98 in.)

As a rule of thumb, the higher the percentage changes in the output are, the more sensitive the output is to the changes in the specific variable. There is no variation in pressure drop with the density change because the flow is laminar under this condition. The results demonstrated that H_{bed} and q are the influential variables that significantly affect the pressure drop under this condition. A 10% decrease in the annulus diameter causes an increase higher than 100% in the pressure drop. Similarly, the increase in bed height causes a significant jump in the pressure drop. Knowing the accurate diameter of the annulus and the bed height is critical to obtain good pressure drop predictions in presence of a thick bed in the annulus.

Figure 6.11 shows the sensitivity analysis for the base fluid at 155 GPM, where the bed is not as high as the case of 35 GPM. In contrast to the previous case, results show a drastic reduction in the importance of the bed height. When the bed gets cleaned, other parameters, such as the rheological properties (K and n), become more influential. The diameter of the annulus is still the most important parameter in determining the pressure drop. In the laboratory-scale experiments, it

is easy to measure the diameter of the annulus. In field situations however, determining the diameter of the drilled hole is not an easy task. It is commonly assumed that the hole is the same as the size of the bit used to drill the well, which may not be always the case due to the instability of the wellbore and the presence of various wellbore irregularities. In real life situations, the pressure drop is more sensitive to the hole diameter.

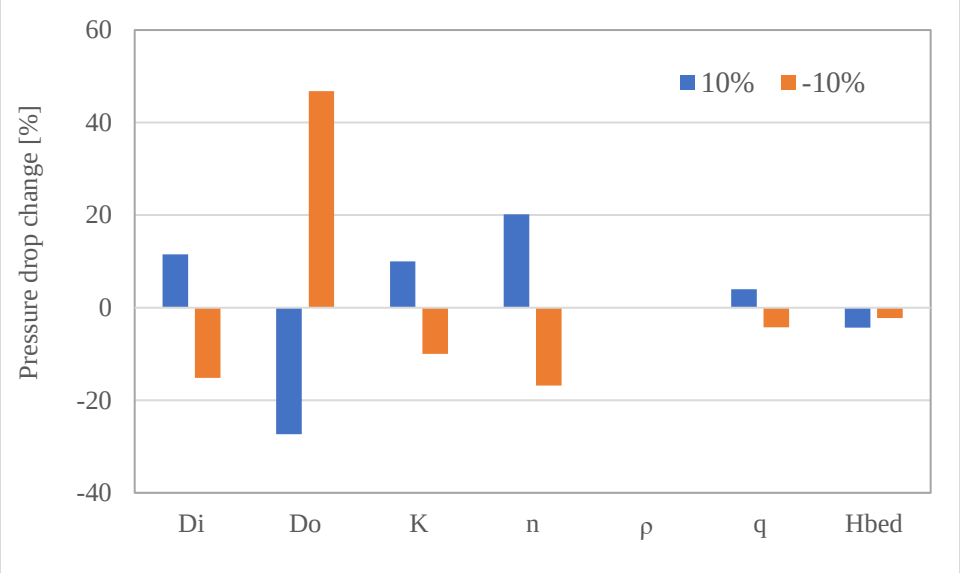

Figure 6.11 Sensitivity plot for base fluid pressure drop (q=155 GPM, H_{bed}=2.17 in)

Figures 6.12 and 6.13 show the sensitivity plots for fibrous fluid experiments at 35 GPM and 155 GPM, respectively. It can be seen that the sensitivity analysis trends for the fibrous fluid are similar to the ones observed for the base fluid. The pressure drop is highly sensitive to the bed height when it is high, and less sensitive when it is low. The diameter of the annulus plays an important role on the frictional pressure loss regardless of the experimental conditions. In addition, the model's sensitivity to rheological properties (K and n) increases with flowrate.

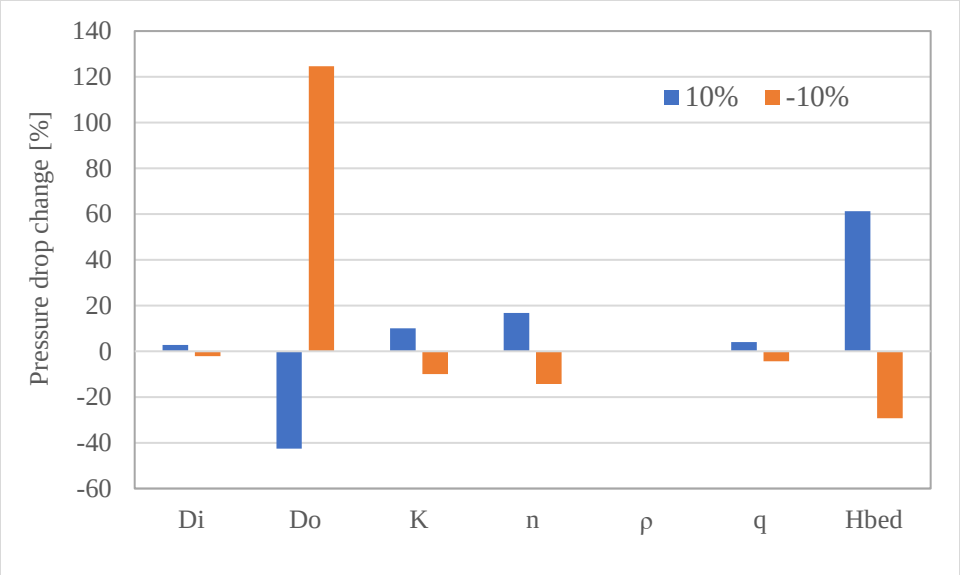

Figure 6.12 Sensitivity plot for fibrous fluid pressure drop prediction (q=35 GPM, H_{bed}=3.73 in)

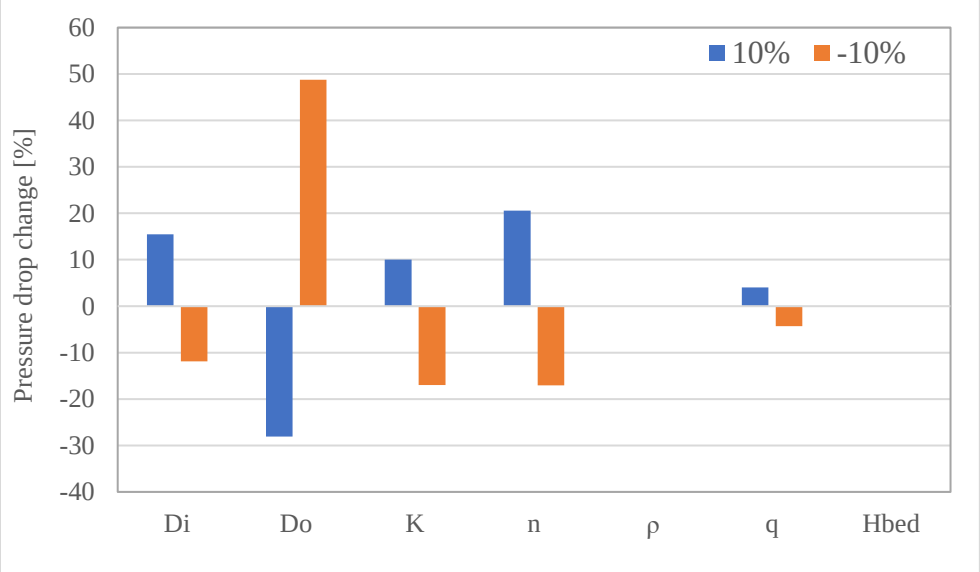

Figure 6.13 Sensitivity plot for fibrous fluid pressure drop prediction (q=155 GPM, H_{bed}=0.60 in)

6.3.2 Sensitivity Analysis for Equilibrium Bed Height

Figure 6.14 shows the sensitivity plot for the equilibrium bed height at 35 GPM. The additional influential factors for the bed height are the fiber concentration parameter (X_f), wellbore

inclination angle (α), angle of repose of the sand (ϕ), particle density (ρ_p) and average diameter of the sand particles (d_p). The rest of the inputs are the same as the ones utilized for the pressure drop analysis. A 10% change in any of the input parameters, other than X_f, does not cause an observable response in the equilibrium bed height. Increasing the fiber concentration (Xf) is the factor that results in the most visible drop in the predicted bed height. At low flowrate (q = 35 GPM) with larger bed heights, the fiber concentration and hole diameter are the most important parameters.

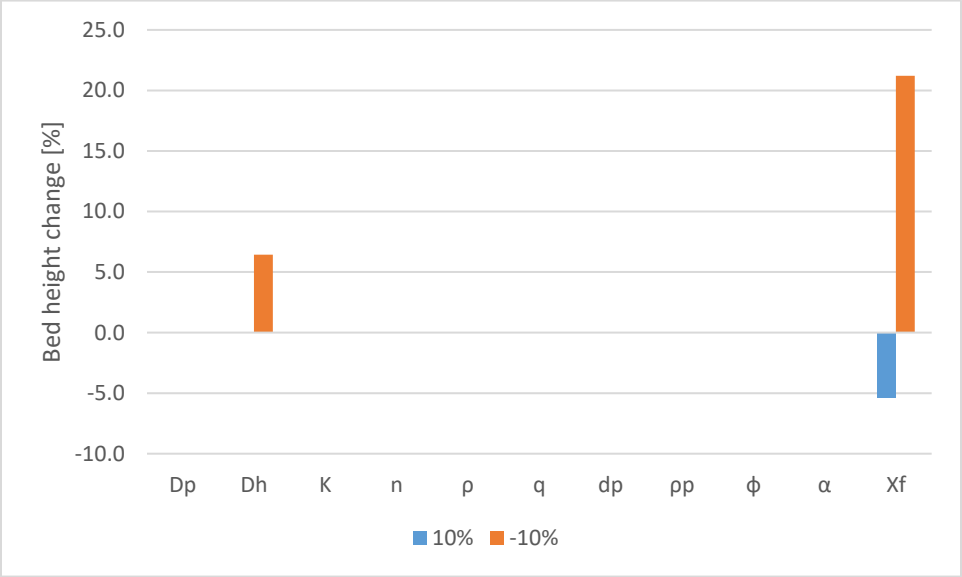

Figure 6.14 Sensitivity plot for equilibrium bed height (q=35 GPM)

Figure 6.15 shows the sensitivity plot for the bed height at the flowrate of 155 GPM. At this flowrate, the bed height is sensitive to various inputs parameters even at 10% input change. The most important parameters are the hole diameter, fluid behavior index, particle density, and fiber concentration. These factors need to be considered in the optimization of cleaning operation in horizontal and highly deviated wells.

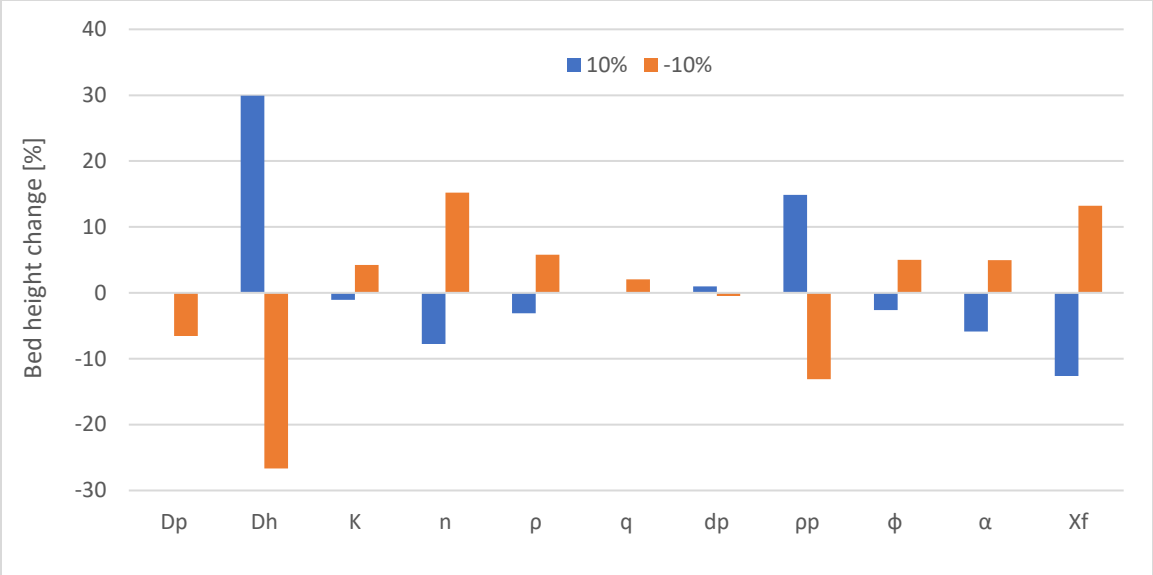

Figure 6.15 Sensitivity plot for equilibrium bed height (q=155 GPM)

Table 6.9 shows large errors in bed height prediction. Future investigations may be performed using the sensitivity plots. At low flowrates, the most important parameter is the fiber concentration that needs to be further investigated to verify the predictions of the model. At higher flowrates, all the parameters play an important role in determining the bed height. Hence, even the slightest change in each parameter can cause significant change in the equilibrium bed height, resulting in a reduced hole cleanout performance and associated operational complications.

Chapter 7: Conclusions and Recommendations

This study is an effort to better understand the effects of fiber and pipe rotation in hole cleaning operations of polymer-based fluids. Three pipe rotation speeds were considered to experimentally evaluate the performance of the base fluid with and without fiber. The tests were carried out using a large-scale flow loop at different flowrates, carefully measuring and recording equilibrium bed height and pressure loss. The conclusions drawn from analyzing the experiments are presented in this chapter. Furthermore, some recommendations are provided to guide future studies.

7.1 Conclusions

The following conclusions are a summary of the main takeaways from this study:

- The presence of fiber in the fluid exceptionally improves its cleaning performance in a horizontal configuration due to the extra drag force provided by the fiber network; the increasing removal of deposited particles is more noticeable starting at a flowrate of 35 gpm.
- Even the slightest pipe rotation improves the horizontal hole cleaning efficiency, agitating, and lifting the settled solids in the bed and preventing new settlements during the cleanout experiments.
- The new model (Elgaddafi et al. 2021) for predicting the pressure drop is more consistent than the existing model. The model's underpredictions can be explained by analyzing the assumptions that are considered in its development.

- The presence of dunes in sand bed causes significant discrepancy in the predictions of pressure drop and bed height. Dunes are more observable in fibrous fluids due to their extra drag force that acts on the deposited bed particles.
- The coefficient of variation CV is a great tool to quantify the lack of homogeneity of the solids bed and by correlating it with the error and the bed shear stress, an improved model that corrects the pressure drop prediction accounting the presence of dunes and variability in the bed was developed. The improved model is consistent and provides better results overall in predicting the pressure drop.
- The diameter of the annulus is the most important parameter in determining the pressure drop. Minor changes in the hole diameter can have significant effect on pressure loss.
- When thick bed is formed in the wellbore, the bed height plays an important role in determining the pressure drop. As the bed gets cleaned, other parameters such as the rheological properties become more important.
- The fiber concentration is the most important parameter affecting the bed height with fibrous fluid. The slightest changes in fiber concentration can cause significant variation in bed height. Optimization of the fiber concentration is critical to improve cleanout operation and to minimize bed height.
- The bed height prediction model is a great tool that can be utilized to design horizontal downhole cleaning programs in real life situations.

7.2 Recommendations

The following recommendations are suggested to be applied in future research:

- Accurately measure and record variations in the flowrate and pressure drop during the experiments and explain the experimental causes of those variabilities. Experimental abnormalities are not taken into account in the models. Knowing their root causes is a good way to explain the discrepancies between measurement and predictions.
- Extend the shear rate range of the rheological experiments for base and fibrous fluids to obtain a more detailed rheological characterization of the fluids.
- Test different concentrations of polymer and fiber, and compare their performances with the fluid utilized in the present work.

Nomenclature

a, b	Geometric parameters, dimensionless
A_f	Flow cross sectional area, m^2
A_i	Inner pipe area, m^2
A_o	Outer wellbore area, m^2
A_p	Area of the particle facing the flow, m^2
C_D	Drag coefficient, dimensionless
C_{Df}	Fiber drag coefficient, dimensionless
C_L	Lift coefficient, dimensionless
D_{eff}	Effective diameter, m
D^*_{eff}	Modified effective diameter, m
D_{hy}	Hydraulic diameter, m
D_i	Inner pipe diameter, m
d_p	Particle diameter, m
f	Fanning friction factor, dimensionless
F_b	Buoyancy force, N
F_D	Hydrodynamic drag force, N
F_{Df}	Fiber drag force, N
F_g	Gravity force, N
F_L	Hydrodynamic lift force, N
g	Gravitational acceleration, m/s^2
G	Dimensionless parameter, dimensionless

H	Annular clearance, m
H_b	Dimensionless bed height, dimensionless
H_{bed}	Bed height, m
I_n	Empirical coefficient, dimensionless
K	Fluid consistency index, $Pa\ s^n$
n	Fluid behavior index, dimensionless
P	Pressure, Pa
r_1	Radius of bob viscometer, m
r_2	Radius of rotor viscometer, m
Re_{gn}	General Reynolds number, dimensionless
Re_k	Generalized Kozicki Reynolds number, dimensionless
R_i	Radius of the inner part of the annulus, m
R_o	Radius of the outer part of the annulus, m
S	Total wetted perimeter, m^2
S_b	cuttings bed perimeter, which is in contact with the fluid, m
S_l	Empirical coefficient, dimensionless
S_o	outer wellbore wall perimeter, which is in contact with the fluid, m
S_p	Inner pipe wall perimeter which is in contact with the fluid, m
U	Average fluid velocity in the channel, m/s
u	Fluid local velocity, m/s
x	hydraulic radius of concentric annulus with no cuttings bed, m
Y	Empirical constant, dimensionless

Z	Empirical constant, dimensionless
θ_i	Inner angle of general wellbore geometry, degrees
θ_o	Outer angle of general wellbore geometry, degrees
ϕ	Angle of repose, degrees
$\frac{\Delta P}{\Delta L}$	Pressure gradient, Pa/m
τ_y	Yield shear stress of the fluid, Pa
μ	Fluid viscosity, $Pa\ s$
ρ_f	Density of the fluid, Kg/m^3
ρ_p	Particle density, Kg/m^3
τ_b	Bed shear stress, Pa
τ_w	Wall shear stress, Pa

References

Adari, Rishi, Stefan Miska, Ergun Kuru, Peter Bern, and Arild Saasen. "Selecting Drilling Fluid Properties and Flow Rates For Effective Hole Cleaning in High-Angle and Horizontal Wells," n.d., 9.

Ahmed, Ramadan Mohammed, Nicholas E. Takach, and M. Savitri. "Experimental Study on Fiber Sweeps in Horizontal and Highly Deviated Configurations." In *All Days*, SPE-120644-MS. Oklahoma City, Oklahoma: SPE, 2009. https://doi.org/10.2118/120644-MS.

Allahvirdizadeh, Payam, Ergun Kuru, and Mahmut Parlaktuna. "Experimental Investigation of Solids Transport in Horizontal Concentric Annuli Using Water and Drag Reducing Polymer-Based Fluids." *Journal of Natural Gas Science and Engineering* 35 (September 2016): 1070–78. https://doi.org/10.1016/j.jngse.2016.09.052.

Aoki, Tatsuyoshi, Shigemi Naganawa, Kazunori Abe, and Ryutaro Mukai. "Evaluating Hole Cleaning Capability of Biodegradable Fiber-Containing Drilling Fluids in Riserless Tophole Drilling." In *Day 1 Mon, November 09, 2020*, D012S116R141. Abu Dhabi, UAE: SPE, 2020. https://doi.org/10.2118/202711-MS.

Awad, Abdelrahman M., Ibnelwaleed A. Hussein, Mustafa S. Nasser, Hamidreza Karami, and Ramadan Ahmed. "CFD Modeling of Particle Settling in Drilling Fluids: Impact of Fluid Rheology and Particle Characteristics." *Journal of Petroleum Science and Engineering* 199 (April 2021): 108326. https://doi.org/10.1016/j.petrol.2020.108326.

Bizhani, M.., F. E. Rodriguez Corredor, and E.. Kuru. "Quantitative Evaluation of Critical Conditions Required for Effective Hole Cleaning in Coiled-Tubing Drilling of Horizontal Wells." *SPE Drilling & Completion* 31, no. 03 (September 8, 2016): 188–99. https://doi.org/10.2118/174404-PA.

Bulgachev, R V. "New Experience in Monofilament Fiber Tandem Sweeps Hole Cleaning Performance on Kharyaga Oilfield, Timan-Pechora Region of Russia," n.d., 12.

Cheung, Erik, Nicholas Takach, Evren Ozbayoglu, Reza Majidi, and Ben Bloys. "Improvement of Hole Cleaning Through Fiber Sweeps." In *All Days*, SPE-154759-MS. Galveston, Texas, USA: SPE, 2012. https://doi.org/10.2118/154759-MS.

Clark, R K. "A Mechanistic Model for Cuttings Transport," n.d., 15.

Dedegil, M. Y. "Drag Coefficient and Settling Velocity of Particles in Non-Newtonian Suspensions." *Journal of Fluids Engineering* 109, no. 3 (September 1, 1987): 319–23. https://doi.org/10.1115/1.3242667.

Duan, Mingqin, Stefan Miska, Mengjiao Yu, Nicholas Takach, Ramadan Ahmed, and Claudia Zettner. "Transport of Small Cuttings in Extended-Reach Drilling," 2008, 8.

Egbue, Jude Chibuike. “Improving The Efficiency Of Transportation Of Cuttings In Wellbore,” n.d., 47.

Elgaddafi, Rida, and Ramadan Ahmed. “Fibrous Cleanout Fluids in Horizontal and Inclined Wells.” In *Day 1 Tue, March 24, 2020*, D012S008R002. The Woodlands, Texas, USA: SPE, 2020. https://doi.org/10.2118/199868-MS.

Elgaddafi, Rida, Ramadan Ahmed, Hamidreza Karami, Mustafa Nasser, and Ibnelwaleed Hussein. “A Mechanistic Model for Wellbore Cleanout in Horizontal and Inclined Wells.” *SPE Drilling & Completion* 36, no. 04 (December 15, 2021): 832–48. https://doi.org/10.2118/204442-PA.

Karimi Rad, Mohammad Saeed, Mojtaba Kalhor Mohammadi, and Kourosh Tahmasbi Nowtarki. “Investigating Hole-Cleaning Fibers’ Mechanism to Improve Carrying Cutting Capacity and Comparing Their Effectiveness with Common Polymeric Pills.” In *Day 1 Mon, November 09, 2020*, D012S116R142. Abu Dhabi, UAE: SPE, 2020. https://doi.org/10.2118/203147-MS.

Li, Jeff, and Bernard Luft. “Overview Solids Transport Study and Application in Oil-Gas Industry-Theoretical Work.” In *All Days*, IPTC-17832-MS. Kuala Lumpur, Malaysia: IPTC, 2014. https://doi.org/10.2523/IPTC-17832-MS.

Mahmoud, Husameldin, Mohammed Alhajabdalla, Mustafa S. Nasser, Ibnelwaleed A. Hussein, Ramadan Ahmed, and Hamidreza Karami. “Settling Behavior of Fine Cuttings in Fiber-Containing Polyanionic Fluids for Drilling and Hole Cleaning Application.” *Journal of Petroleum Science and Engineering* 199 (April 2021): 108337. https://doi.org/10.1016/j.petrol.2020.108337.

Masuda, Y, Q Doan, M Oguztoreli, S Naganawa, T Yonezawa, and A Kobayash. “Critical Cuttings Transport Velocity in Inclined Annulus: Experimental Studies and Numerical Simulation,” n.d., 12.

Mendez, Michael; Garcia, Sergio; Ahmed, Ramadan; Karami, Hamidreza; Nasser, Mustafa; and Ibnelwaleed Hussein. "Effect of Fluid Rheology on the Performance of Fibrous Fluid in Horizontal Well Cleanout." Paper presented at the SPE/ICoTA Well Intervention Conference and Exhibition, The Woodlands, Texas, USA, March 2022. doi: https://doi-org.ezproxy.lib.ou.edu/10.2118/209018-MS

Morrison, Faith A. *Understanding Rheology*. Topics in Chemical Engineering. New York: Oxford University Press, 2001.

Naik, S. 2015. Effect of Fluid Rheology and Flow Rate on Wellbore Cleanout Operations in Horizontal and Deviated Wells. PhD dissertation, University of Oklahoma, Norman, Oklahoma.

Ozbayoglu, Evren M, Middle East Technical University, Arild Saasen, and Statoil Asa. “Estimating Critical Velocity To Prevent Bed Development for Horizontal-Inclined Wellbores,” n.d., 6.

Pandya, S., Ahmed, R., and Shah, S. 2020. Wellbore Cleanout in Inclined and Horizontal Wellbores: The Effects of Flow Rate, Fluid Rheology, and Solids Density. SPE Drill & Compl 35 (1): 48–68. SPE-194240-PA. https://doi.org/10.2118/194240-PA

Power, D J, C Hight, D Weisinger, and C Rimer. "Drilling Practices and Sweep Selection for Efficient Hole Cleaning in Deviated Wellbores," n.d., 9.

Ramadan, A, P Skalle, and S.T Johansen. "A Mechanistic Model to Determine the Critical Flow Velocity Required to Initiate the Movement of Spherical Bed Particles in Inclined Channels." *Chemical Engineering Science* 58, no. 10 (May 2003): 2153–63. https://doi.org/10.1016/S0009-2509(03)00061-7.

Rodriguez Corredor, Fabio Ernesto, Majid Bizhani, and Ergun Kuru. "A Comparative Study of Hole Cleaning Performance — Water Versus Drag Reducing Fluid." In *Volume 5: Materials Technology; Petroleum Technology*, V005T11A018. San Francisco, California, USA: American Society of Mechanical Engineers, 2014. https://doi.org/10.1115/OMAE2014-24083.

Sanchez, R. Alfredo, J. J. Azar, A. A. Bassal, and A. L. Martins. "Effect of Drillpipe Rotation on Hole Cleaning During Directional-Well Drilling." *SPE Journal* 4, no. 02 (June 1, 1999): 101–8. https://doi.org/10.2118/56406-PA.

Sifferman, T. R., and T. E. Becker. "Hole Cleaning in Full-Scale Inclined Wellbores." *SPE Drilling Engineering* 7, no. 02 (June 1, 1992): 115–20. https://doi.org/10.2118/20422-PA.

Song, Xianzhi, Zhengming Xu, Mengshu Wang, Gensheng Li, S. N. Shah, and Zhaoyu Pang. "Experimental Study on the Wellbore-Cleaning Efficiency of Microhole-Horizontal-Well Drilling." *SPE Journal* 22, no. 04 (August 11, 2017): 1189–1200. https://doi.org/10.2118/185965-PA.

Valluri, S. G., Miska, S. Z., Ahmed, R. et al. 2008. Experimental Study of Effective Hole Cleaning Using "Sweeps" in Horizontal Wellbores. Paper presented at the SPE Annual Technical Conference and Exhibition, San Antonio, Texas, USA, 24–27 September. SPE-101220-MS. https://doi.org/10.2118/101220-MS.

Walker, S., and J. Li. "The Effects of Particle Size, Fluid Rheology, and Pipe Eccentricity on Cuttings Transport." In *All Days*, SPE-60755-MS. Houston, Texas: SPE, 2000. https://doi.org/10.2118/60755-MS.

Appendix

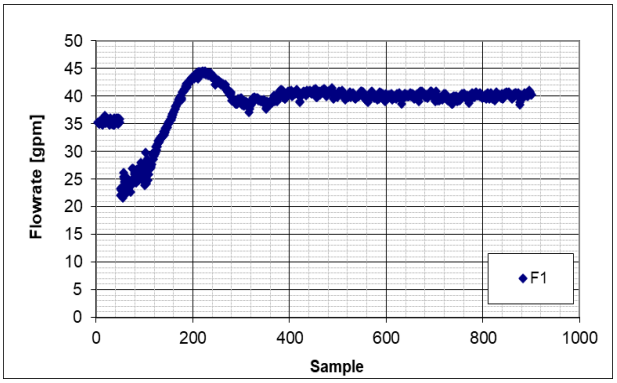

a) Stabilized flowrate (40 GPM) @0 RPM

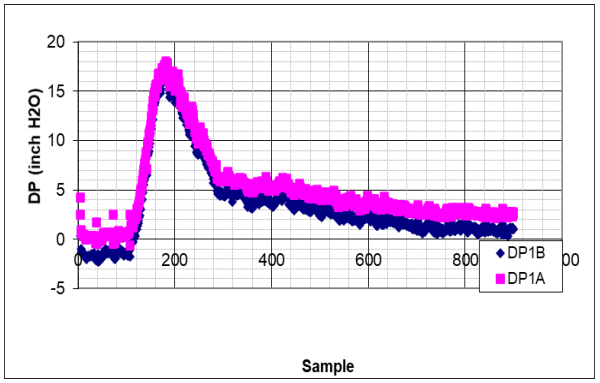

b) Pressure during the test at 40 GPM @0 RPM

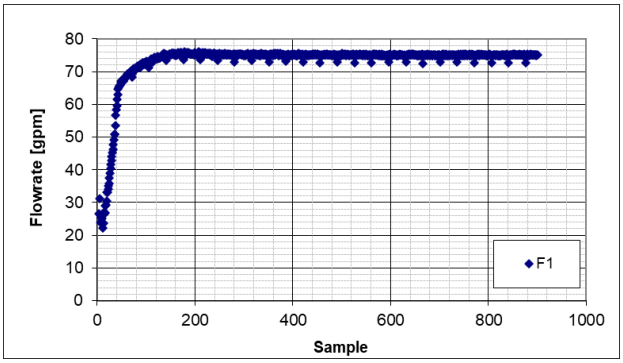

c) Stabilized flowrate (75 GPM) @0 RPM

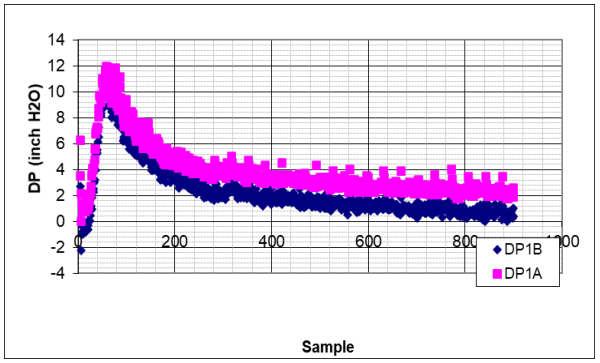

d) Pressure during the test at 75 GPM @0 RPM

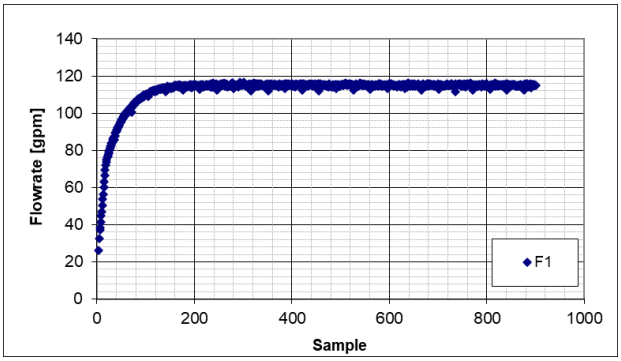

e) Stabilized flowrate (115 GPM) @0 RPM

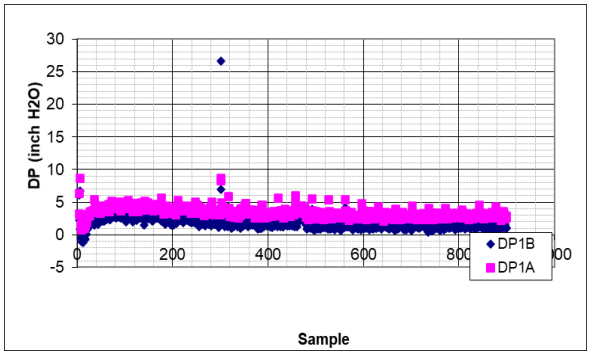

f) Pressure during the test at 115 GPM @0 RPM

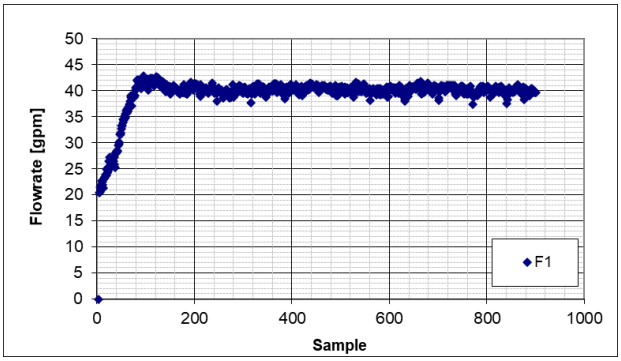

a) Stabilized flowrate (40 GPM) @50 RPM

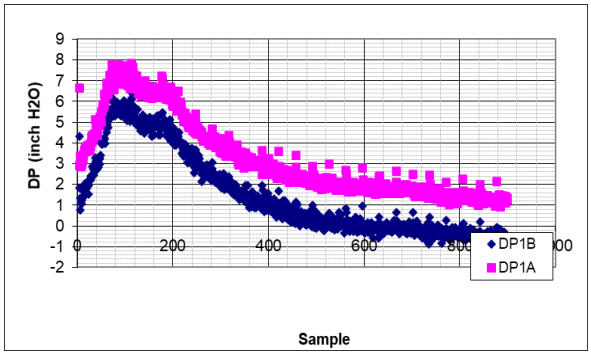

b) Pressure during the test at 40 GPM @50 RPM

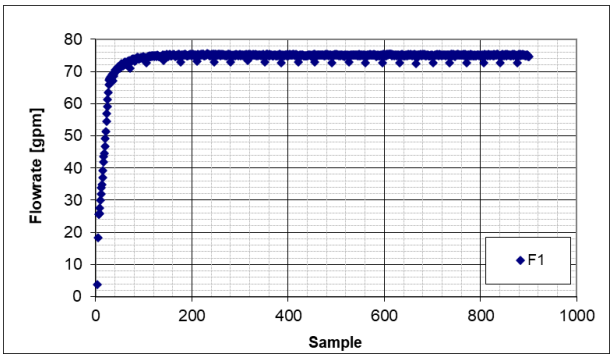

c) **Stabilized flowrate (75 GPM) @50 RPM**

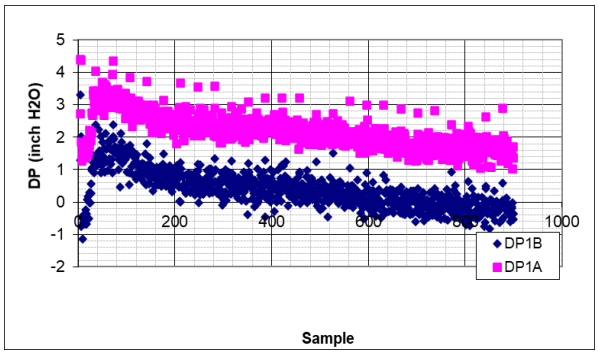

d) **Pressure during the test at 75 GPM @50 RPM**

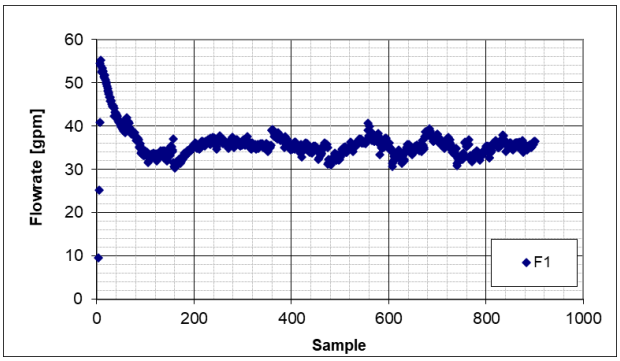

e) **Stabilized flowrate (35 GPM) @100 RPM**

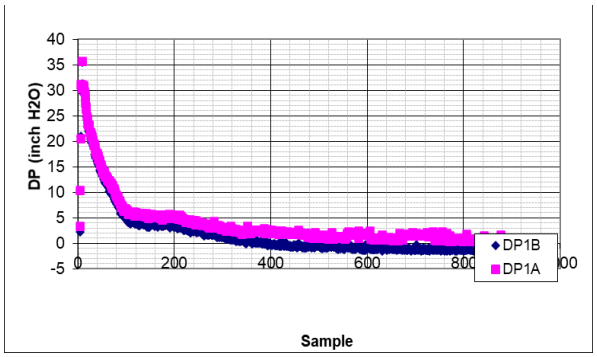

f) **Pressure during the test at 35 GPM @100 RPM**

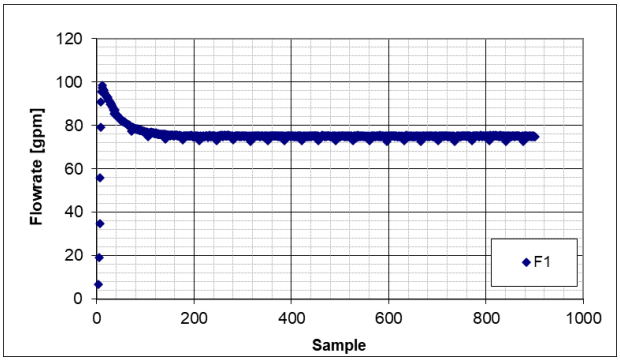

g) **Stabilized flowrate (75 GPM) @100 RPM**

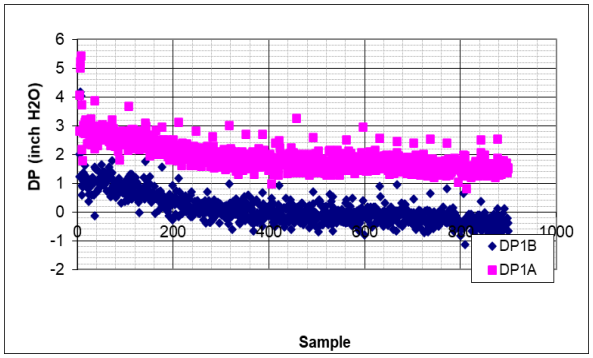

h) **Pressure during the test at 75 GPM @100 RPM**

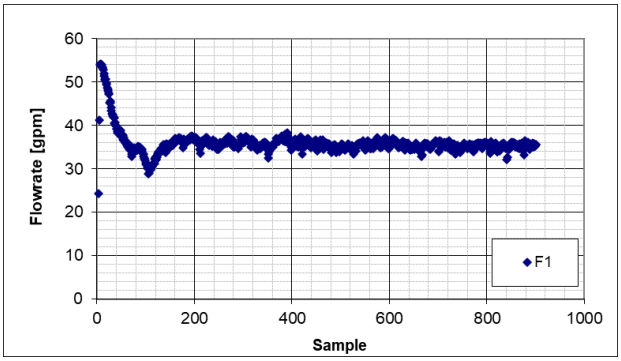

i) **Stabilized flowrate (35 GPM) @150 RPM**

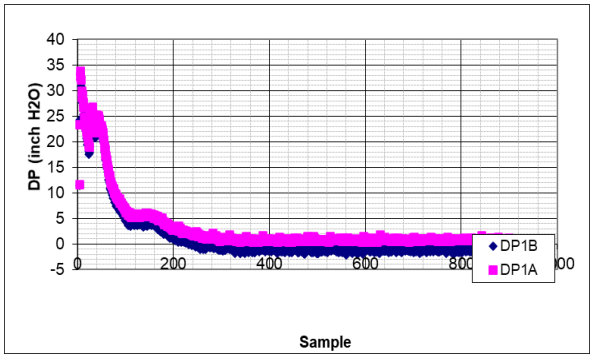

j) **Pressure during the test at 35 GPM @150 RPM**

Figure A.1 Water test flowrate and pressure plots

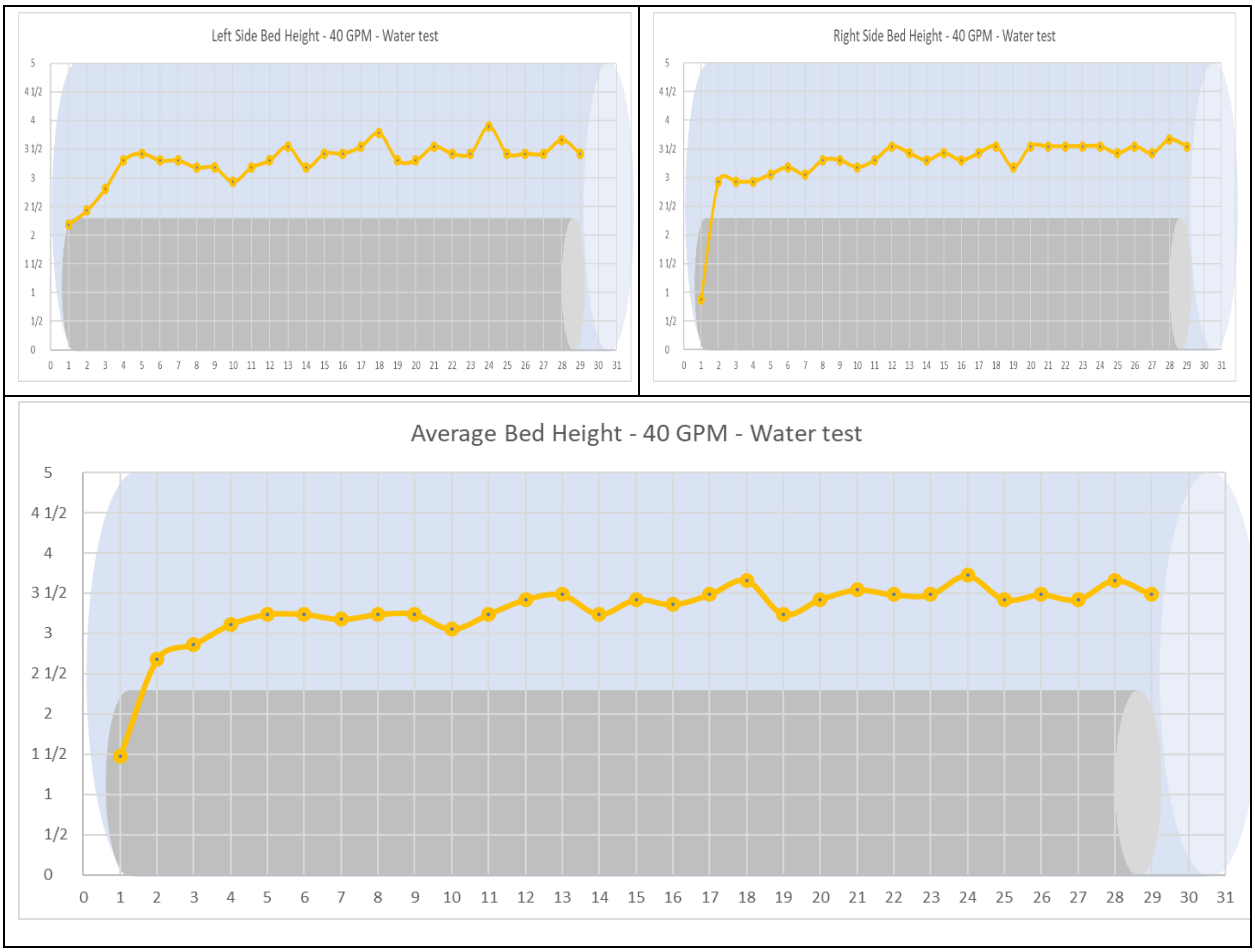

Figure A.2 Water test left-side, right-side, and average bed profiles (40 GPM, 0 RPM)

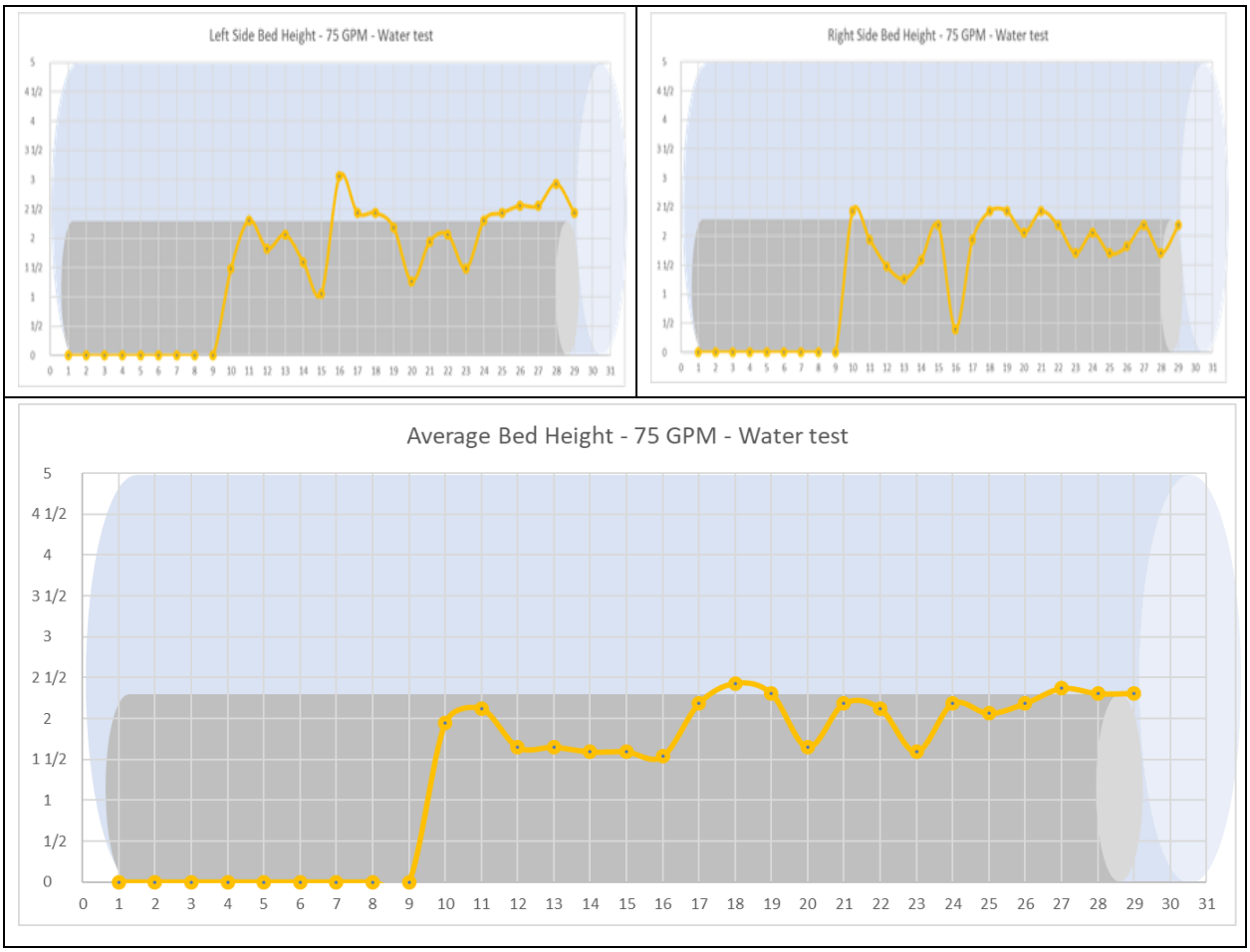

Figure A.3 Water test left-side, right-side, and average bed profiles (75 GPM, 0 RPM)

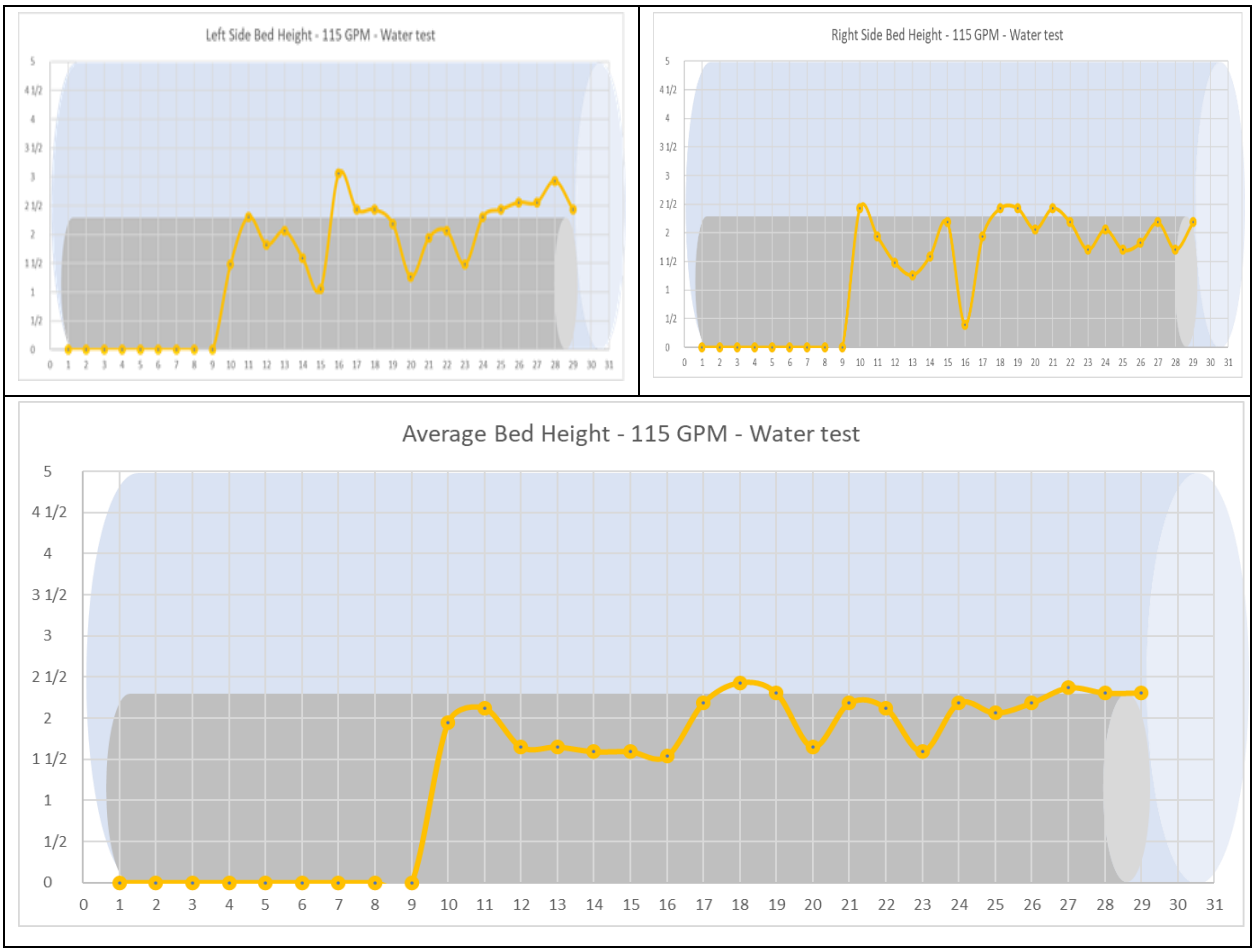

Figure A.4 Water test left-side, right-side, and average bed profiles (115 GPM, 0 RPM)

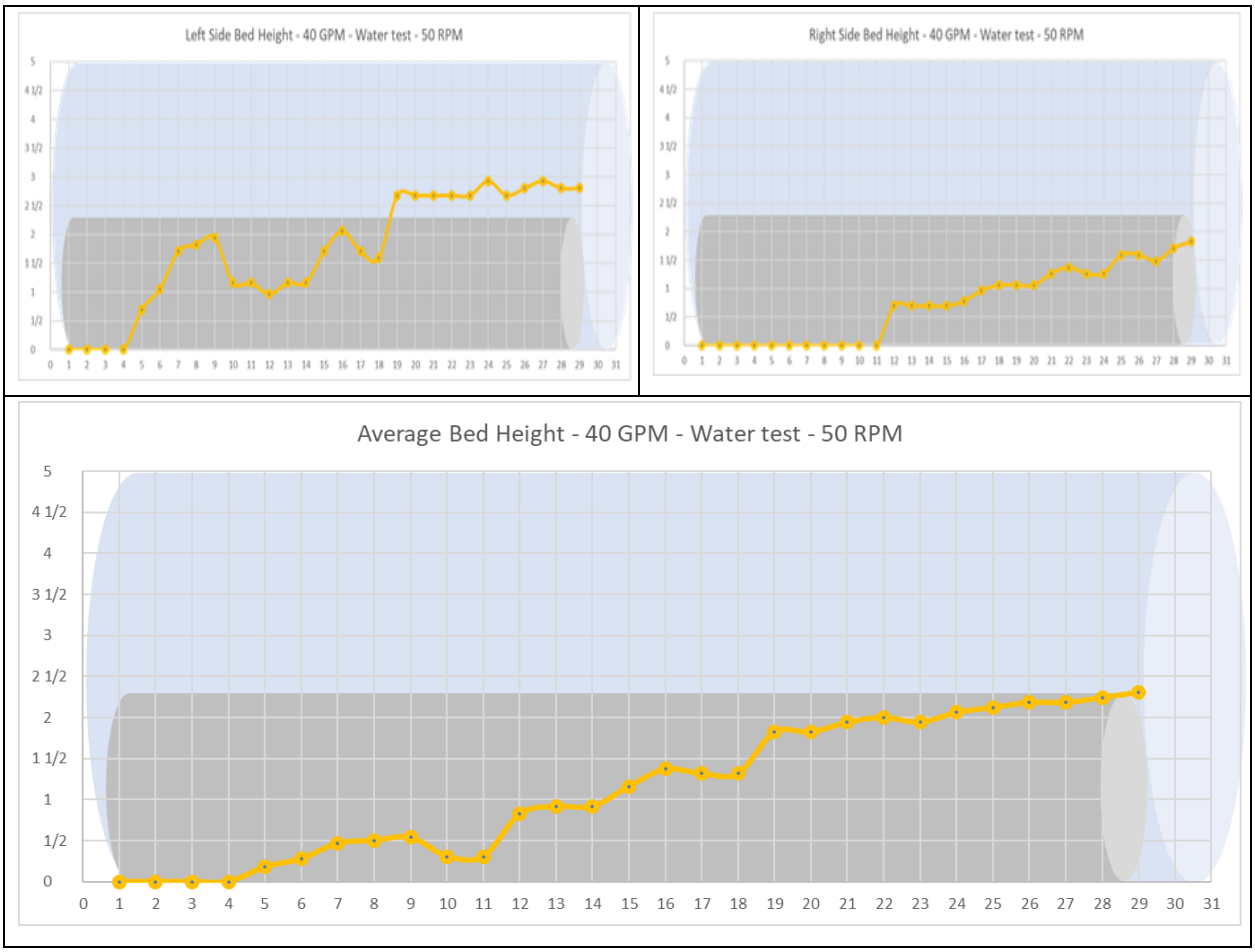

Figure A.5 Water test left-side, right-side, and average bed profiles (40 GPM, 50 RPM)

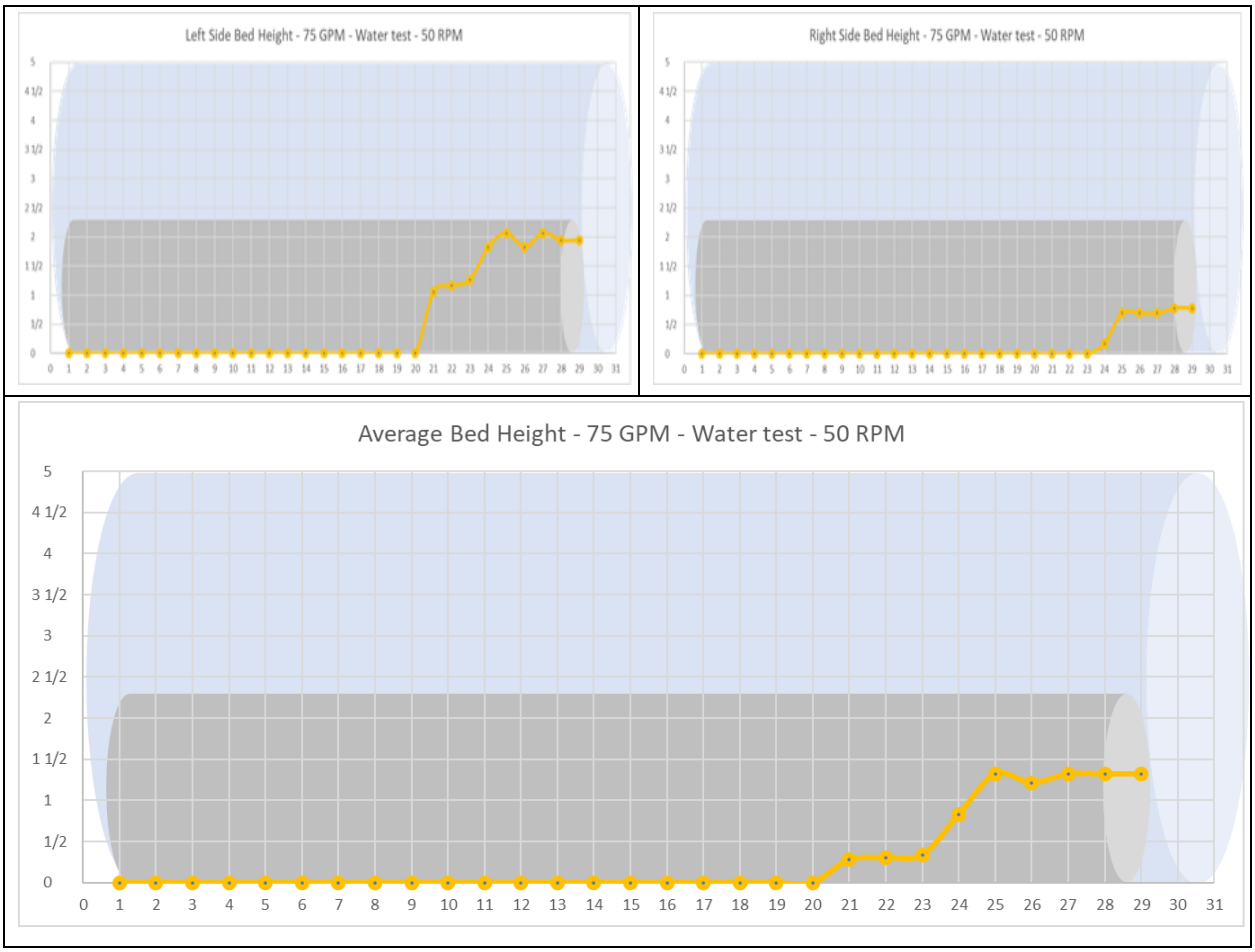

Figure A.6 Water test left-side, right-side, and average bed profiles (75 GPM, 50 RPM)

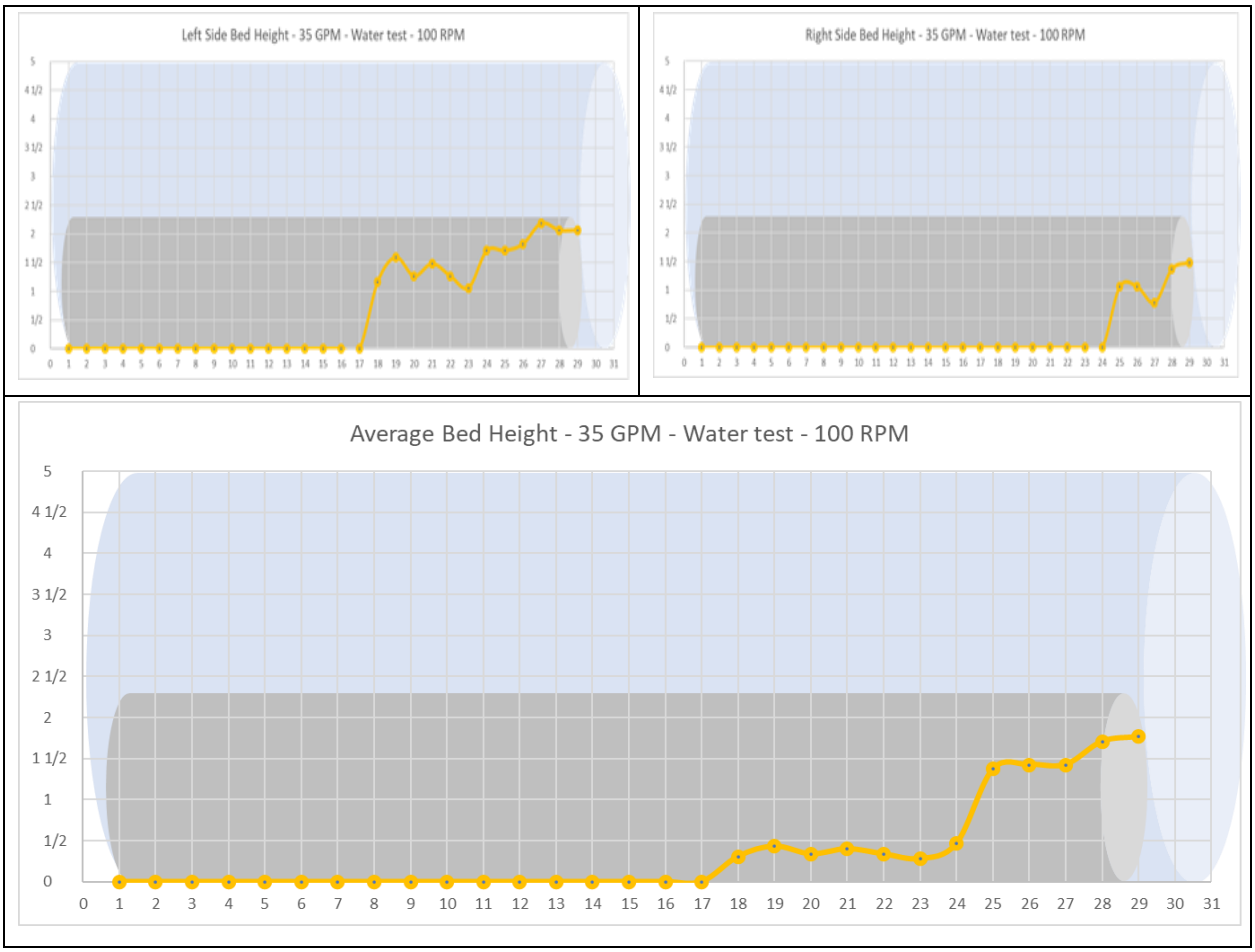

Figure A.7 Water test left-side, right-side, and average bed profiles (35 GPM, 100 RPM)

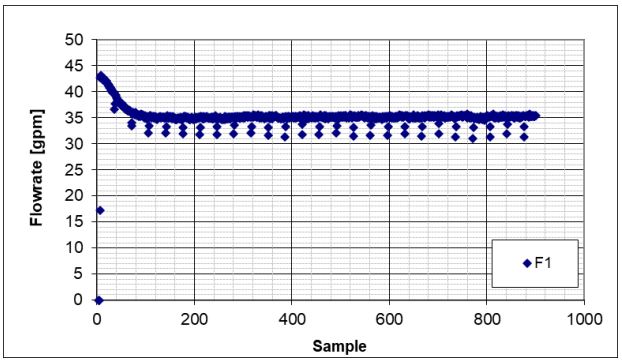

a) Stabilized flowrate (35 GPM) @0 RPM

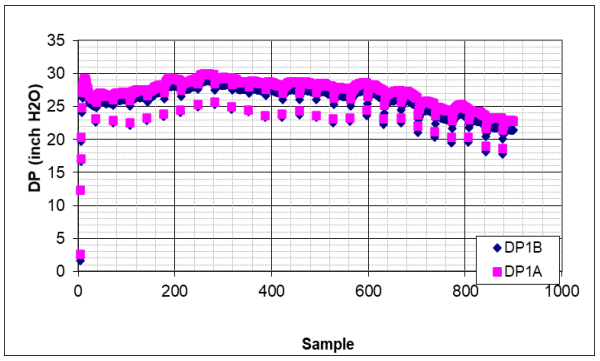

b) Pressure during the test at 35 GPM @0 RPM

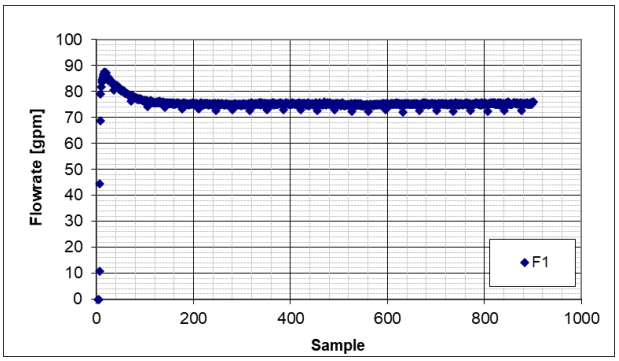

c) Stabilized flowrate (75 GPM) @0 RPM

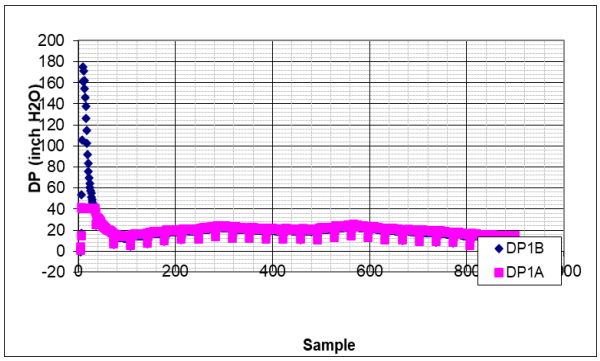

d) Pressure during the test at 75 GPM @0 RPM

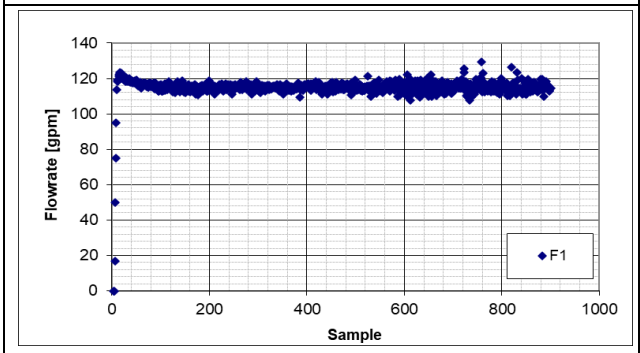

e) Stabilized flowrate (115 GPM) @0 RPM

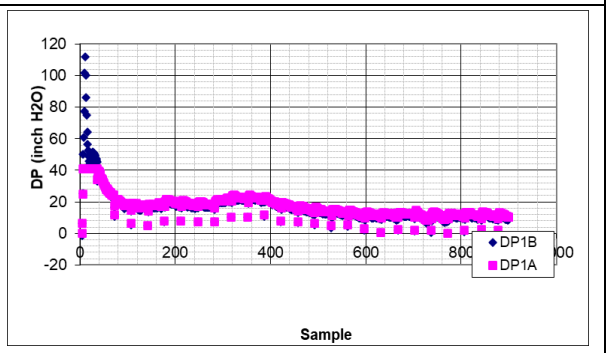

f) Pressure during the test at 115 GPM @0 RPM

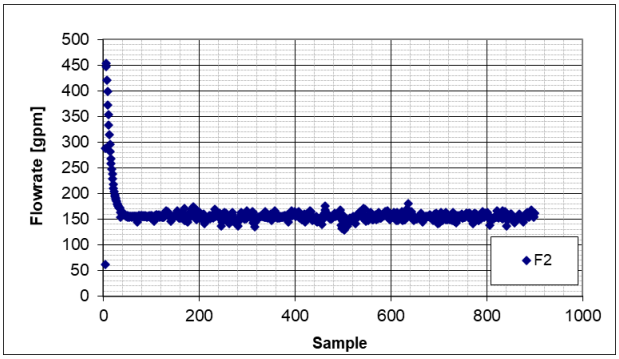

g) Stabilized flowrate (155 GPM) @0 RPM

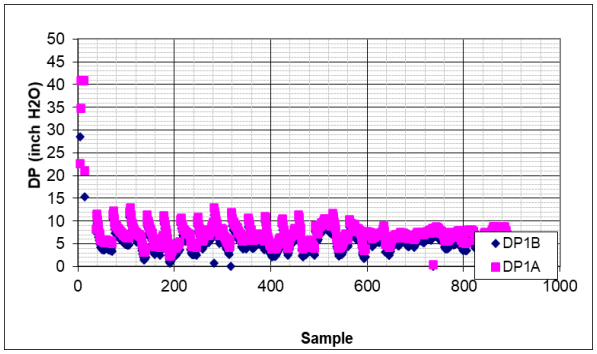

h) Pressure during the test at 155 GPM @0 RPM

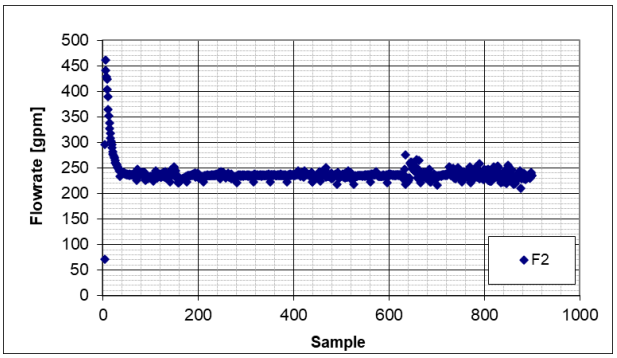

i) **Stabilized flowrate (195 GPM) @0 RPM**

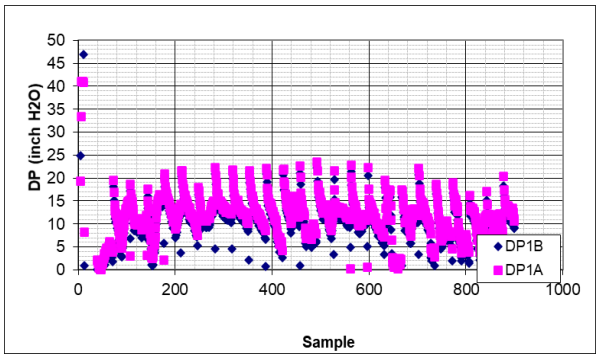

j) **Pressure during the test at 195 GPM @0 RPM**

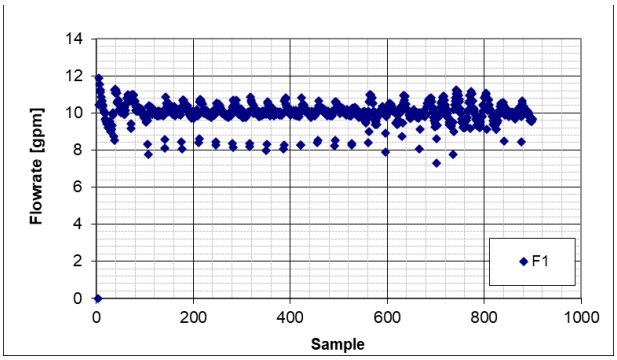

k) **Stabilized flowrate (10 GPM) @50 RPM**

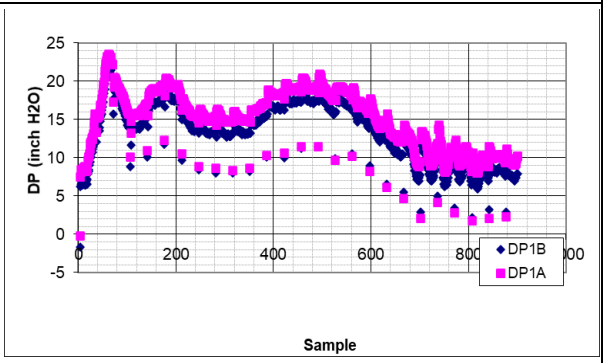

l) **Pressure during the test at 10 GPM @50 RPM**

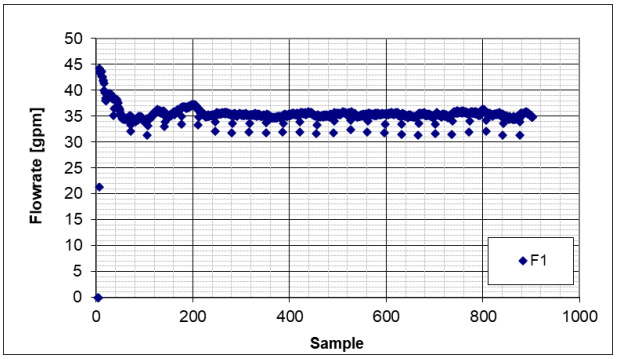

m) **Stabilized flowrate (35 GPM) @50 RPM**

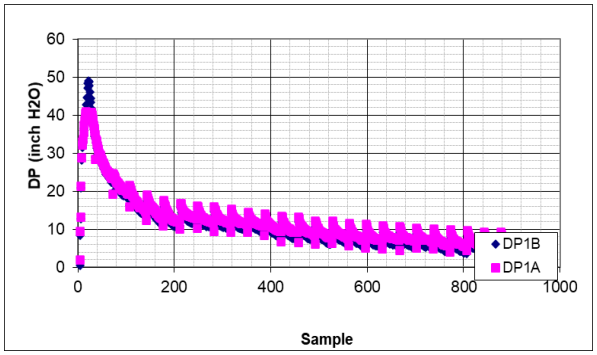

n) **Pressure during the test at 35 GPM @50 RPM**

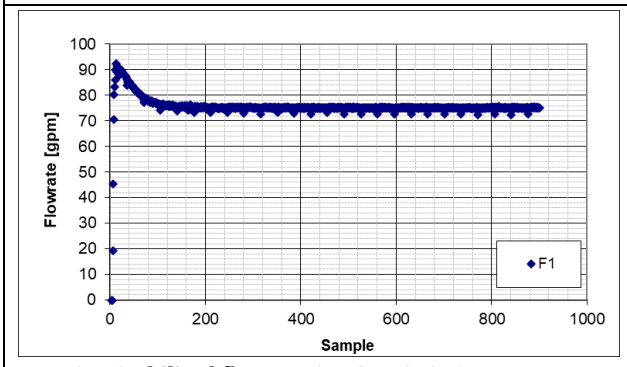

o) **Stabilized flowrate (75 GPM) @50 RPM**

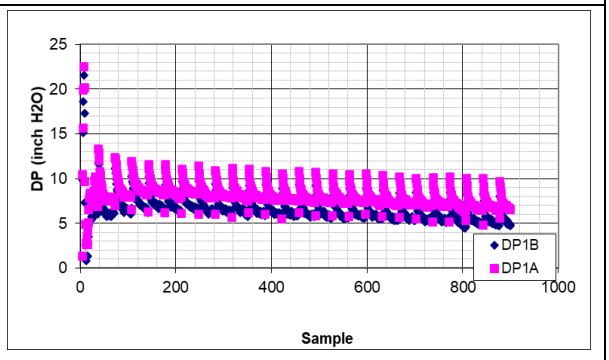

p) **Pressure during the test at 75 GPM @50 RPM**

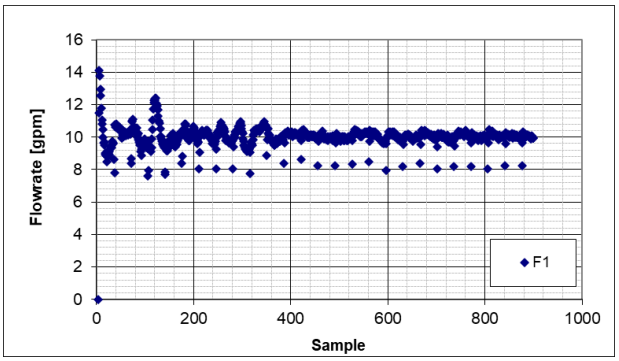

q) **Stabilized flowrate (10 GPM) @100 RPM**

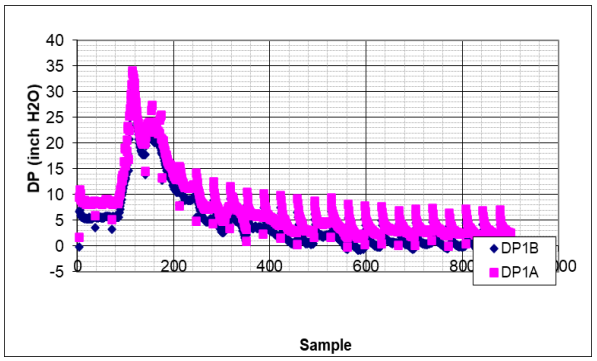

r) **Pressure during the test at 10 GPM @100 RPM**

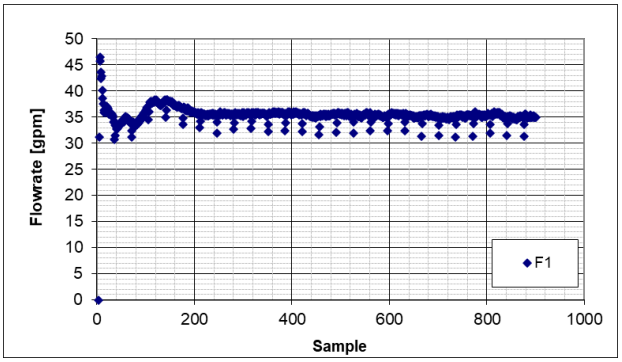

s) **Stabilized flowrate (35 GPM) @100 RPM**

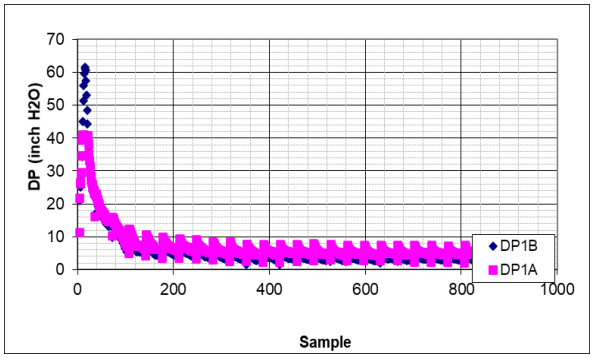

t) **Pressure during the test at 35 GPM @100 RPM**

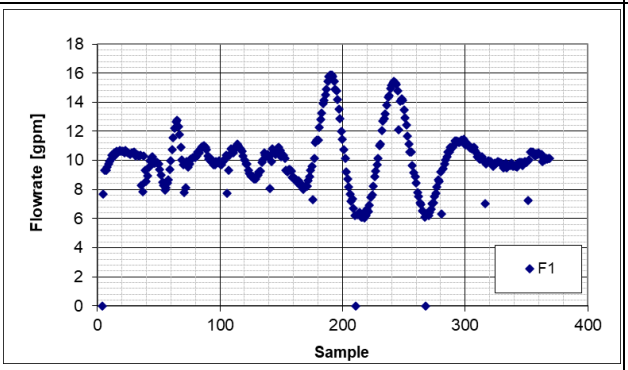

u) **Stabilized flowrate (10 GPM) @150 RPM**

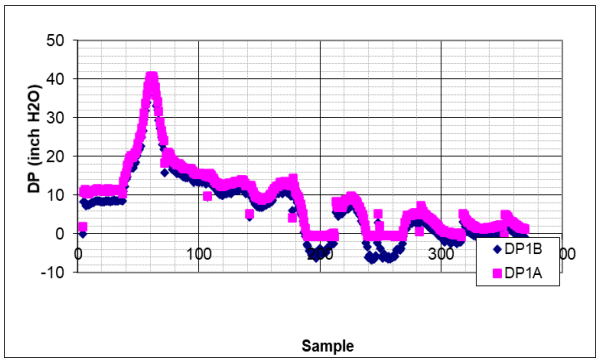

v) **Pressure during the test at 10 GPM @150 RPM**

Figure A.8 Base cleaning flowrate and pressure plots

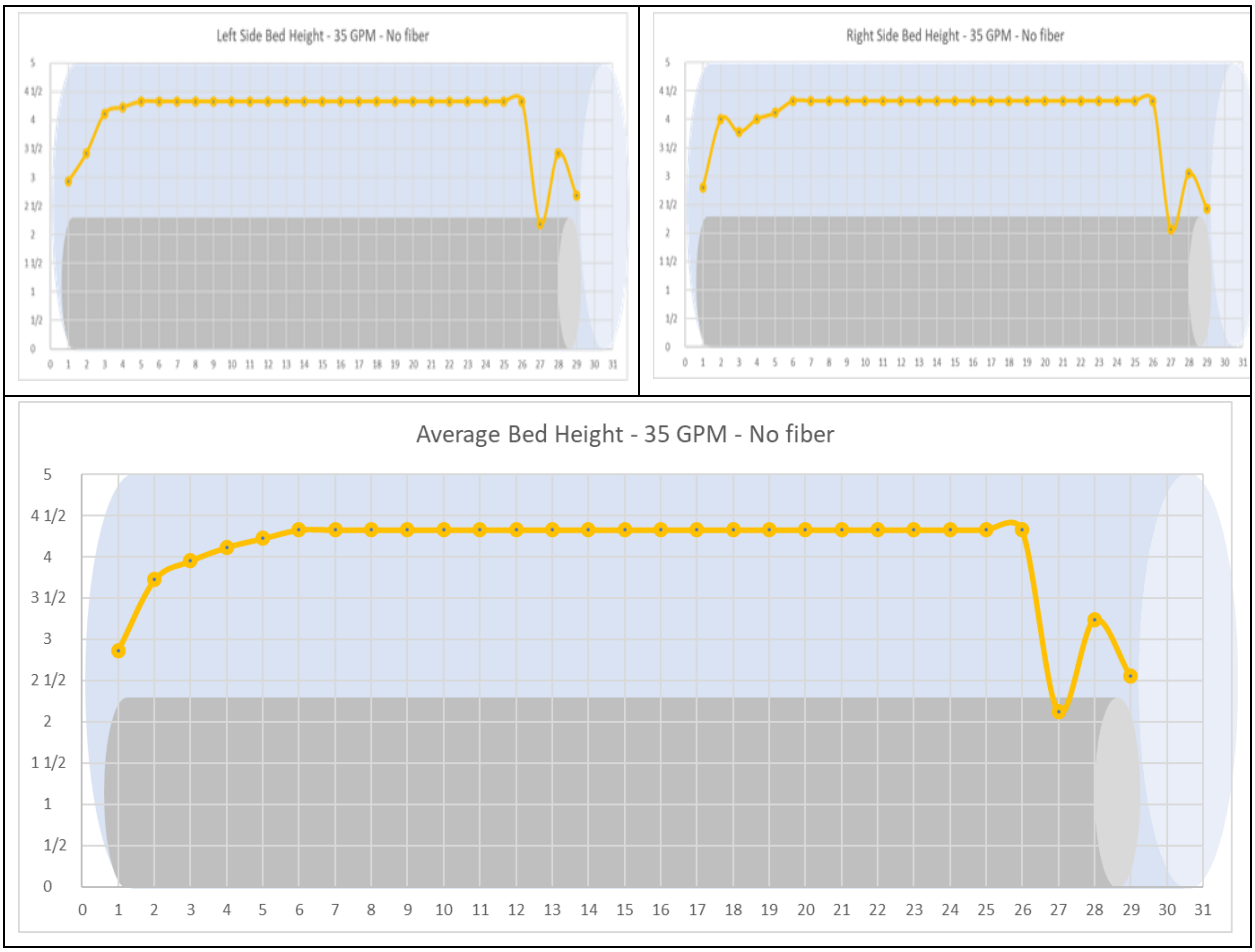

Figure A.9 Base cleaning fluid left-side, right-side, and average bed profiles (35 GPM, 0 RPM)

Figure A.10 Base cleaning fluid left-side, right-side, and average bed profiles (75 GPM, 0 RPM)

Figure A.11 Base cleaning fluid left-side, right-side, and average bed profiles (115 GPM, 0 RPM)

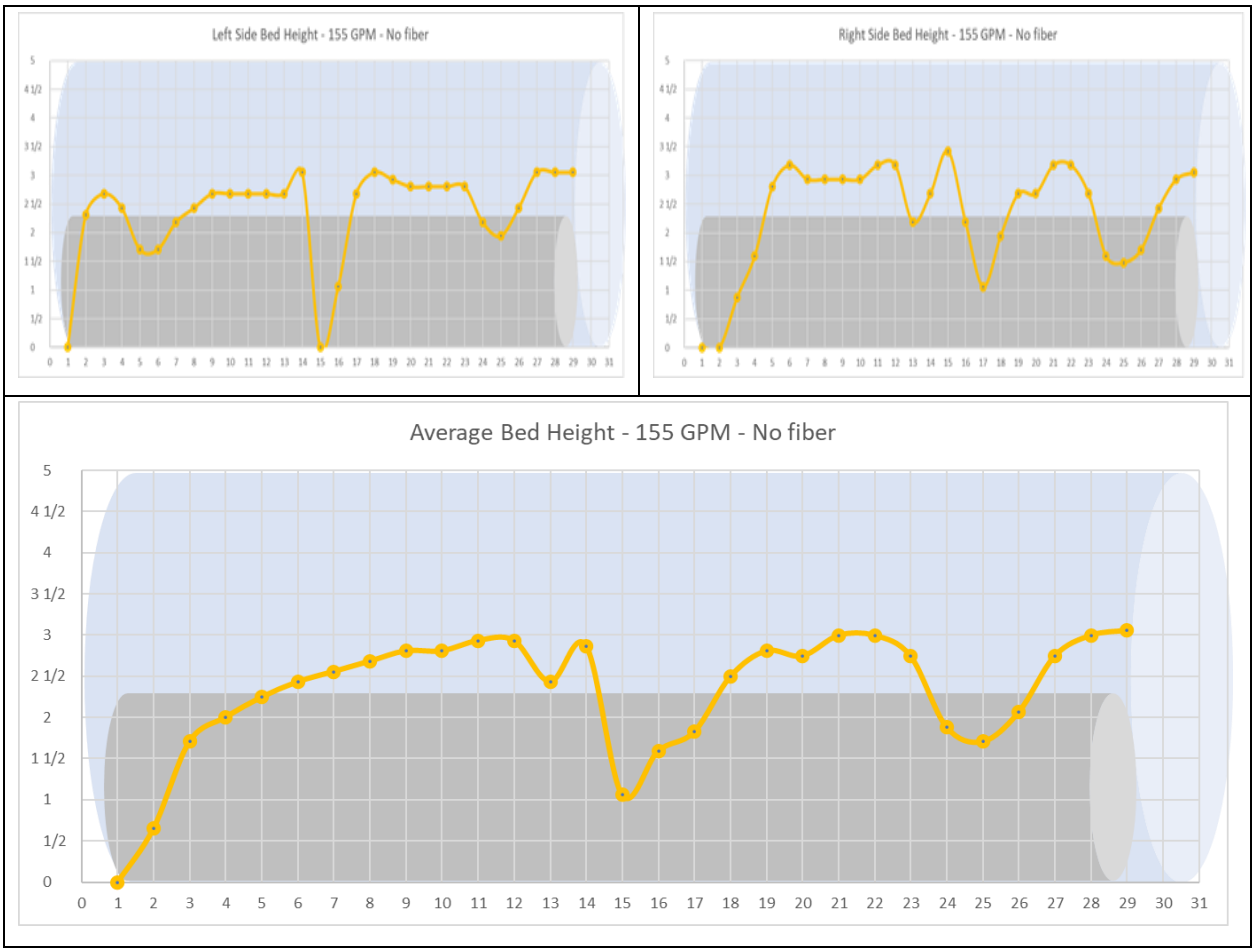

Figure A.12 Base cleaning fluid left-side, right-side, and average bed profiles (155 GPM, 0 RPM)

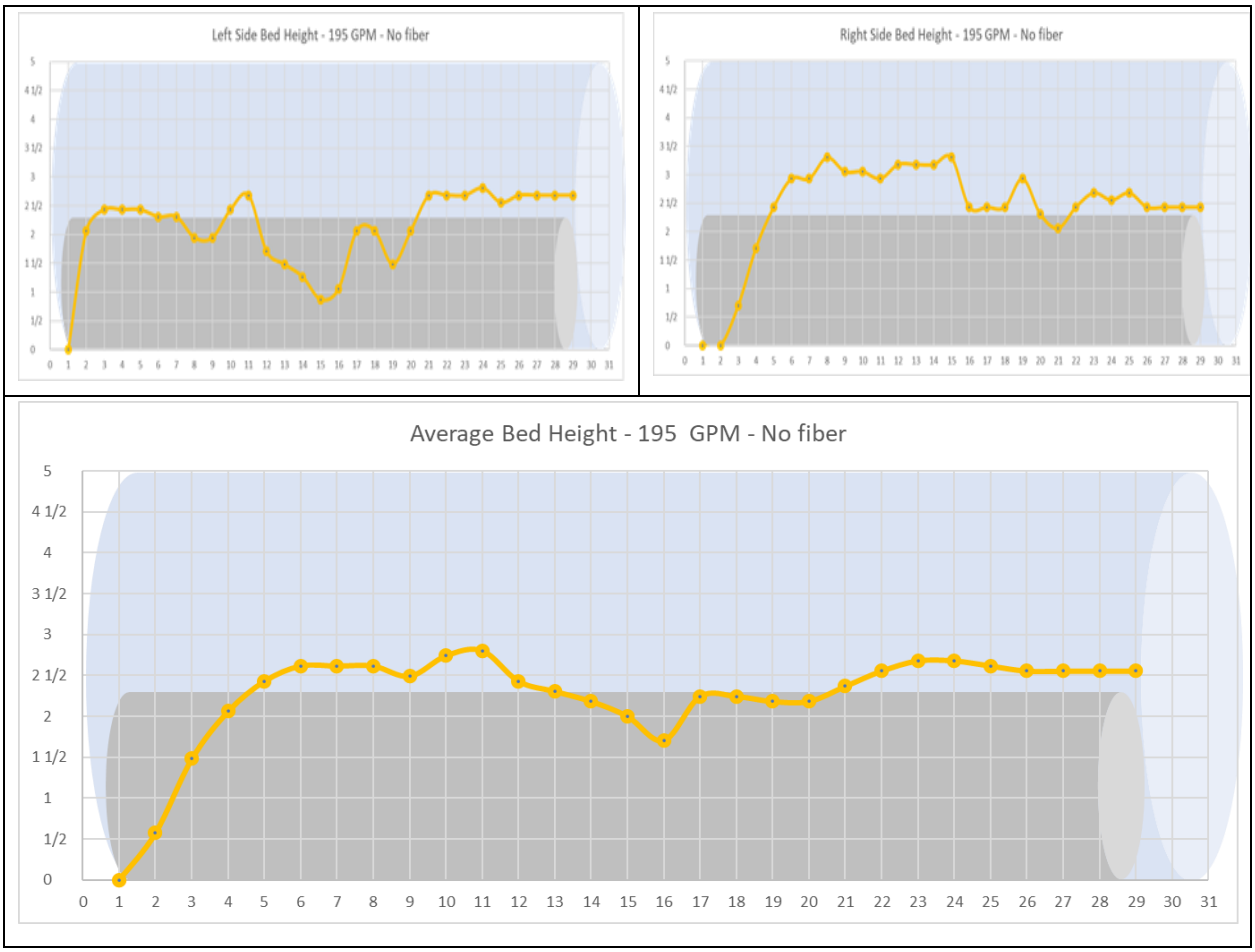

Figure A.13 Base cleaning fluid left-side, right-side, and average bed profiles (195 GPM, 0 RPM)

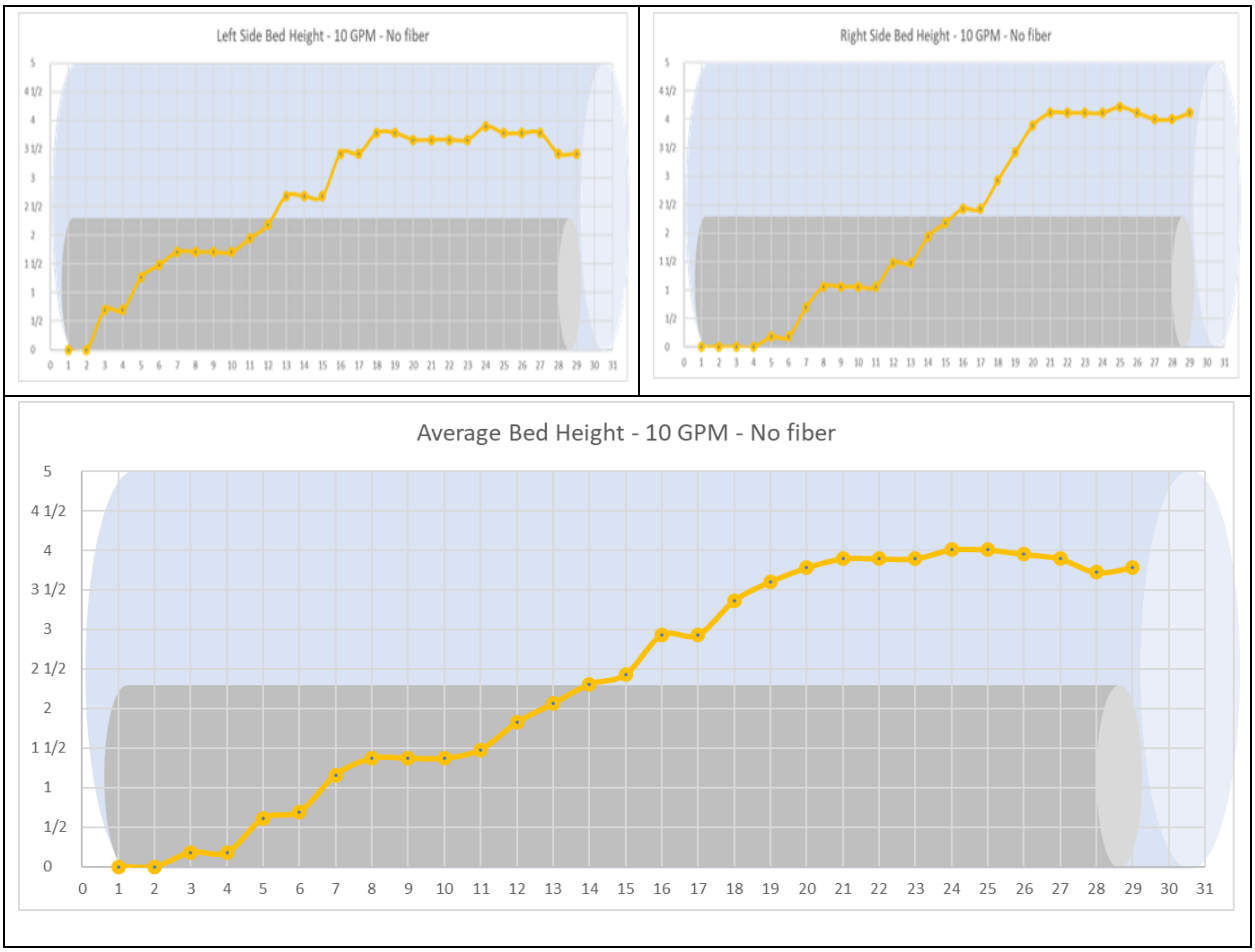

Figure A.14 Base cleaning fluid left-side, right-side, and average bed profiles (10 GPM, 50 RPM)

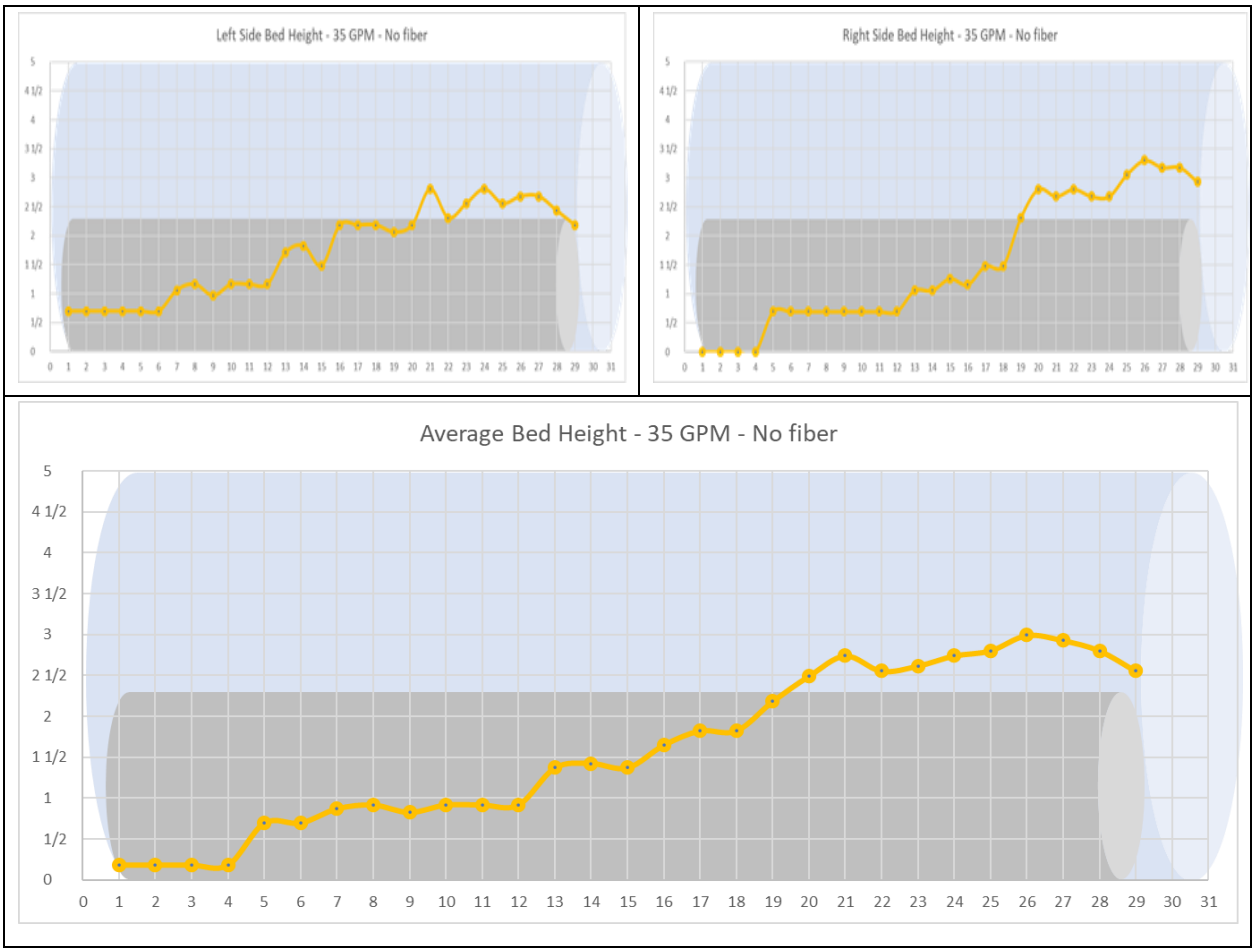

Figure A.15 Base cleaning fluid left-side, right-side, and average bed profiles (35 GPM, 50 RPM)

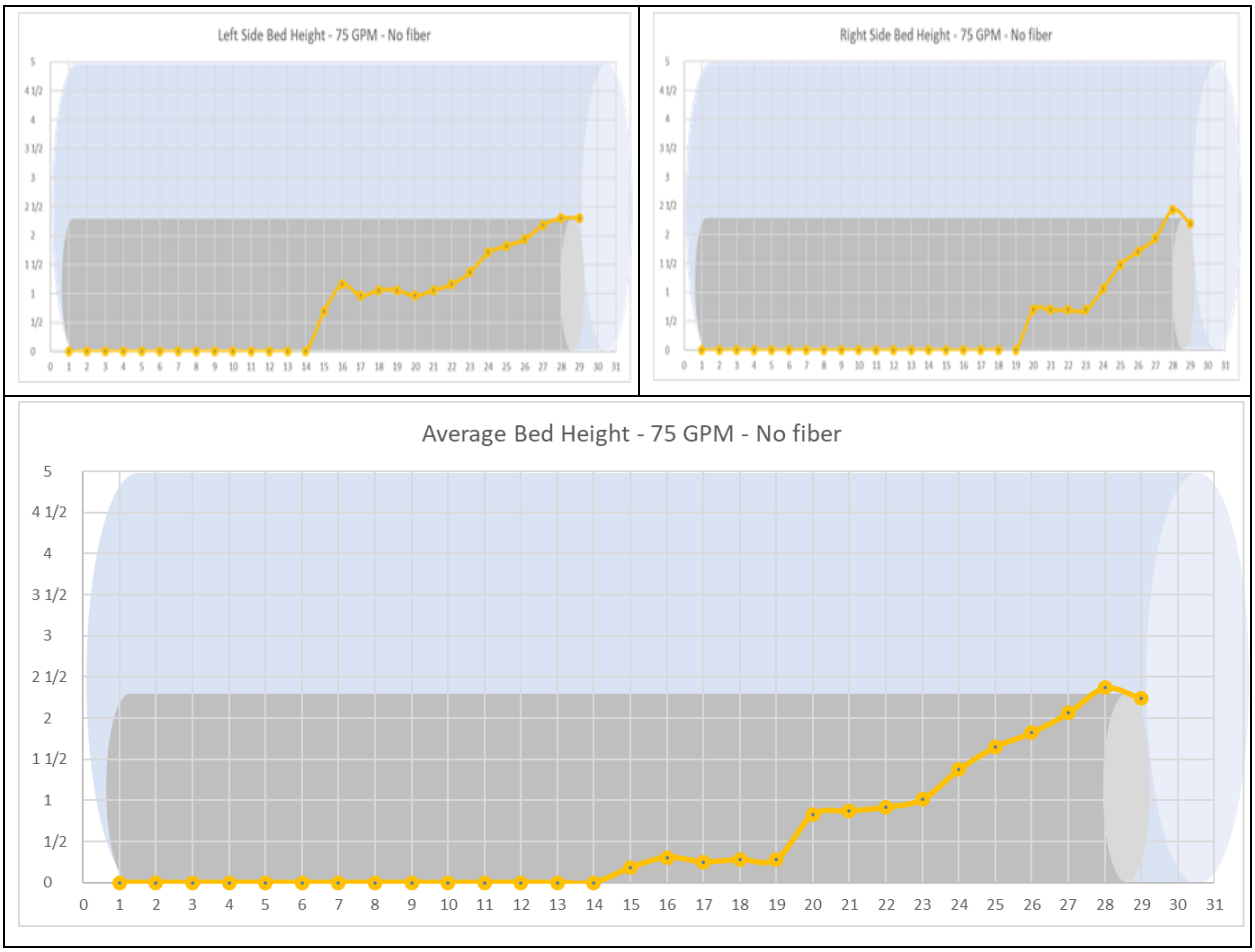

Figure A.16 Base cleaning fluid left-side, right-side, and average bed profiles (75 GPM, 50 RPM)

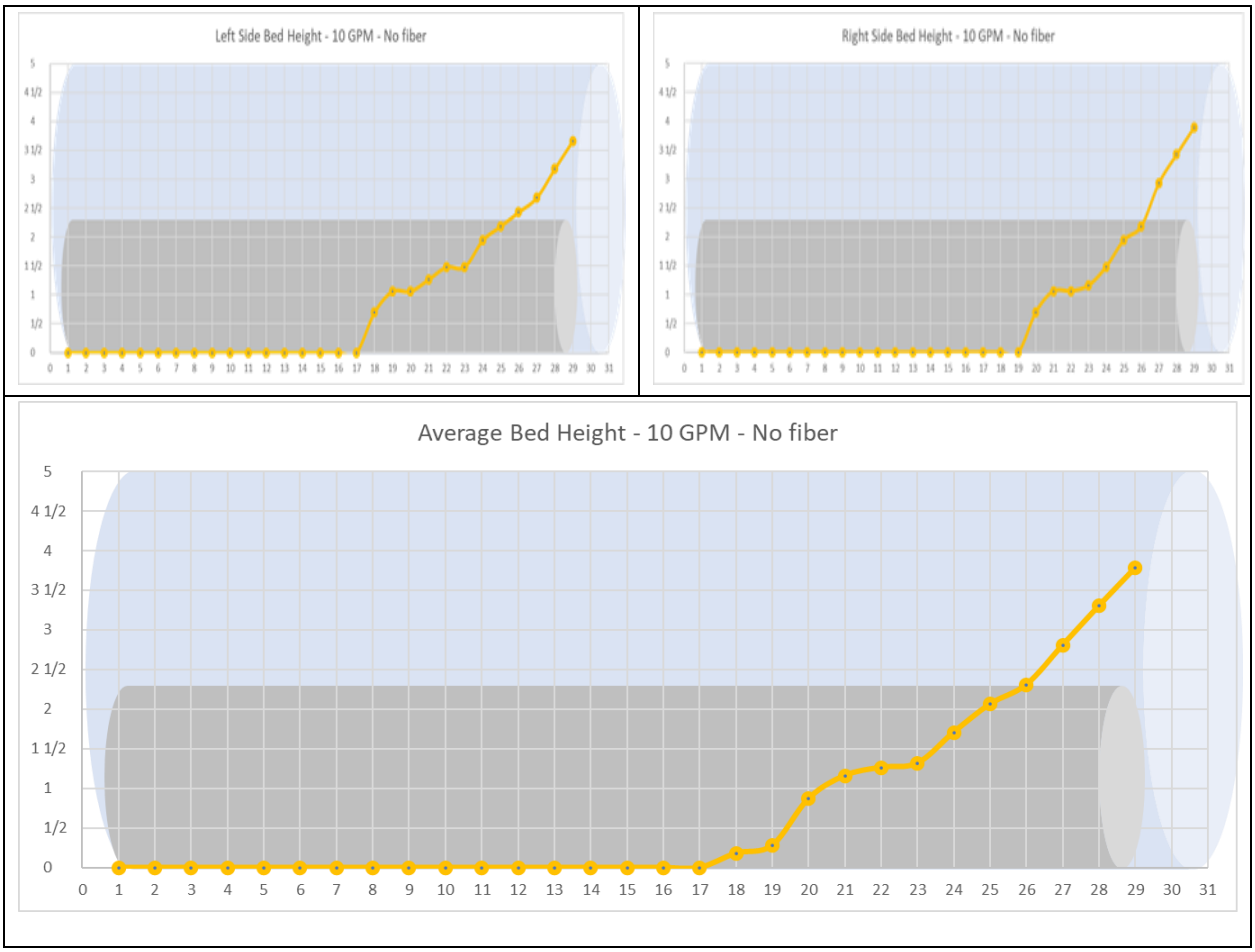

Figure A.17 Base cleaning fluid left-side, right-side, and average bed profiles (10 GPM, 100 RPM)

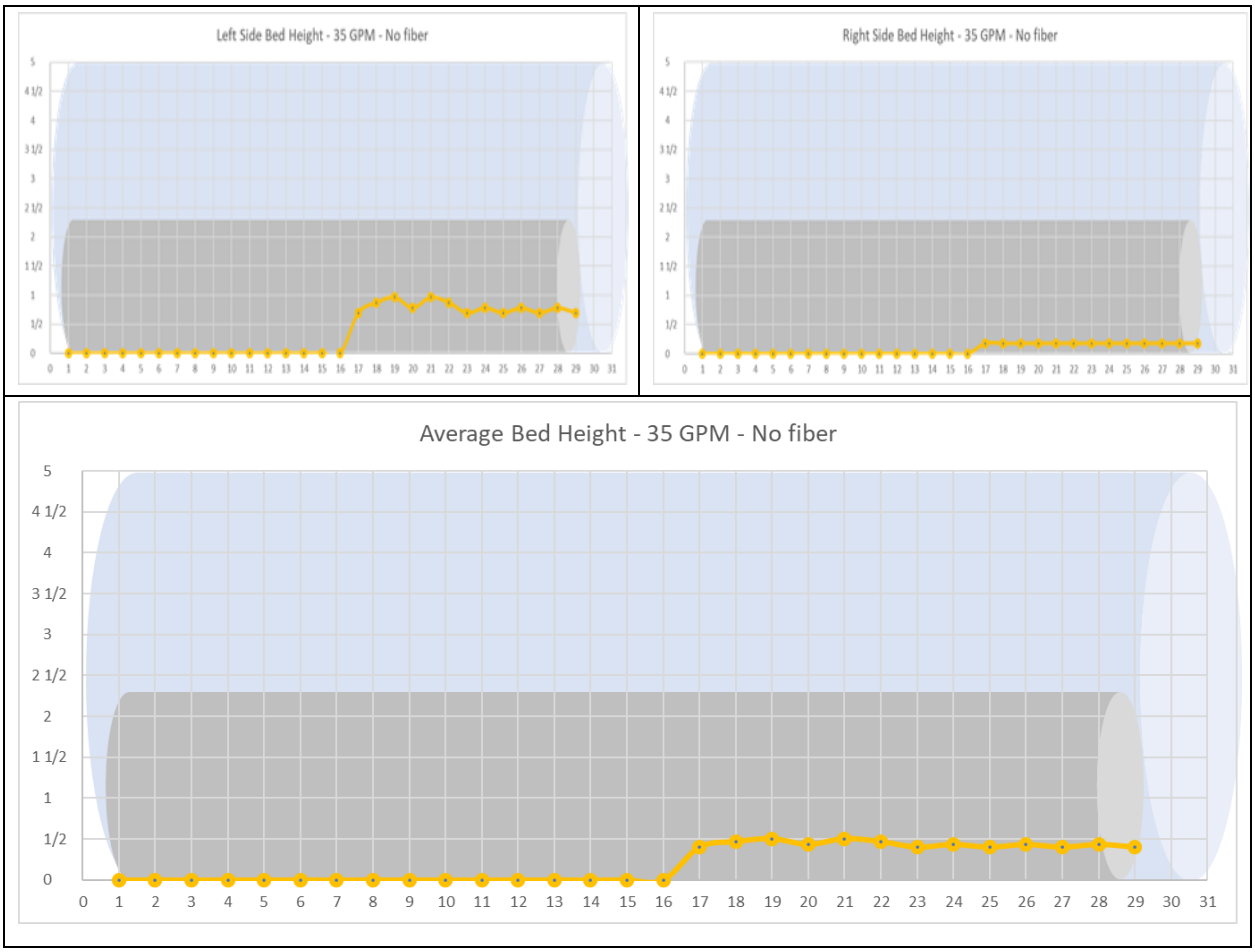

Figure A.18 Base cleaning fluid left-side, right-side, and average bed profiles (35 GPM, 100 RPM)

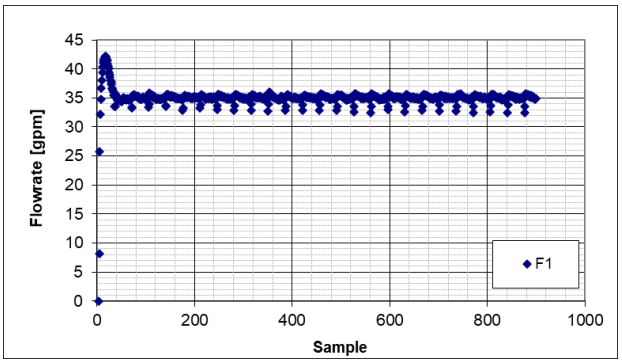

a) Stabilized flowrate (35 GPM) @0 RPM

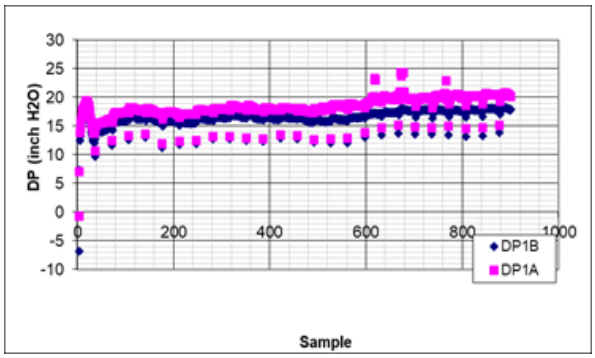

b) Pressure during the test at 35 GPM @0 RPM

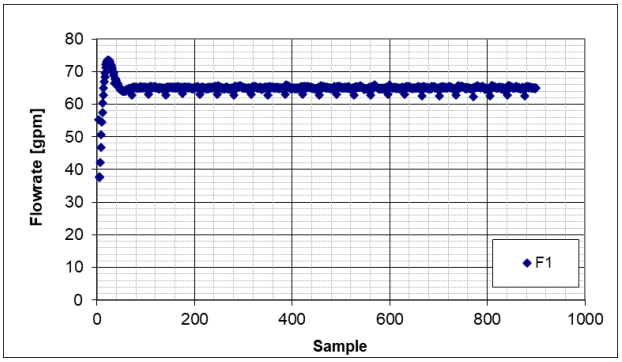

c) Stabilized flowrate (65 GPM) @0 RPM

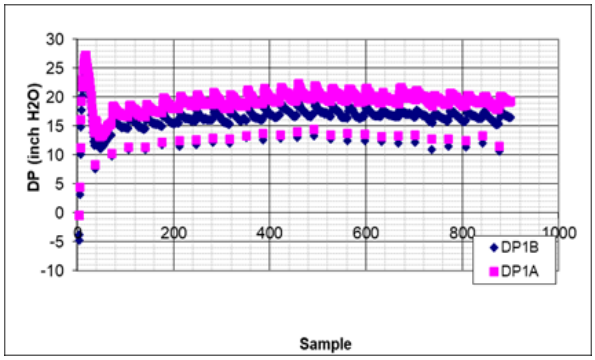

d) Pressure during the test at 65 GPM @0 RPM

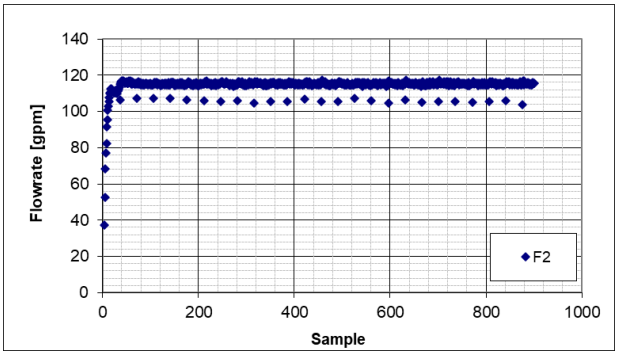

e) Stabilized flowrate (115 GPM) @0 RPM

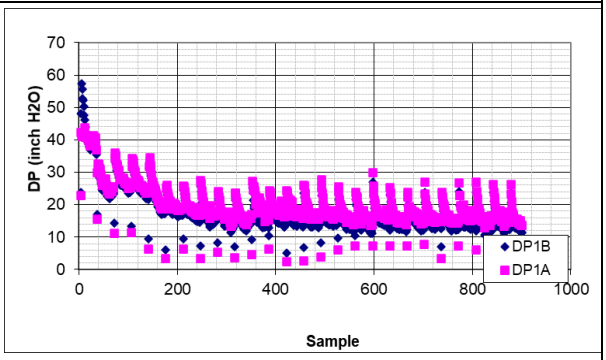

f) Pressure during the test at 115 GPM @0 RPM

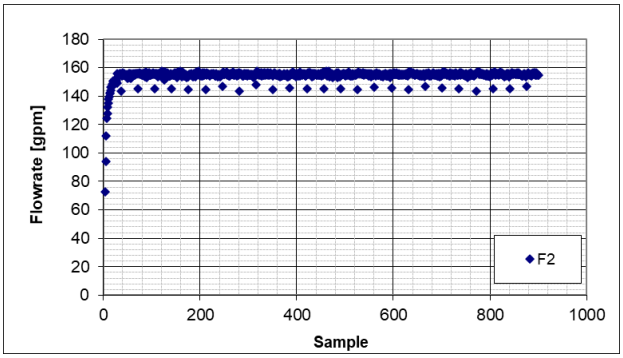

g) Stabilized flowrate (155 GPM) @0 RPM

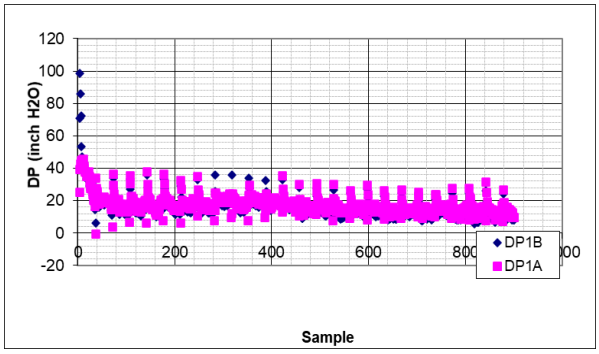

h) Pressure during the test at 155 GPM @0 RPM

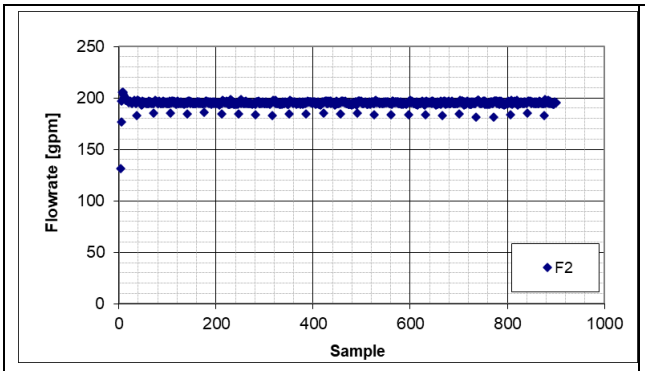

i) **Stabilized flowrate (195 GPM) @0 RPM**

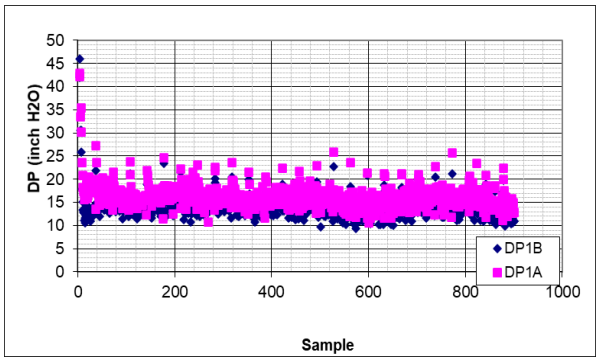

j) **Pressure during the test at 195 GPM @0 RPM**

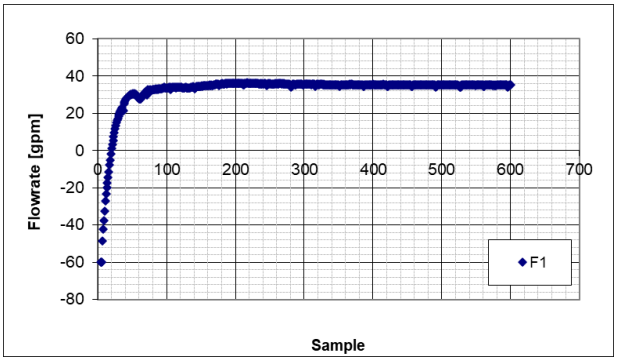

k) **Stabilized flowrate (35 GPM) @50 RPM**

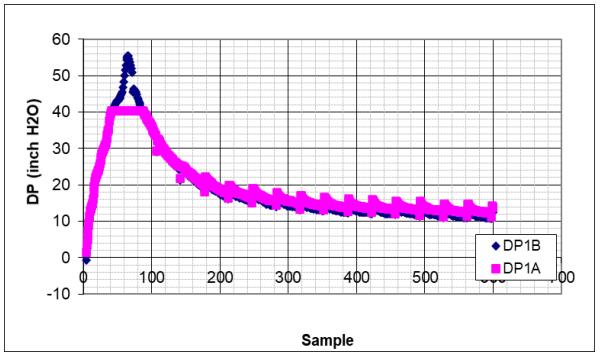

l) **Pressure during the test at 35 GPM @50 RPM**

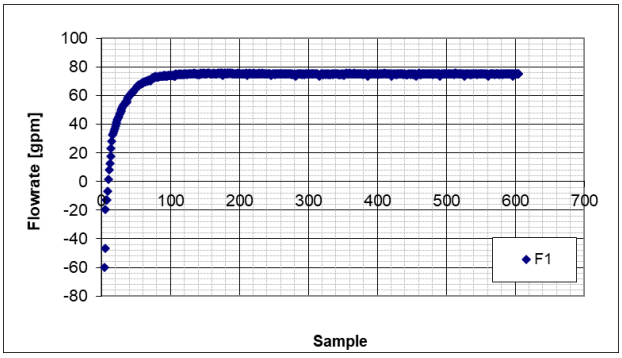

m) **Stabilized flowrate (75 GPM) @50 RPM**

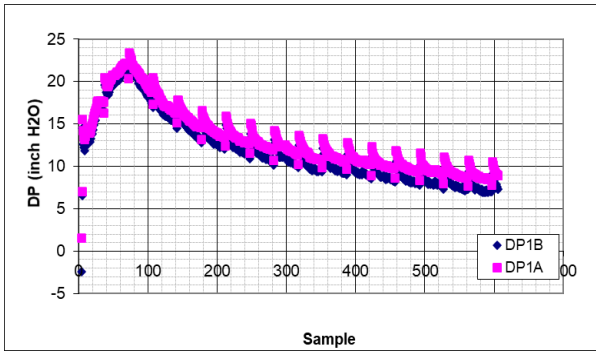

n) **Pressure during the test at 75 GPM @50 RPM**

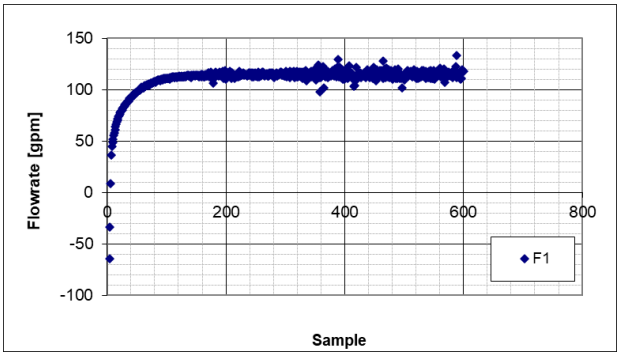

o) **Stabilized flowrate (115 GPM) @50 RPM**

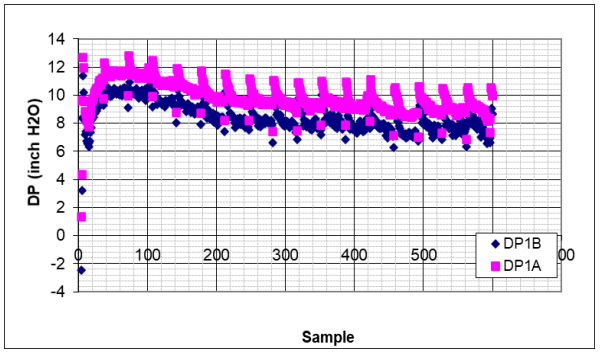

p) **Pressure during the test at 115 GPM @50 RPM**

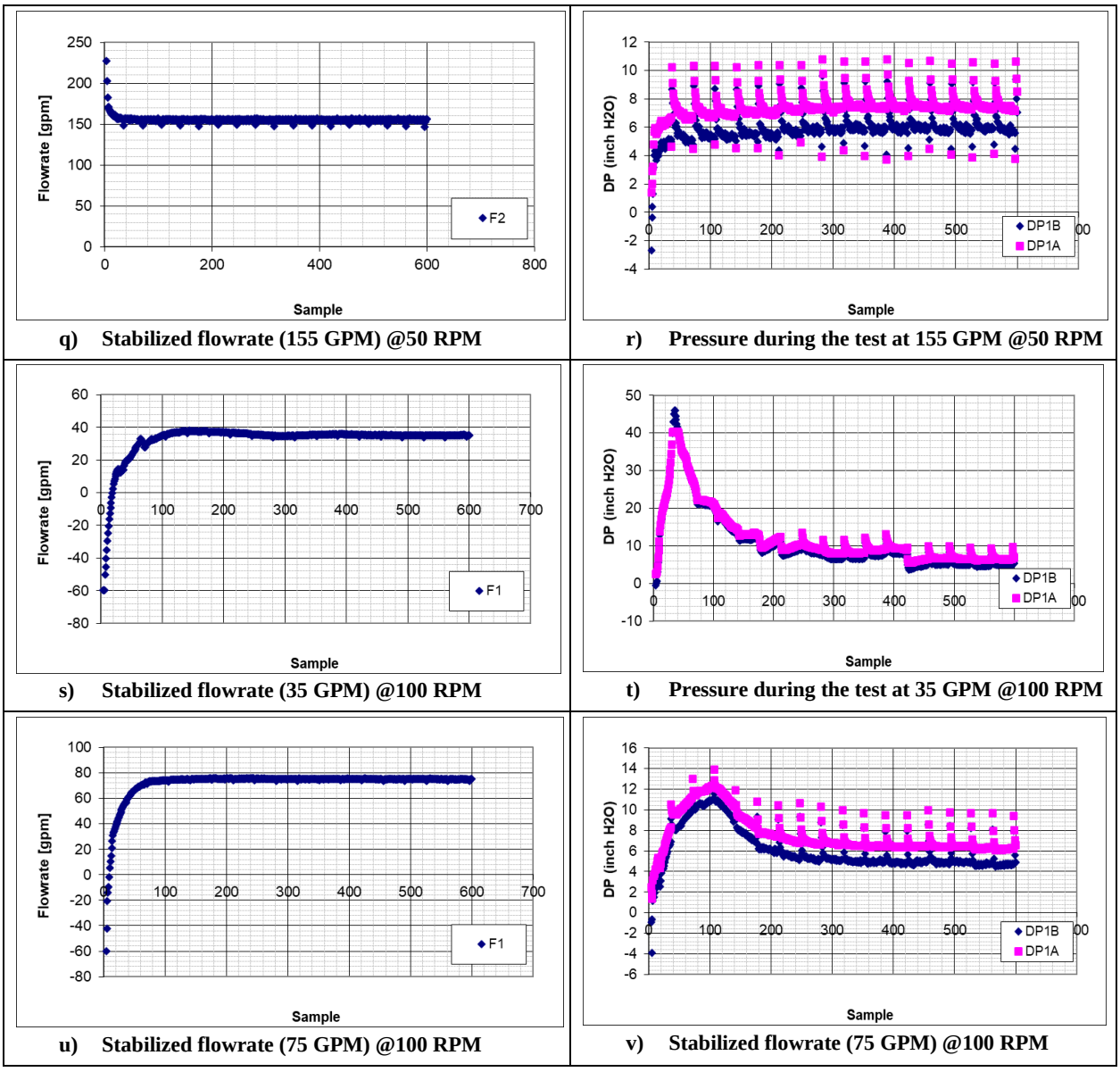

q) **Stabilized flowrate (155 GPM) @50 RPM**

r) **Pressure during the test at 155 GPM @50 RPM**

s) **Stabilized flowrate (35 GPM) @100 RPM**

t) **Pressure during the test at 35 GPM @100 RPM**

u) **Stabilized flowrate (75 GPM) @100 RPM**

v) **Stabilized flowrate (75 GPM) @100 RPM**

Figure A.19 Fibrous cleaning fluid flowrate and pressure plots

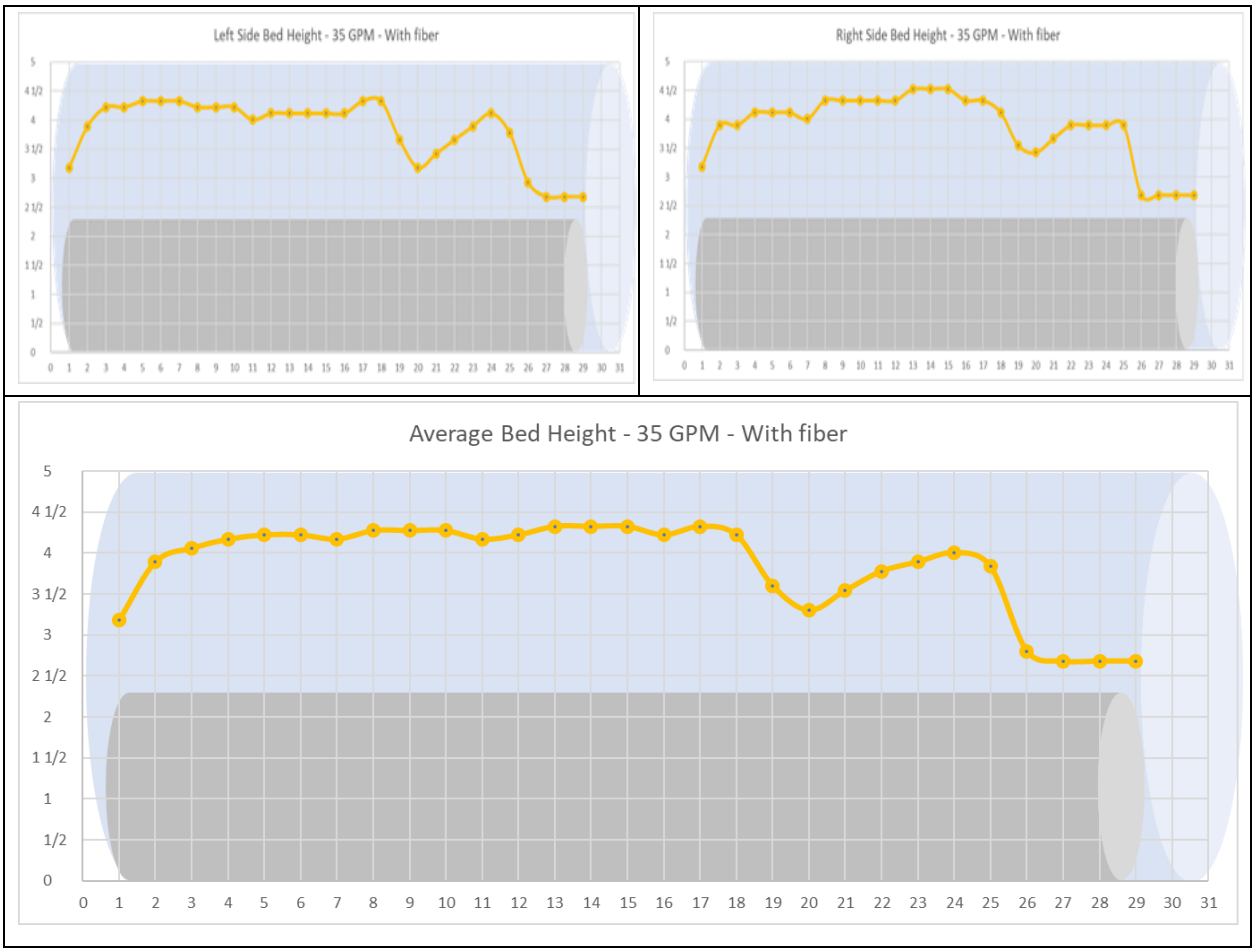

Figure A.20 Fibrous cleaning fluid left-side, right-side, and average bed profiles (35 GPM, 0 RPM)

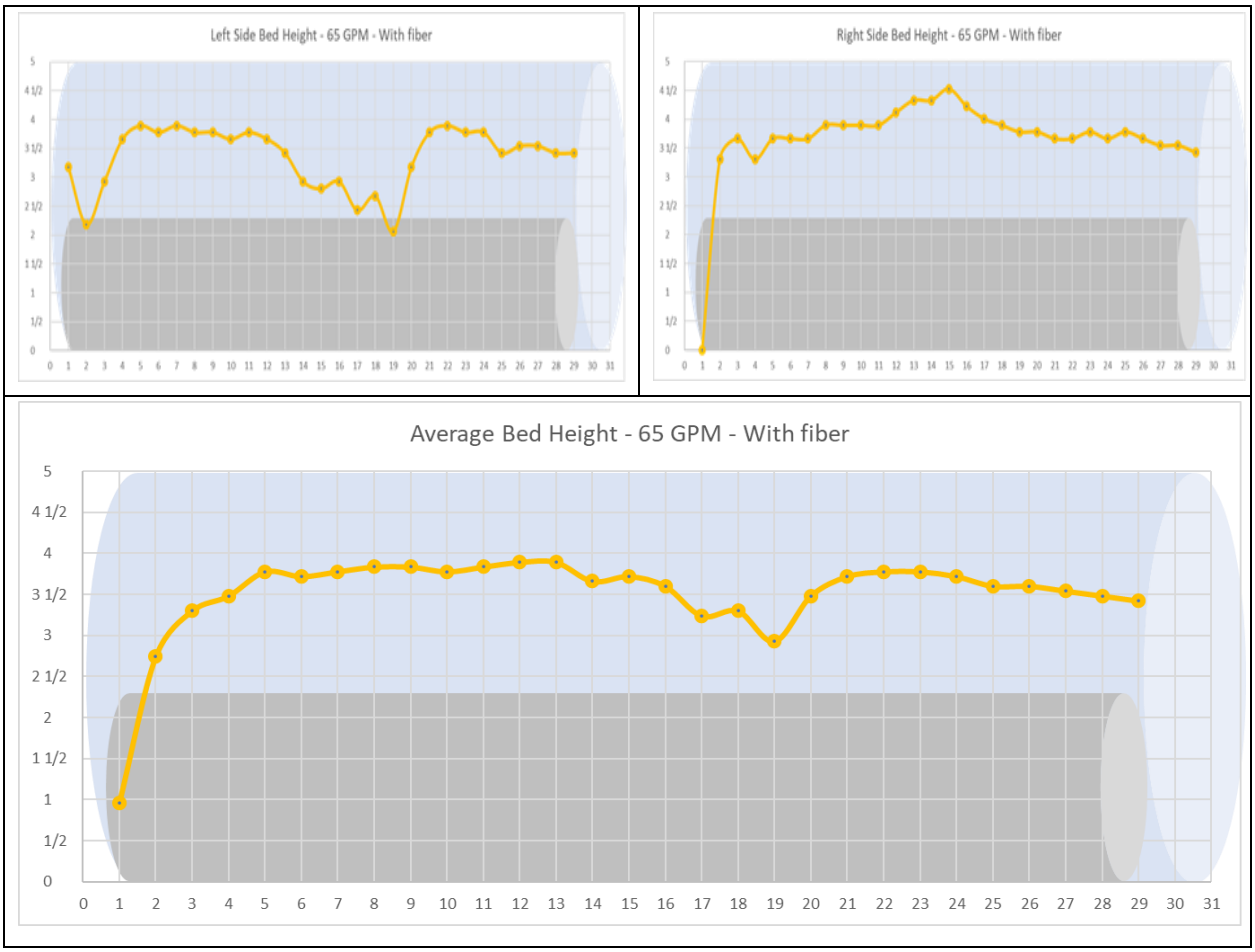

Figure A.21 Fibrous cleaning fluid left-side, right-side, and average bed profiles (65 GPM, 0 RPM)

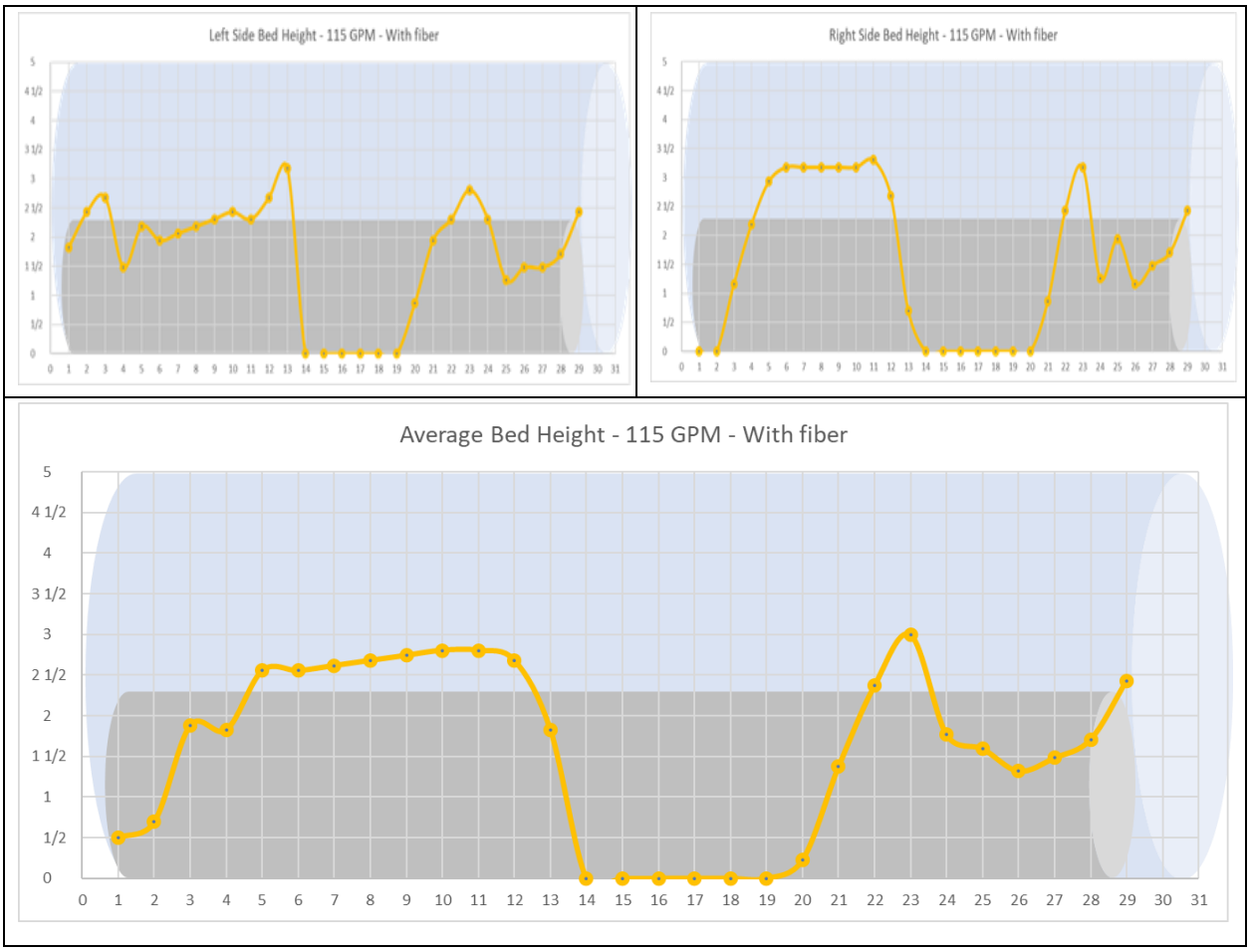

Figure A.22 Fibrous cleaning fluid left-side, right-side, and average bed profiles (115 GPM, 0 RPM)

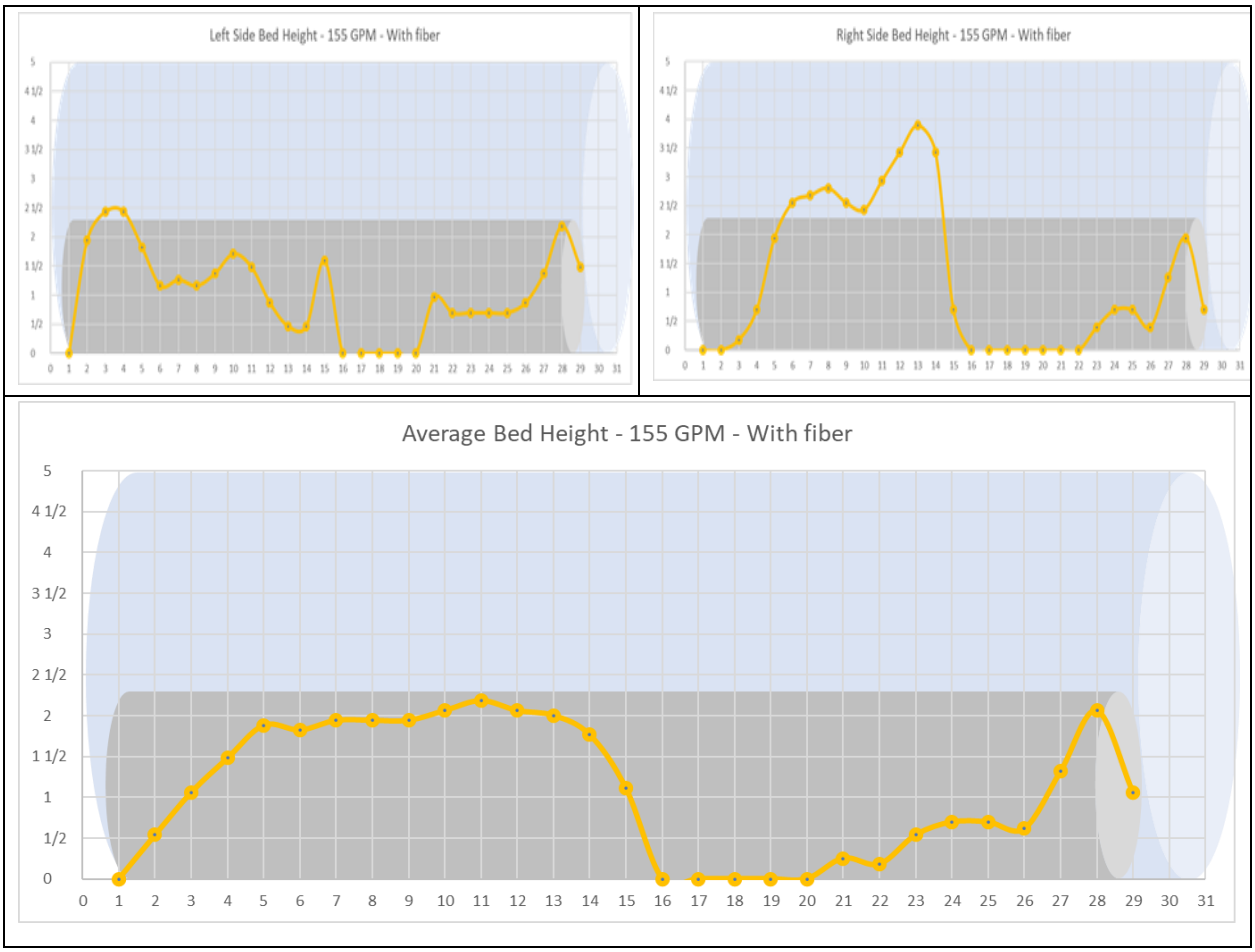

Figure A.23 Fibrous cleaning fluid left-side, right-side, and average bed profiles (155 GPM, 0 RPM)

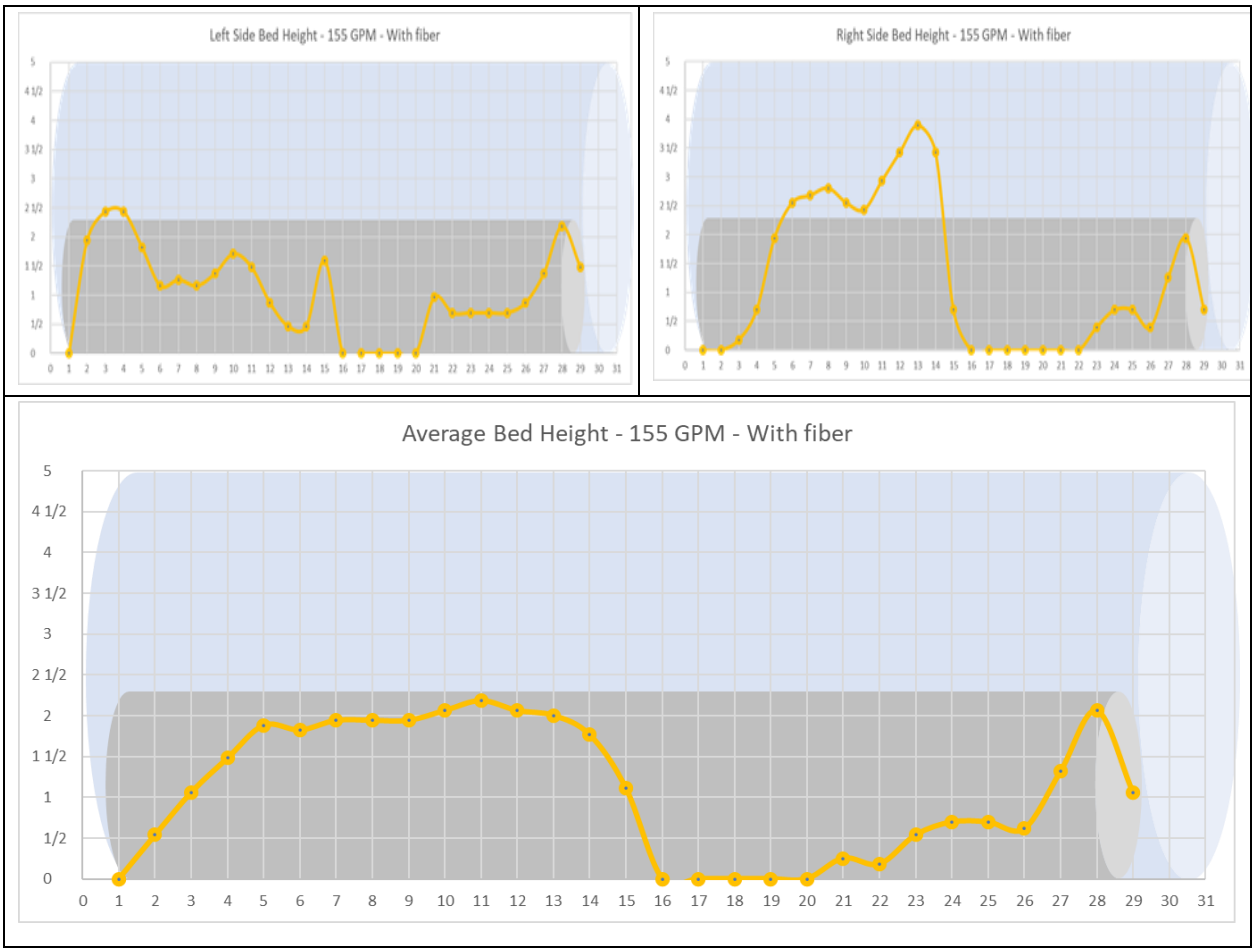

Figure A.24 Fibrous cleaning fluid left-side, right-side, and average bed profiles (155 GPM, 0 RPM)

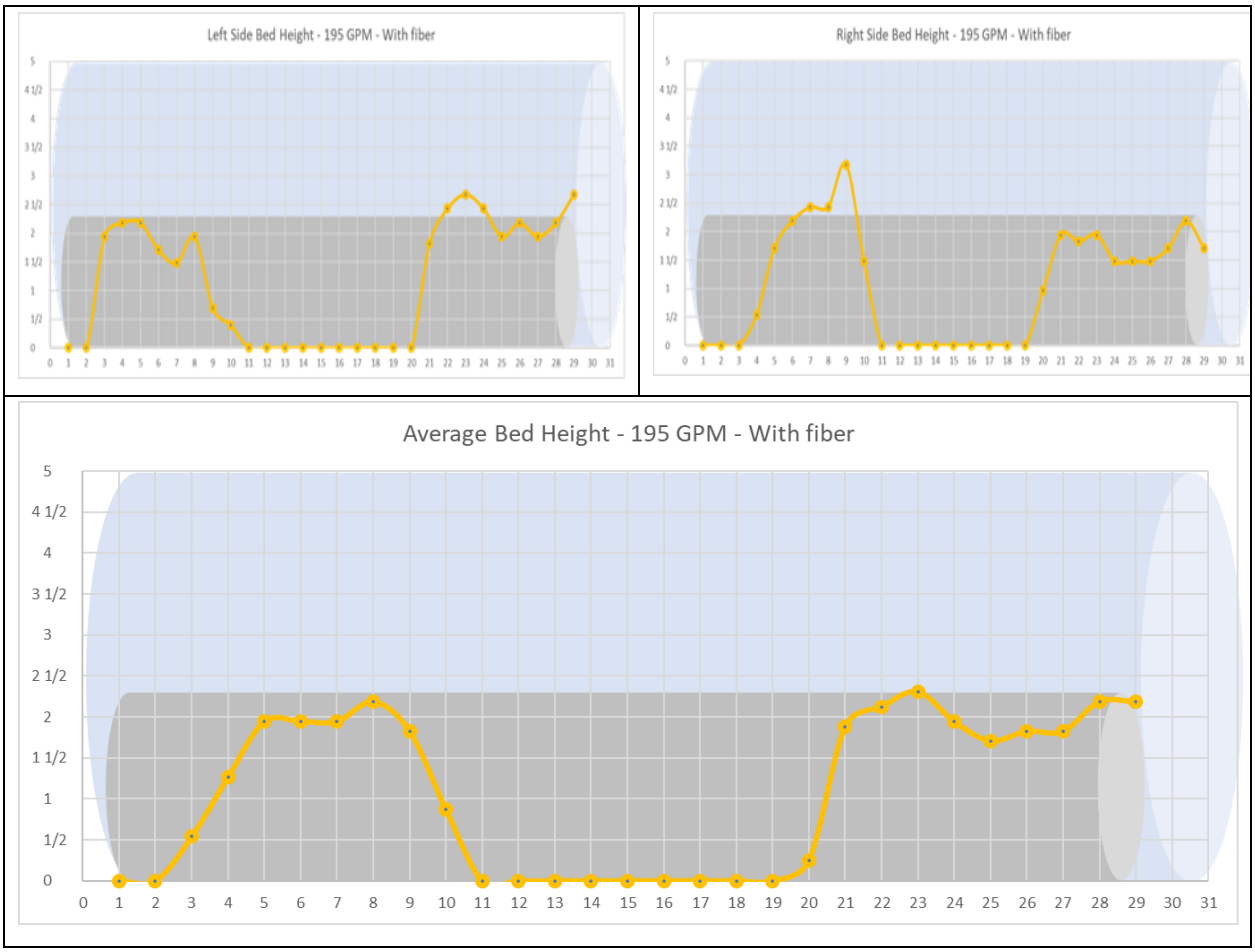

Figure A.25 Fibrous cleaning fluid left-side, right-side, and average bed profiles (195 GPM, 0 RPM)

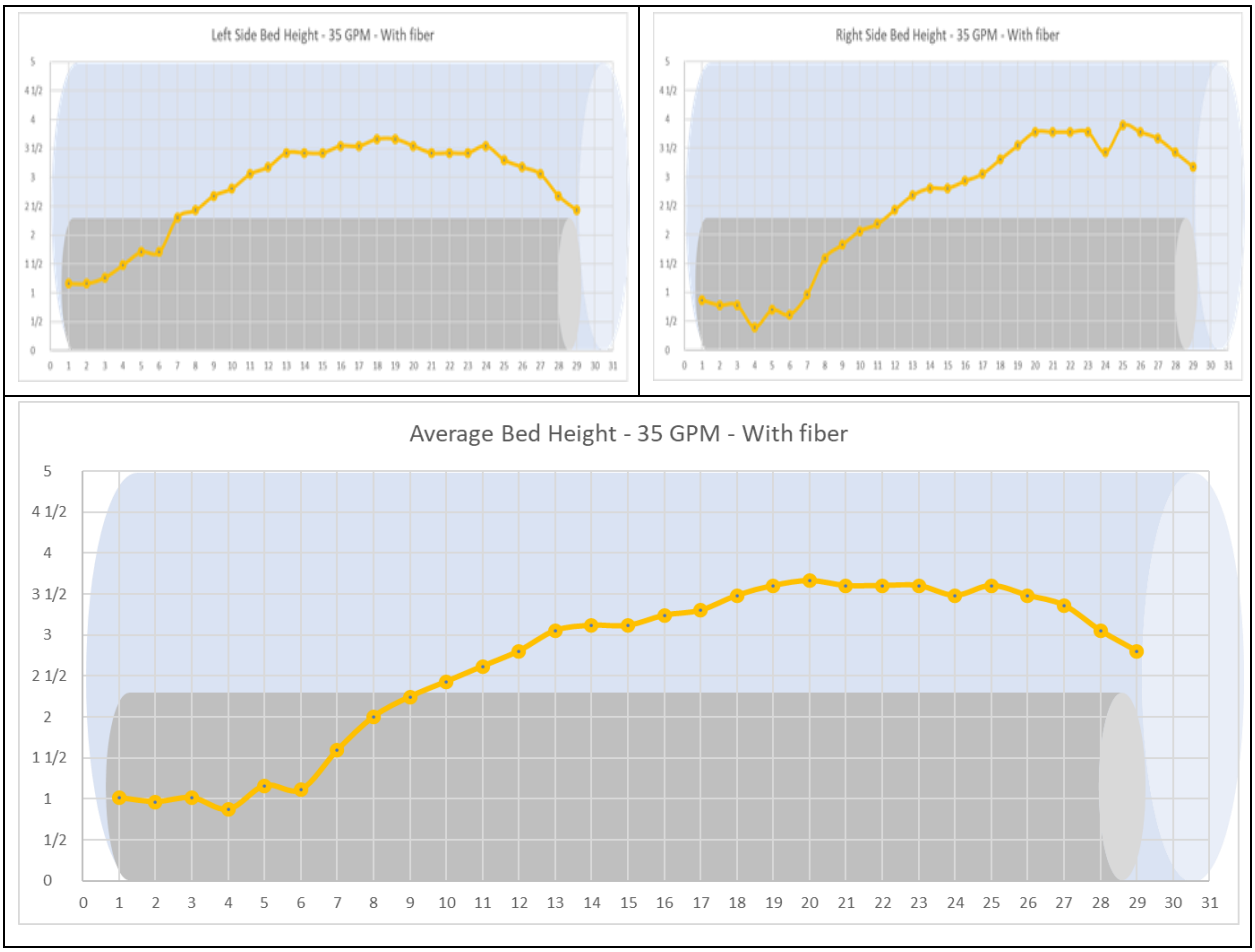

Figure A.26 Fibrous cleaning fluid left-side, right-side, and average bed profiles (35 GPM, 50 RPM)

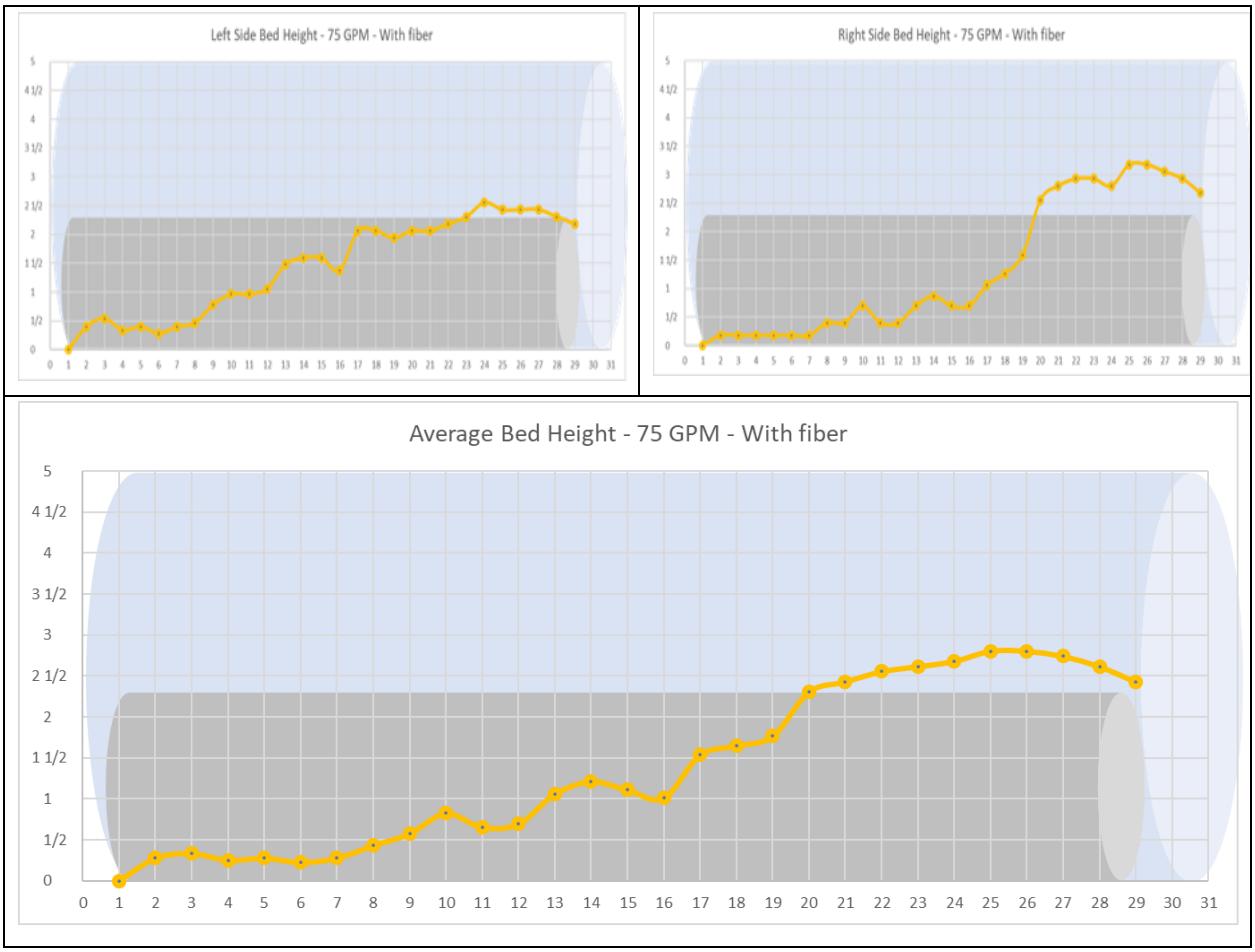

Figure A.27 Fibrous cleaning fluid left-side, right-side, and average bed profiles (75 GPM, 50 RPM)

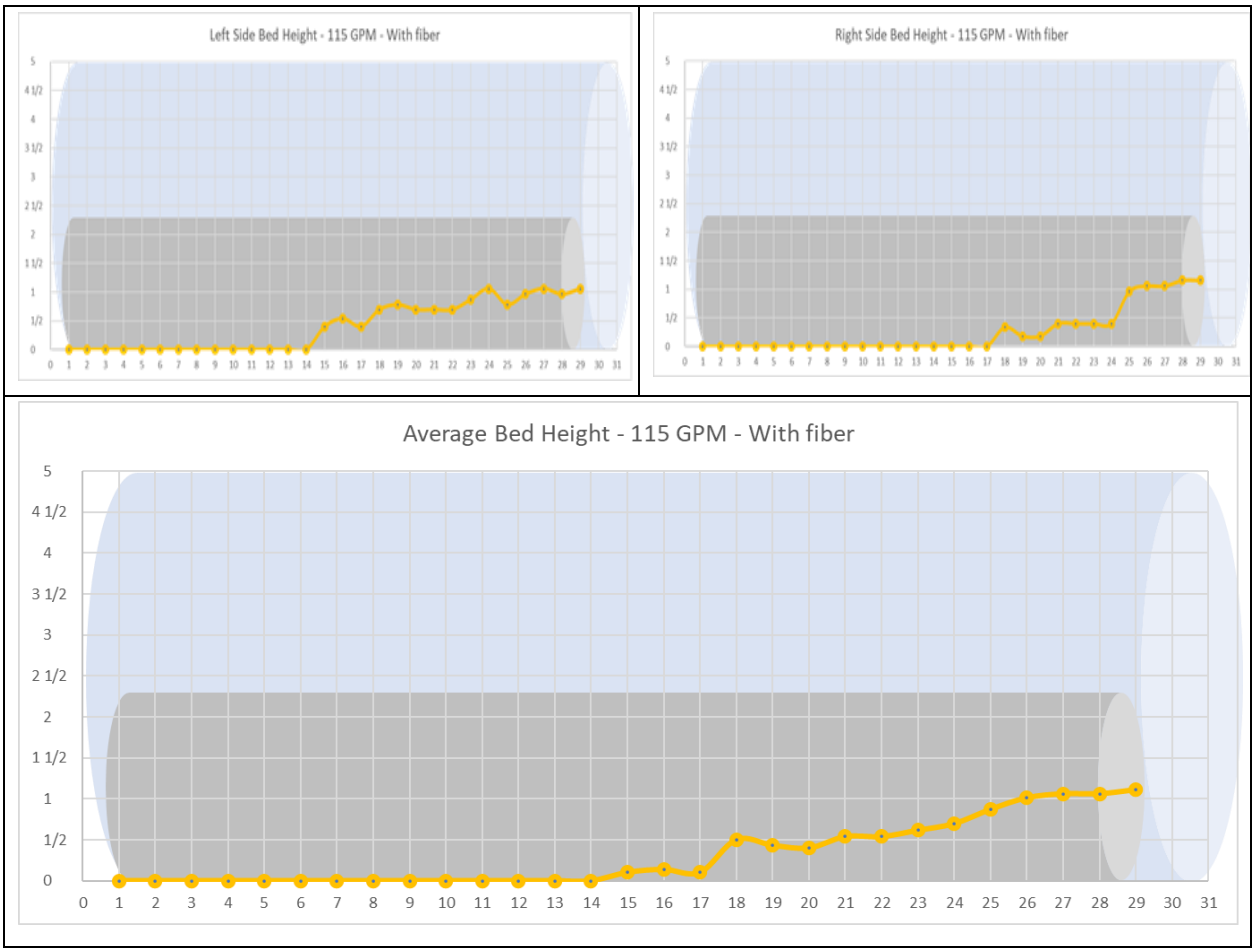

Figure A.28 Fibrous cleaning fluid left-side, right-side, and average bed profiles (115 GPM, 50 RPM)

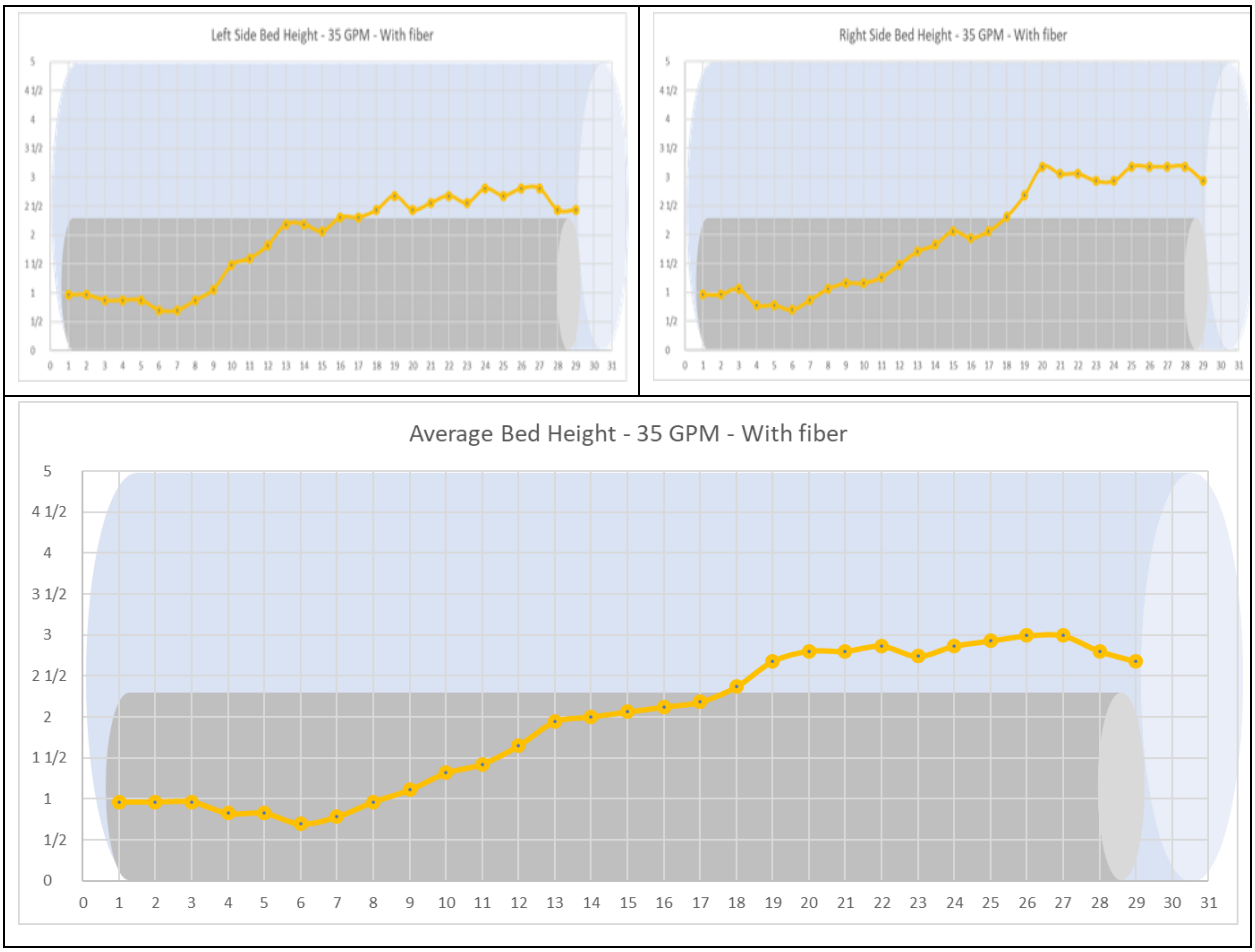

Figure A.29 Fibrous cleaning fluid left-side, right-side, and average bed profiles (35 GPM, 100 RPM)

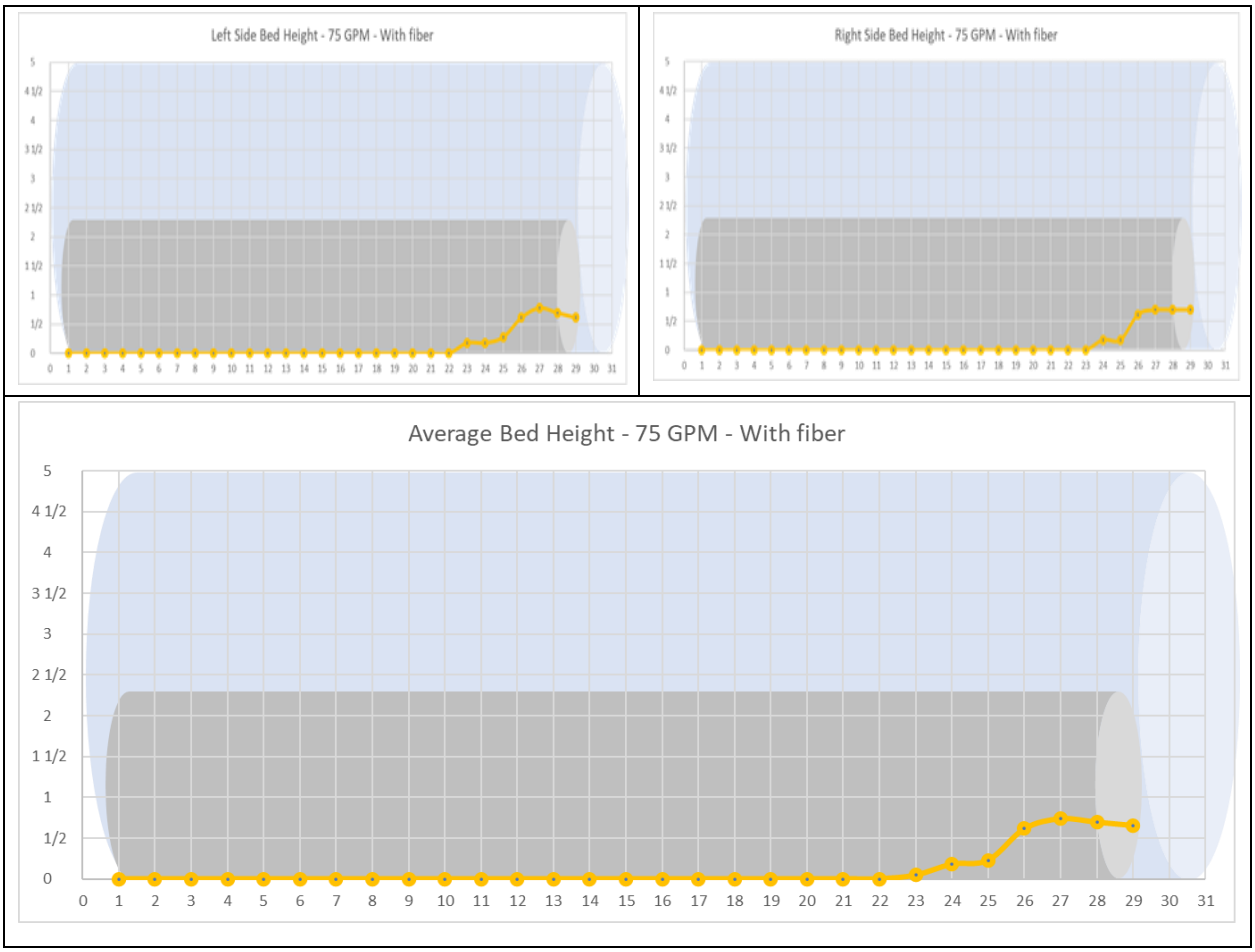

Figure A.30 Fibrous cleaning fluid left-side, right-side, and average bed profiles (75 GPM, 100 RPM)